# Interactions of metal and metalloid ions with fungal biomass

**PhD research thesis by**

Joseph M. Brady *B.Sc.*

**Supervisor**

Dr. John M. Tobin

School of Biological Sciences,

Dublin City University,

Dublin 9,

Ireland.

September, 1996

I hereby certify that this material, which I now submit for assessment on the programme of study leading to the award of PhD is entirely my own work and has not been taken from the work of others save and to the extent that such work has been cited and acknowledged within the text of my own work.

Signed:.....Joseph M. Brady..... ID No.: 92701191

Date: 26th August 1996

*Dedicated to Yvonne, my father, and all my family*

**TABLE OF CONTENTS** Page

# ABSTRACT


***Interactions of metal and metalloid ions with fungal biomass***

***PhD Research Thesis by***

***Joseph M. Brady* B.Sc.**

In theory, the higher the covalent index value of a metal ion, the greater its potential to form covalent bonds with biological ligands. Metabolism-independent equilibrium metal ion adsorption to freeze dried *Rhizopus arrhizus* biomass was found to increase in the order $Sr^{2+} < Mn^{2+} < Zn^{2+} < Cd^{2+} < Cu^{2+} < Pb^{2+}$ and positively correlated with covalent index. Adsorption was rapid and 95% complete within five minutes of metal-microbe contact, and equilibrium was independent of solution biomass concentrations.

The potential of a metal to displace other preloaded cations from the biomass ligands, and the extent to which a preloaded ion inhibited the adsorption of another both increased with increasing covalent index for $Mn^{2+}$, $Zn^{2+}$, $Cd^{2+}$, $Cu^{2+}$ and $Pb^{2+}$. An almost complete inversion of this order was observed in the case where $Sr^{2+}$ was the primary binding test ion. According to the *hard and soft* principle of metal ions, $Mn^{2+}$, $Zn^{2+}$, $Cd^{2+}$, $Cu^{2+}$ and $Pb^{2+}$ are classified as *soft-borderline*, $Sr^{2+}$ is classified as *hard*, and theoretically the polar nature of these cations increase in the same order as covalent index.

As a consequence of metal ion adsorption, $Ca^{2+}$ and $Mg^{2+}$ displacement from the biomass ligands was observed for both *hard* and *soft borderline* ions, whereas displacement of $H^{+}$ was observed for *soft borderline* ions only. Overall, the *soft borderline* ions exhibited a significant degree of both covalent and ionic binding, and the *hard* metal $Sr^{2+}$ was found to exhibit ionic binding only. Linear reciprocal Langmuir and Scatchard transformation plots reflected the predominantly ion exchange mechanism of $Sr^{2+}$ and $Cd^{2+}$ adsorption, and a curved Scatchard transformation plot reflected the more covalent nature of $Cu^{2+}$ adsorption.

The transformation and accumulation of the oxyanion selenite (1000 $\mu mol\ l^{-1}$) by a growing *Penicillium* species was investigated over a 2 week period. Selenium in the aqueous phase decreased by *ca.* 49.8%, and selenium accumulated by the fungal biomass totalled *ca.* 36.6%. Transformation into volatile selenium compounds amounted to an average value of *ca.* 8.8%, and the process was determined to be both growth and non-growth associated. Activated charcoal traps were successfully used to retain the volatile selenium compounds which were determined to be organic in nature. The reduction of selenite to amorphous elemental selenium was observed only during the decline phases of growth. Selenite transformation, particularly reduction to amorphous elemental selenium, was enhanced by the addition of amino acids and vitamins to the aqueous medium, and with such amendments selenite reduction was observed both during the rapid and stationary phases of growth.

# LIST OF FIGURES

**Figure 3.1.6**: Representative reciprocal Langmuir plots for $Sr^{2+}$, $Cd^{2+}$ and $Cu^{2+}$ adsorption by freeze-dried *Rhizopus arrhizus* biomass.

**Figure 3.1.7**: Representative BET plots for $Sr^{2+}$, $Cd^{2+}$ and $Cu^{2+}$ adsorption by freeze-dried *Rhizopus arrhizus* biomass.

**Figure 3.1.8**: Representative Freundlich plots for $Sr^{2+}$, $Cd^{2+}$ and $Cu^{2+}$ adsorption by freeze-dried *Rhizopus arrhizus* biomass.

**Figure 3.1.9**: Representative Scatchard transformation plots for $Sr^{2+}$, $Cd^{2+}$ and $Cu^{2+}$ adsorption by freeze-dried *Rhizopus arrhizus* biomass.

**Figure 3.2.1**: Time profiles of the adsorption of $Sr^{2+}$, $Cd^{2+}$ and $Cu^{2+}$ ions by freeze-dried *Rhizopus arrhizus* biomass, and of the subsequent displacement and inhibition effects when a second metal is introduced into the systems at $t_{180}$.

**Figure 3.3.1**: Equilibrium adsorption isotherms for $Sr^{2+}$, $Cd^{2+}$ and $Cu^{2+}$ ions using freeze-dried *Rhizopus arrhizus* biomass, at biosorbent concentrations of 1, 0.5 and 0.25 g $l^{-1}$.

**Figure 3.3.2**: Reciprocal Langmuir plots of $Sr^{2+}$, $Cd^{2+}$ and $Cu^{2+}$ equilibrium adsorption isotherms at biosorbent concentrations of 1, 0.5 and 0.25 g $l^{-1}$.

**Figure 3.3.3**: Equilibrium $Ca^{2+}$ ion displacement from freeze dried *Rhizopus arrhizus* biomass by $Sr^{2+}$, $Cd^{2+}$ and $Cu^{2+}$ ions, versus metal uptake, at biosorbent concentrations of 1, 0.5 and 0.25 g $l^{-1}$.

**Figure 3.3.4**: Equilibrium $Mg^{2+}$ ion displacement from freeze dried *Rhizopus arrhizus* biomass by $Sr^{2+}$, $Cd^{2+}$ and $Cu^{2+}$ ions, versus metal uptake, at biosorbent concentrations of 1, 0.5 and 0.25 g $l^{-1}$.

**Figure 3.3.5**: Final pH values at equilibrium versus metal ion uptake for $Cd^{2+}$ and $Cu^{2+}$ freeze-dried *Rhizopus arrhizus* biomass systems, at biosorbent concentrations of 1, 0.5 and 0.25 g $l^{-1}$.

**Figure 3.3.6**: Equilibrium $H^{+}$ ion displacement from freeze-dried *Rhizopus arrhizus* biomass by $Cd^{2+}$ and $Cu^{2+}$ ions, versus metal uptake, at biosorbent concentrations of 1, 0.5 and 0.25 g $l^{-1}$.

**Figure 3.4.1**: Experimental column breakthrough curves determined over the flowrate range 3.40-11.63 ml $min^{-1}$. Effluent $Cu^{2+}$ concentration versus time (a), and effluent $Cu^{2+}$ concentration versus effluent volume (b).

**Figure 3.4.2**: Representative $Ca^{2+}$ and $Mg^{2+}$ displacement plots versus effluent volume for a column operating at 5.88 ml $min^{-1}$ flowrate.

**Figure 3.4.3**: Plots of $\sigma^2$ versus flowrate (Q), and $t_{50}$ versus $Q^{-1}$ for columns over the flowrate range 3.40-11.63 ml $min^{-1}$.

**Figure 3.4.4**: Mathematically predicted and experimental column breakthrough curves determined over the flowrate range 3.40-11.63 ml $min^{-1}$ ($Cu^{2+}$ effluent concentrations versus effluent volumes).

**Figure 3.4.5**: Mathematically predicted column breakthrough curves determined over the flowrate range 3.40-11.63 ml $min^{-1}$. Effluent $Cu^{2+}$ concentration versus time (a), and effluent $Cu^{2+}$ concentration versus effluent volume (b).

**Figure 3.6.1**: Growth of a *Penicillium* species in the absence of selenite. Biomass growth and pH change are profiled versus time.

**Figure 3.6.2**: Growth of a *Penicillium* species in the presence of 1000 µmol $l^{-1}$ sodium selenite. Biomass growth, pH change, total selenium remaining in the aqueous phase, selenium associated with the biomass, selenium per unit biomass dry weight, and overall selenium mass balance are plotted versus time.

**Figure 3.7.1**: Growth of a *Penicillium* species in the presence of 1000 µmol $l^{-1}$ sodium selenite and, a 50 ml DMEM addition at $t_0$, two 25 ml DMEM additions at $t_0$ and on day 7, and one 50 ml DMEM addition on day 7.

**Figure 3.7.2**: Media pH profile for a *Penicillium* species growth in the presence of 1000 μmol $l^{-1}$ sodium selenite and, a 50 ml DMEM addition at $t_0$, two 25 ml DMEM additions at $t_0$ and on day 7, and one 50 ml DMEM addition on day 7.

**Figure 3.7.3**: Profile of selenium remaining in the aqueous phase as a result of a *Penicillium* species growth in the presence of 1000 μmol $l^{-1}$ sodium selenite and, a 50 ml DMEM addition at $t_0$, two 25 ml DMEM additions at $t_0$ and on day 7, and one 50 ml DMEM addition on day 7.

**Figure 3.7.4**: Profile of selenium associated with the biomass for a *Penicillium* species grown in the presence of 1000 μmol $l^{-1}$ sodium selenite and, a 50 ml DMEM addition at $t_0$, two 25 ml DMEM additions at $t_0$ and on day 7, and one 50 ml DMEM addition on day 7.

**Figure 3.7.5**: Selenium associated with the biomass per unit dry weight for a *Penicillium* species grown in the presence of 1000 μmol $l^{-1}$ sodium selenite and, a 50 ml DMEM addition at $t_0$, two 25 ml DMEM additions at $t_0$ and on day 7, and one 50 ml DMEM addition on day 7.

**Figure 4.2.1**: Correlation of metal uptake with ion covalent index values for $Sr^{2+}$, $Mn^{2+}$, $Zn^{2+}$, $Cd^{2+}$, $Cu^{2+}$ and $Pb^{2+}$.

**Figure 4.3.1**: Ionic/covalent ratios ($Ca^{2+}$+$Mg^{2+}$/$H^{+}$) for $Cd^{2+}$ and $Cu^{2+}$ freeze-dried *Rhizopus arrhizus* biomass systems, at biosorbents concentrations of 1 $gl^{-1}$, 0.5 g $l^{-1}$ and 0.25 $gl^{-1}$.

# LIST OF TABLES

**Table 3.2.3**: Percentage uptake inhibition of $t_{180}$ metals caused by preloaded $t_0$ metals for *equilibrium studies*.

**Table 3.2.4**: Percentage of $t_0$ metals displaced by the addition of $t_{180}$ metals for *time-course studies*.

**Table 3.2.5**: Percentage uptake inhibition of $t_{180}$ metals caused by preloaded $t_0$ metals for *time-course studies*.

**Table 3.4.1**: $Cu^{2+}$ ion uptake values ($q$) and consequent $Ca^{2+}$, $Mg^{2+}$ and $H^+$ ion displacement at equilibrium with native freeze-dried *Rhizopus arrhizus* biomass.

**Table 3.4.2**: $Cu^{2+}$ ion uptake values ($q$) and consequent $Ca^{2+}$, $Mg^{2+}$ and $H^+$ ion displacement at equilibrium with freeze-dried *Rhizopus arrhizus* biomass treated with dichloromethane (DCM).

**Table 3.4.3**: $Cu^{2+}$ ion uptake values ($q$) at equilibrium with freeze-dried *Rhizopus arrhizus* biomass immobilised in polyvinyl-formal (PVF), with biosorbent loading values of 40, 50, 60, 70 and 80%.

**Table 3.4.4**: $Ca^{2+}$ ion displacement values at equilibrium from freeze-dried *Rhizopus arrhizus* biomass immobilised in PVF, with biosorbent loading values of 40, 50, 60, 70 and 80%.

**Table 3.4.5**: $Mg^{2+}$ ion displacement values at equilibrium from freeze-dried *Rhizopus arrhizus* biomass immobilised in PVF, with biosorbent loading values of 40, 50, 60, 70 and 80%.

**Table 3.4.6**: $H^{+}$ ion displacement values at equilibrium from freeze-dried *Rhizopus arrhizus* biomass immobilised in PVF, with biosorbent loading values of 40, 50, 60, 70 and 80%.

**Table 3.4.7**: Overall column $Cu^{2+}$ uptake values ($q$) and consequent $Ca^{2+}$ and $Mg^{2+}$ ion displacement for PVF immobilised *Rhizopus arrhizus* biomass (60% biosorbent loading), over the influent flowrate range 3.40-11.63 ml $min^{-1}$.

**Table 3.5.1**: $Ca^{2+}$, $Mg^{2+}$, $H^{+}$ and $K^{+}$ ion release at equilibrium from live non-metabolising *Rhizopus arrhizus* biomass following selenite-microbe contact.

**Table 3.5.2**: $Ca^{2+}$, $Mg^{2+}$, $H^{+}$ and $K^{+}$ ion release at equilibrium from live non-metabolising *Penicillium* species biomass following selenite-microbe contact.

**Table 3.6.1**: Volatile selenium compounds recovered from activated charcoal traps during growth of a *Penicillium* species in a bioreactor containing 5000 µmol of sodium selenite.

**Table 3.7.1**: Volatile selenium compounds recovered from activated charcoal traps during growth a *Penicillium* species in 5 l bioreactors amended with 50 ml of Dulbecco's Modified Eagle Medium and 5000 µmol of sodium selenite.

**Table 4.5.1**: Maximum equilibrium $Ca^{2+}$, $Mg^{2+}$, $H^{+}$ and $K^{+}$ ion release levels from *Rhizopus arrhizus* and a *Penicillium* species following selenite-microbe contact.

# CURRENT PUBLICATIONS

Brady, J.M. & Tobin, J.M. (1994). Adsorption of metal ions by *Rhizopus arrhizus* biomass: Characterisation studies. *Enzyme and Microbial Technology* **16**, 671-675.

Brady, J.M. & Tobin, J.M. (1995). Column studies of metal removal by immobilised biomass. *ICHEME Research Event/First European Conference* **1**, 213-215.

Brady, J.M. & Tobin, J.M. (1995). Binding of hard and soft metal ions to *Rhizopus arrhizus* biomass. *Enzyme and Microbial Technology* **17**, 791-796.

Brady, J.M., Tobin, J.M. & Gadd, G.M. (1996). Volatilization of selenite in aqueous medium by a *Penicillium* species. *Mycological Research* **00**, 00-00. (*In press*)

# ACKNOWLEDGEMENTS

I would like to sincerely thank my supervisor Dr. John Tobin for the opportunity to study and work in his laboratory in Dublin City University. Thanks for all the advice, encouragement and professionalism during the course of my research, I am forever grateful. Thanks also to the head of the department, Professor Richard O'Kennedy, for his confidence in me in all my academic pursuits, and to Professor Geoffrey Gadd in the University of Dundee, Scotland, for his support and guidance during my 6 month research visit to his laboratory.

To my colleagues and very good friends, Kevin, Robert and Marianne, thanks for making each working day fun, we had a lot of great times together. Many thanks to Damian for his assistance and expertise in solving my many computer problems, and to Dr. Brendan O' Connor, Dr. Padraig Walsh and Dr. Greg Foley for all their time, assistance and friendly advice in writing this thesis.

Special thanks to Yvonne, my father and all the family for all the kind and encouraging words. Their expressions of pride in my achievements is always a great source of encouragement and inspiration.

# FOREWORD

*Interactions of metal and metalloid ions with fungal biomass*

*PhD Research Thesis by*

*Joseph M. Brady* **B.Sc.**

## FOREWORD

The interaction of metal ions with biological cell surfaces is a prerequisite for intracellular accumulation where metals fulfill essential metabolic functions or, in certain cases, exhibit toxic effects (Avery & Tobin, 1993). Microbial mechanism for the detoxification of metal ions include chemical transformations to more volatile compounds (Gadd, 1993*a*,*b*; Morley *et al.*, 1995; Tebo, 1995; Brady, Tobin & Gadd, 1996) or different valency states (Hassett & Kosman, 1995), physico-chemical accumulation of dissolved and particulate ions usually referred to as *biosorption* (Lin, Crawford & Koswan, 1993*a*; Yazgan & Ozcengiz, 1994; Yoshida & Murooka, 1994; Gelmi *et al.*, 1994; Brady & Tobin, 1994; 1995*a*,*b*; Berhe, Fristedt & Persson, 1995; Engl & Kunz, 1995; Chen & Ting, 1995; Akthar, Sastry & Mohan, 1995), formation of metabolic products that make the contaminant insoluble (Corzo *et al.*, 1994; Farcasanu *et al.*, 1995), and utilisation of efflux systems (Gadd 1990; 1992). After transport into viable cells, metals may be compartmentalised in specific organelles, and rendered non-toxic by binding or precipitation (Gadd & White, 1985, 1989*a*; Gadd, 1990; 1992; Lin, Crawford & Koswan, 1993*a*,*b*; Klapcinska, 1994; Gelmi *et al.*, 1994; Golab & Breitenbach; 1995; Volesky & May-Phillips, 1995; Bode *et al.*, 1995; Appanna *et al.*, 1995; Donnellan *et al.*, 1995).

This research thesis divides naturally into a number of sections as described below. Initially the work seeks to characterise and explain physico-chemical interactions of a range of divalent metal cations with nonviable fungal biomass, and is then extended to continuous flow immobilised biomass systems. In later sections fungal biosorption and

volatilisation of the metalloid selenium is investigated and various enhancement strategies are studied. The sections may be summarised as follows, and this format is followed throughout the thesis.

***Biosorption characterisation*** investigates equilibrium $Sr^{2+}$, $Cd^{2+}$ and $Cu^{2+}$ ion adsorption by freeze-dried, oven-dried and live non-metabolising biomasses of *Rhizopus arrhizus*. Ionic and covalent contributions were calculated by monitoring $Ca^{2+}$+$Mg^{2+}$ and $H^+$ ion displacement values respectively. The biosorbent surfaces were characterised by application of mathematical adsorption isotherm models and Scatchard transformation plots to the adsorption data. In ***Application of hard and soft principle***, the *hard* and *soft* principle of metal ions was applied to the study of $Sr^{2+}$, $Mn^{2+}$, $Zn^{2+}$, $Cd^{2+}$, $Cu^{2+}$ and $Pb^{2+}$ adsorption by freeze-dried *Rhizopus arrhizus* biomass, and also to the study of displacement and inhibition effects of one ion by another. Time profiles of adsorption, displacement and inhibition were also examined for $Sr^{2+}$, $Cd^{2+}$ and $Cu^{2+}$ systems. The effect of biomass solution concentration on equilibrium $Sr^{2+}$, $Cd^{2+}$ and $Cu^{2+}$ biosorption by freeze-dried *Rhizopus arrhizus* biomass was examined in ***Effects of biomass concentration***, along with the relevant ionic and covalent contributions. ***Continuous flow systems*** examined continuous fixed-bed adsorption of $Cu^{2+}$ ions by polyvinyl formal immobilised freeze-dried *Rhizopus arrhizus* biomass, and the resultant breakthrough curves were characterised by mathematical modelling. Ionic and covalent contributions were again evaluated. ***Selenite adsorption studies*** examined the toxic effects of selenite on live non-metabolising biomasses of *Rhizopus arrhizus* and a *Penicillium* species by monitoring the release of $Ca^{2+}$, $Mg^{2+}$, $H^+$ and $K^+$ ions.

***Selenite transformation studies*** characterises the transformation of selenite in aqueous media by the *Penicillium* species over a 2 wk period at 25°C under aerobic and acidic conditions. The design of the bioreactors, the trapping and recovery of volatile selenium compounds, and a suitable selenium assay are all explained in detail. ***Transformation enhancement studies*** investigates the beneficial effects of Dulbecco's Modified Eagle Medium (DMEM) components, particularly a range of amino acids and vitamins, on selenite transformation, both volatilisation and reduction to amorphous elemental selenium.

# CHAPTER 1

# INTRODUCTION

*Interactions of metal and metalloid ions with fungal biomass*

*PhD Research Thesis by*

*Joseph M. Brady* **B.Sc.**

## CHAPTER 1: INTRODUCTION

*The first part of this literature review (sections 1.1 to 1.6) examines the potential of microbial biomass to adsorb metal ions from aqueous environments and considers the mechanisms involved. It examines physical and chemical properties of metal ions and the nature of ligands available for sequestration. Mathematical models used for describing adsorbent surfaces, and quantifying receptor sites and binding affinities are also examined.*

*The second part of this survey (sections 1.7 to 1.11) examines the microbial transformation of selenium oxyanions, particularly selenite, into volatile selenium compounds and amorphous elemental selenium. It considers the mechanisms involved and some experimental techniques designed to monitor and enhance such transformations. Accumulation/biosorption aspects of selenium oxyanion reduction are also discussed.*

### 1.1 *Metals and Microorganisms*

Metals and metalloids considered necessary for biological growth and function are the macro-elements sodium, potassium, magnesium and calcium, and the micro-trace elements vandium, chromium, manganese, iron, cobalt, nickel, copper, zinc, selenium and molybdenum (Hughes & Poole, 1989; 1991; Gadd, 1992). In general terms, they are known to be involved in the stabilisation of a range of biological structures, from cell walls to protein conformations. Some are considered highly effective catalysts of a range of diverse biochemical processes that can initiate, moderate or inhibit reactions (Hughes

& Poole, 1989). Non-essential metals/metalloids with no known biological functions include, aluminium, arsenic, silver, cadmium, mercury, tin, tellerium and lead. At relatively high concentrations of both essential and non-essential metals toxic effects can be experienced by a range of organisms (Hughes & Poole, 1989; 1991; Gadd, 1993*b*).

Metal ions arise in quantity from a range of domestic and industrial processes and waste streams (Azab, Peterson & Young, 1990; Gadd, 1992; Andreoni *et al.*, 1994; Mishra, Singh & Tiwari, 1995), and their release into the environment can lead to the contamination of the food chain. They occur in a range of physical and chemical forms that greatly influence their bioavailability and effect on the aquatic environment. Most are in the form of inorganic salts and tend to be predominantly associated with suspended solids (Zabel, 1993). Organoderivatives of lead, tin and mercury, where the metals are bound to a variety of organo groups through metal-carbon bounds, frequently have a higher toxicity than simple inorganic derivatives (Gadd, 1992). This results from greater lipid solubility of organoderivatives and resulting enhancement of incorportation into viable cells (Gadd, 1993a,b). Microorganisms, including bacteria, algae, yeasts and fungi can sequester metal ions from solution with relatively high efficiencies by a process commonly referred to as *biosorption* (Gadd, 1990; Enzminger, 1991; Tebo, 1995; Volesky & Holan, 1995). Such a process is presently being considered as a novel metal decontamination-recovery technique.

## 1.2 *Biosorption*

Biosorption can be simply defined as the removal of metal or metalloid species, compounds and particulates from solution by biological material (Volesky, 1986; Gadd, 1990, 1992; Tebo, 1995; Chong & Volesky, 1995; Volesky & Holan, 1995). The term biosorption has mainly been applied to microbial biomass, although most biological material has biosorptive capacity. The process of biosorption by microbial biomass is considered to involve a variety of metabolic-dependent and -independent mechanisms that are influenced by environmental factors including pH, temperature and the presence of other metal ions (Wainwright, 1990; Wnorowski, 1991; Gadd, 1992; Brady & Duncan, 1994*a*; Blackwell, Singleton & Tobin, 1995; Chen & Ting, 1995). Bisorption by viable biomass is considered a biphasic process: an initial metabolism-independent rapid binding of metal ions onto the cell surface followed by a slower metabolism-dependent intracellular uptake (Trevors, Stratton & Gadd, 1986; de Rome & Gadd, 1987; Duncan & Brady, 1994*a*; Sloof & Viragh, 1995). In the case of non-viable biomass, biosorption proceeds exclusively by metabolically independent passive adsorptive processes (de Rome & Gadd, 1987; Wainwright, 1990), which under certain conditions has been reported to adsorb metal ions in larger quantities than viable biomass (Kuyucak & Volesky, 1988; Wainwright, 1990; Andreoni *et al.*, 1991; Urruita Mera *et al.*, 1992; Volesky & May-Phillips, 1995). The three major classes of microbial biopolymers, proteins, nucleic acids and polysaccharides, all provide sites at which metal ions will bind. The ligand groups available for biosorption include the amine function, and the negatively charged groups, carboxylate, thiolate and phosphate (Hughes & Poole, 1989; Tobin, Cooper & Neufeld, 1990).

### 1.2.1 *Potential applications of biosorption*

Potential industrial applications of this phenomenon include the use of immobilised microbial biomass in suitably constructed bioreactors for reclamation or containment of metal ions in industrial waste/process streams (Treen-Sears, Volesky & Neufeld, 1984; Volesky, 1986; 1990; Tsezos, Noh & Baird, 1988; Tsezos, McCready & Bell, 1989; Gadd, 1990; Wainwright, 1990; Tobin, L'Homme & Roux, 1993; Tobin, White & Gadd, 1994; Brady & Duncan, 1994*a*; Volesky & Holan, 1995). Biosorptive processes are rapid and would in theory be suitable for the extraction of metal ions from large volumes of water (Azab *et al.*, 1990; Melcer, Monteith & Nutt, 1992; Artola & Rigola, 1992; Blais, Tyagi & Auclair, 1993; Geddie & Sutherland, 1993). For industrial scale processes, the cost of producing biomass may be a serious economic disadvantage and consequently the use of waste microbial biomass which arises in quantity from several industrial fermentations would be desirable (Volesky, 1986; Leuf, Prey & Kubicek, 1991; Simmons, Tobin & Singleton, 1995).

## 1.3 *Classification of hard and soft metals and ligands*

The *hard* and *soft* theory of metal ions originates from a study that examined the relative affinities of ligand atoms for acceptor molecules and ions (Ahrland, Chatt & Davies, 1958). The work examined trends in the magnitude of equilibrium constants that describe the formation of acceptor-ligand complexes. Two prominent features of the study emerged:

(1) Significant differences exist between the co-ordinating affinities of the first and the second element from each of the three groups of ligand atoms V, VI, VII, from the

Periodic Table, *i.e.*, between N and P, O and S, and F and Cl.

(2) Two classes of acceptors exist:

(a) those that form their most stable complexes with the first ligand atom of each group, N, O and F

(b) those that form their most stable complexes with the second or subsequent ligand atom.

Some acceptors exhibit both *class (a)* and *class (b)* characteristics and are separated into a border region. This border region leads to a gradual transition between class (a) and (b) within the Periodic Table.

**1.3.1** *Pearson's Classification of hard and soft acids and bases (1963)*

Metal ions act as Lewis acids by accepting electron pairs from ligands. From a study conducted by Pearson (1963), the relative stability of complexes formed between various Lewis bases (electron pair donors) from group VII of the Periodic Table and various Lewis acids were compared. Derived from the work of Ahrland *et al.* (1958), a number of diverse Lewis acids were classified as *class (a)*, *class (b)*, or *borderline*. Class (a) and (b) Lewis acids are referred to as *hard* and *soft* respectively. Pearson's classification of a range of Lewis acids is outlined in *Appendix A*.

The majority of all ligands are from groups VII, VI and V of the Periodic Table, and the atoms in each group become progressively polar or *soft* with increasing atomic weight. Thus, increasing softness and decreasing hardness of the ligands from each group follow the trends:

Group VII: F < Cl < Br < I

Group VI: O < S < Se < Te

Group V: N < P < As < Sb < Bi

Therefore, the atoms F, O and N are the hardest in each group. Hard acids form their most stable complexes with the first ligand atom of each group and soft acids form their most stable complexes with the second or subsequent member of each group.

Common features inherent to class (a) Lewis acids are small ionic sizes and high positive oxidation states, and to class (b) acids, are low or zero oxidation states and/or large ionic sizes. Features that promote class (a) behaviour are those that lead to low polarisability, and those that promote class (b) behaviour are those that lead to high polarisability. This makes it convenient to refer to class (a) Lewis acids as hard acids and class (b) Lewis acids as soft acids. For hard acids, low polarisability is proportional to high ionisation potential and high electronegativity and vice versa for soft acids. Hard acids, with high positive charges and small ionic sizes favour strong ionic binding with bases of large negative charges and small ionic sizes. Soft acids prefer to bond to soft or polarisable soft bases by primarily covalent bonds, and bonding is strong if the electron affinity of the acid is large, and the ionisation potential of the base is low. Some Lewis acids exhibit both class (a) and class (b) character and are consequently refered to as *borderline*.

### **1.3.2** *Nieboer & Richardson's classification of metal ions (1980)*

In considering a biologically significant classification system, Nieboer & Richardson again separated metal ions into the distinctive classes, (a), (b) and borderline. Class (a)

ions are characterised by a high affinity for oxygen molecules in ligands, and class (b) ions are characterised by a high affinity for nitrogen and sulphur molecules. Similar to the studies by Ahrland *et al.* (1958) and Pearson (1963), the classification of metal ions was also based on trends in the magnitude of equilibrium constants that describe the formation of metal-ligand complexes. Class (a) metals were determined to have the following preference for ligands:

$$F^- > Cl^- > Br^- > I^-$$

and for metal binding donor atoms significant to biological ligands:

$$O > N > S$$

In contrast, class (b) metal ions exhibit the opposite preference sequence:

$$S > N > O$$

and $$I^- > Br^- > Cl^- > F^-$$

Borderline metal ions form an intermediate group and form stable complexes with all classes of ligands. There is a sharp separation between class (a) and borderline metal ions, but the distinction between class (b) and borderline metal ions is not well defined (Gadd, 1992).

The energy of the empty valence orbital of a metal ion is considered a measure of its potential to accept electrons and thus form covalent bonds. Orbital energy may be considered representative of the covalent potential of the ion and is related to electronegativity ($X_m$), which is subsequently related to ionic radius ($r$). The ionic potential of a metal ion is its charge to size ratio, and is considered a measure of its capacity to form ionic bonds with a ligand. In the formation of a covalent bond, a metal ion receives electrons from a ligand. This increases the electron density around the metal

ion and reduces its formal charge. The bond energy between atoms of unequal electronegativity has both covalent and ionic contributions, and there is an unequal sharing of the electrons. For a metal ion, the value of the expression, $X_m^2 r$, is considered a measure of the importance of covalent interactions relative to ionic interactions. This is defined as its potential to form covalent bonds and is referred to as *covalent index*. Thus, the greater the covalent index value of a metal ion, the greater its potential to form covalent bonds with a ligand. For a range of metal ions classified as class (a), class (b) and borderline, $X_m^2 r$ index values as computed by Nieboer & Richardson, are outlined in *Appendix B*. In contrast to Pearson system, $Cd^{2+}$ is classified as borderline instead of soft, and $H^+$ as borderline instead of hard.

### **1.3.3** *General metal-ligand interactions*

Considering the classification systems presented by Pearson and Nieboer & Richardson, it appears that the extent to which a metal ion will bind to a ligand largely depends upon the chemistry of the metal ion and its preference to form ionic or covalent bonds. Class (a) metal ions are described as nonpolarisable Lewis acids which prefer binding to nonpolarisable hard bases by bonds which are principally ionic, and class (b) metal ions are described as polarisable Lewis acids which prefer binding to polarisable soft bases by bonds which are principally covalent (Pearson, 1963; Nieboer & McBryde, 1973; Nieboer & Richardson, 1980; Darnall *et al.*, 1986; Gardae-Torresday *et al.*, 1990; Remacle, 1990; Gadd, 1992). In biological systems soft metals will bind to an extent with hard oxygen donor ligands, and this depends on the degree of polarisation.

In biological systems, oxygen donor ligands and sulphur and nitrogen donor ligands are described as hard and soft respectively. For typical soft metal ions encountered in metal-microbial studies, the order of increasing stability of complexes for a range of common ligand atoms is:

$$F < O < N < Cl < Br < I < S < C$$

This trend is the same as that of increasing softness, decreasing hardness, and also of decreasing electronegativity. For hard metal ions a strong inversion of this order occurs.

It is apparent that all macro-nutrient metals are class (a) ions, and trace/micro-nutrient and toxic metals are class (b) or borderline ions (see *Appendix C*). The essential *s-block* elements are the monovalent cations $K^+$ and $Na^+$ and the divalent cations $Mg^{2+}$ and $Ca^{2+}$. These cations are of noble gas configuration and their chemistry is essential ionic in nature. They prefer to bind to oxygen donor ligands and interact weakly with most biological ligands. The transition elements have filled or partially filled *d* orbitals and bind biological ligands more strongly than the s-block elements. Common examples of toxic elements are the *d-block* elements $Cd^{2+}$ and $Hg^{2+}$, and the *p-block* elements $Tl^{+,3+}$, Sb(III), $Pb^{2+}$ and As(III). These are readily polarisable and bind strongly to biological ligands, particularly soft ligands such as thiols. They exert toxic effects in several ways including, displacing native metals from their normal binding sites, binding to proteins and nucleic acids thereby altering their conformation, and affecting membrane permeability (Hughes & Poole, 1989).

It is possible to qualitatively predict the interaction of metal ions with ligands based on knowledge of polarizing potentials. The ability of a metal ion to complex a ligand depends on its polarising power, its charge/radius ratio. Polarisation potential

increases directly with covalent index and general trends indicate that covalent index values increase in magnitude from left to right across the Periodic Table, and from top to bottom down the table. A cation of high polarising power is described as a strong Lewis acid, and if hard and soft metal ions are present in solution, soft ions tend to bind preferentially to biological ligands and displace essential-hard metal ions from their sites (Hughes & Poole, 1991). This displacement of one cation by another depends on the strength of the individual ligand complexes (Remacle, 1990). In the first series of transition elements, $Cu^{2+}$ is the strongest Lewis acid and will bind preferentially to microbial biomass ligands (Hughes & Poole, 1989; 1991), with a higher affinity for amines over carboxylates (Beveridge & Murray, 1980). For this series, increasing covalent index, softness and polarisation potential, and subsequent enhanced ability to bind to biological ligands increase in the following order:

$$Mn^{2+} < Ti^{2+} < V^{2+} < Zn^{2+} < Cr^{2+} < Ni^{2+} < Fe^{2+} < Co^{2+} < Cu^{2+}$$

(Hughes & Poole, 1989; 1991). This is similar to the Irving-Williams series (1949), that describes formation constants for complexes of the divalent transition metal ions with inorganic nitrogen donor ligands, and increases in the series:

$$Mn^{2+} < Fe^{2+} < Co^{2+} < Ni^{2+} < Cu^{2+} > Zn^{2+}$$

A relationship between covalent index and toxicity is illustrated in a study of $Zn^{2+}$, $Cd^{2+}$ and $Hg^{2+}$ accumulation by freeze dried fungal cell walls of *Trichoderma harzianum* (Rulcker, Frandberg & Schnurer, 1995). Overall uptake at low residual concentrations, and metal ion inhibition of cell wall enzymatic hydrolysis by the lytic enzyme Novozym 234, increased in the order, $Zn^{2+} < Cd^{2+} < Hg^{2+}$, both reflecting increasing covalent index and toxicity. It was postulated that additional components besides chitin were involved in the adsorption of the ions by the fungal cell walls.

**1.3.4** *pH and metal chemistry*

A further consideration for metal-microbial interactions is pH. This is an important factor regulating access to binding sites in biological molecules since the proton directly competes with metal ions. In biological systems, a metal ion frequently has to displace a proton from the binding site. When an amino acid is the ligand, a borderline metal ion would be considered to bind to the carboxylate moiety in mildly acidic solution. Binding to the amino group would not occur until the pH was raised to depronate this group (Nieboer & Richardson, 1980; Hughes & Poole, 1989). Electrophoretically determined isoelectric points of bacterial species showed no fundamental differences in the range of values for Gram-positive and Gram-negative bacteria, and an increase of the net negative charge was detected at pH 10.7, while a positive charge was apparent at pH 2.0 (Yoshida & Murooka, 1994). These findings are consistent with an ionic surface consisting mainly of acidic carboxyl groups, and some basic amino groups. In a similar study, metal ions were divided into three classes based upon pH dependence of binding to algae biomass (Darnall *et al.*, 1986). Class I ions bind at pH > 5, and includes divalent and trivalent hard and borderline cations. Class II comprises of metallic anions that bind at pH < 2 and includes $SeO_4^{2-}$, $CrO_4^{2-}$ and $PtCl_4^{2-}$. Class III ions exhibit no discernible pH dependence and includes the soft cations, $Ag^+$ and $Hg^{2+}$, and the metallic anion $AuCl_4^-$, and were found to exhibit the highest affinity for algal ligands. At pH values above the isoelectric point of the algal biomass, there is a net negative charge on the cell surface. This ionic state of ligands such as, carboxyl, phosphate, imidazole and amino acid groups promotes interaction with positively charged class I cations. As the pH decreases, $H^+$ ions bind to these class I receptors and the overall surface charge on

the cells becomes positive. This inhibits class I cation interaction, and promotes class II anion binding. Interaction of class II anions with the biomass was considered to consist of primarily electrostatic interactions (Tobin, Cooper & Neufeld, 1984). Metal ions from class III were described as soft, and were considered to form covalent complexes with soft ligands containing nitrogen and sulphur. During competition studies, binding of $Ag^{+}$ and $Al^{3+}$ were relatively unaffected by each other. This suggested two classes of binding sites, one with specificity for hard ions such as $Al^{3+}$, and others with specificity for soft ions as $Ag^{2+}$.

### **1.3.5** *Metal-binding groups*

A range of *hard* and *soft* ligands, as compiled by Nierboer & Richardson (1980) and Hughes & Poole (1989; 1991) are presented in *Appendix D*. Metal-binding groups available in proteins are the amino and carboxylate termini, the deprotonated peptide link and the side chain substituents. Nitrogen donor ligands include the imidazole side chain of the histidine residue, and sulphur donor ligands include the thiol side chain of the cysteine residues. Oxygen donor ligands are largely the carboxylate groups of aspartic acid and glutamic acid residues, and also hydroxyl groups of serine and threonine. Ligand groups associated with nucleotides and nucleic acids include phosphate oxygen donor atoms and nitrogen groups of adenine, guanine, cytosine, uracil and thymine. Also, ADP and ATP exist as intracellular chelate complexes of $Mg^{2+}$. Polysaccharides and their analogues, as important components of cell walls and membranes, have a range of metal-binding compounds. Oxygen donor ligands appear to be the most abundant and include carboxylate groups of *N*-acetylglucosamine: a component of both fungal chitin

and bacterial peptidoglycan, and phosphate groups of teichoic acid: a linear polymer of glycerol phosphate.

### 1.4 *Mathematical adsorption isotherm models*

By considering the cell wall components of microbes as anionic, the cation adsorption potential can be described by surface complex formation equilibrium models (Remacle, 1990). Adsorption involves the interphase accumulation or concentration of substances at a surface or interface. Adsorption on solids, particularly activated carbon, is a widely used operation for purification of waters and wastewaters. The material being concentrated or adsorbed is referred to as the *adsorbate*, and the adsorbing phase is termed the *adsorbent* (Weber, 1972).

#### 1.4.1 *Adsorption isotherms*

Adsorption in liquid-solid systems involves the immobilisation of an adsorbate onto the surface of an adsorbent. Adsorption continues until such time as the concentration of adsorbate remaining in solution is in dynamic equilibrium with the adsorbate attached to the adsorbents surface. Equilibrium positions are usually represented graphically by adsorption isotherms. Isotherms express the quantity $q_e$, the amount of adsorbate attached to the adsorbent (per unit weight), as a function of $C_f$, the adsorbate concentration in the liquid phase in contact with the adsorbent at the liquid-solid interface. Values for $q_e$ and $C_f$ are given on the ordinate and abscissa respectively. Commonly, the amount of adsorbed material per unit weight of adsorbent increases with increasing concentration but not in direct proportion, and curves concave to the abscissa represents *favourable*

adsorption (Weber, 1972; Belter *et al.*, 1988). Isothermal plots are independent of adsorbate solution volume in contact with a known quantity of adsorbent.

In metal-microbial interactions, the maximum adsorption capacity of the biosorbent, $q_{max}$, is considered a measure of the ability of the material to accumulate metal ions from concentrated solutions, and the slope of the curve as it leaves the origin quantifies the ability of the biosorbent to accumulate metal ions from dilute solutions (Brady & Duncan, 1994).

### **1.4.2** *Langmuir adsorption isotherm*

The Langmuir adsorption model is valid for single-layer adsorption (de Rome & Gadd, 1987*b*; Crist *et al.*, 1988; Guibal, Roulph & Le Cloirec, 1992; Volesky *et al.*, 1993; Brady & Tobin, 1994), based on the assumptions: Maximum adsorption corresponds to a saturated monolayer of adsorbate molecules on the adsorbent surface, the energy of adsorption is constant, and there is no transmigration of adsorbate in the plane of the surface (Langmuir, 1918; Weber, 1972). The model is usually presented as

$$q_e = \frac{q_0 b C_f}{1 + b C_f}$$

The term $b$ is a constant related to the energy or net enthalpy of adsorption and can serve as an indicator of the isotherm rise in the region of the lower residual concentrations which reflects the affinity of the sorbent material for the solute (Volesky, May & Holan, 1993). The term $q_0$ is the number of moles of adsorbate adsorbed per unit weight of adsorbent in forming a complete monolayer on the surface. The common linear form of the model is a plot of $q_e^{-1}$ versus $C_f^{-1}$, where the intercept on the ordinate gives $q_0^{-1}$, and the slope is $1/bq_0$.

### 1.4.3 *BET adsorption isotherm*

The Brunauer, Emmett, Teller (BET) model represents isotherms reflecting apparent multilayer adsorption (de Rome & Gadd, 1987*b*; Guibal, Roulph & Le Cloirec, 1992), and reduces to the Langmuir model when the limit of adsorption is a monolayer. The BET model is formulated on a number of assumptions: a number of layers of adsorbate molecules form at the surface and that the Langmuir model assumptions apply to each, a given layer need not complete formation prior to initiation of subsequent layers, and layers beyond the first have equal energies of adsorption (Weber, 1972). The BET equation is given by

$$q_e = \frac{BC_f q_0}{(C_s - C_f)[1 + (B - 1)(C/C_s)]}$$

The terms $C_s$ is the the saturation concentration of the adsorbate and $B$ is a constant, expressive of the energy of interaction with the surface. All other symbols are as previously described. The common linearised form of this equation is

$$\frac{C_f}{(C_s - C_f)q_e} = \frac{1}{Bq_0} + \frac{(B - 1)}{(Bq_0)}\frac{C_f}{C_s}$$

For data conforming to the BET model, a plot of $C/(C_s - C)q_e$ versus $C/C_s$ gives a straight line of slope $(B - 1)/Bq_0$ and intercept $1/Bq_0$.

### 1.4.4 *Freundlich adsorption model*

The Freundlich equation represents the case of heterogeneous energies of adsorption on adsorbent surfaces (de Rome & Gadd, 1987*b*; Guibal, Roulph & Le Cloirec, 1992). In the Langmuir equation, the term $b$ varies as a function of surface coverage, $q_e$, due to variations in heat of adsorption (Weber, 1972). The Freundlich equation is basically empirical and has the general form

$$q_e = k_f C_f^{1/n}$$

The constants $n$ and $K_f$ are determined experimentally by means of a log-log plot of $q_e$ versus $C_f$.

$$\log q_e = \log K_f + \frac{1}{n} \text{ Log } C_f$$

The slope of such a plot is $1/n$ with an intercept of $K_f$. For favourable adsorption, $n > 1$. In general, as the affinity of an adsorbent increases for a particular adsorbate, the $k$ value increases (Namasivayam & Yamuna, 1992).

The Freundlich equation predicts that the adsorbate on the adsorbent will increase as long as there is an increase in the adsorbate concentration in the liquid. The Freundlich equation generally agrees well with the Langmuir equation over moderate ranges of adsorbate concentration, but unlike the Langmuir equation, it does not reduce to a linear adsorption expression at very low concentrations. Furthermore, experimental evidence indicates that an isotherm plateau is reached at a limiting value of the solid phase concentration (Allen & Brown, 1995), and since $n$ reaches a limit when the adsorbent surface is completely covered, this region is not predicted by the Freundlich equation.

### **1.4.5** *Scatchard transformation plots*

Scatchard transformation plots (Scatchard, 1949) are routinely applied to the study of the attractions of ions and small molecules to protein ligands (Chamness & McGuire, 1975), and has been applied to metal-microbial adsorption data (Tobin *et al.*, 1990; Saucedo *et al.*, 1992; Avery & Tobin, 1993; Brady & Tobin, 1994; Brady & Duncan, 1994*b*). Scatchard plots of adsorption data are presented as $q_e/C_f$ on the ordinate, versus

$q_e$ on the abscissa. Linear plots result when single distinct types of binding site are present, and nonlinear plots are interpreted as reflecting multiple, nonequivalent binding sites. The Scatchard plot allows for the determination of the affinity constant between the cation and the ligand from the slope of the graph, and the number of binding sites from the abscissa intercept (Brady & Duncan, 1994*b*).

### 1.5 *Efflux studies and cation displacement*

A number of studies report the efflux/displacement of cellular $K^+$, $H^+$, $Ca^{2+}$ and $Mg^{2+}$ ions following metal biosorption. Efflux of the ions, particularly $K^+$, can be interpreted as a microbial detoxification mechanism in response to harmful external cations, whereas the displacement of $H^+$ and $Ca^{2+}$+$Mg^{2+}$ is considered to represent covalent and ionic binding respectively. Both hypotheses are discussed below.

#### 1.5.1 *$K^+$ efflux*

Efflux of $K^+$ ions has been observed in many cases from viable *Saccharomyces cerevisiae* cells that were exposed to metal ions. For each of the divalent ions $Co^{2+}$ and $Cu^{2+}$ accumulated, two $K^+$ ions were released, representing stoichiometric exchange (Norris & Kelly, 1977; Kessels, Belde & Borst-Pauwels, 1985; Gadd & Mowll, 1985; de Rome & Gadd, 1987*a*). In contrast, studies with $Cd^{2+}$ displayed no single relationship between the rate of $K^+$ efflux and cellular $Cd^{2+}$ levels (Norris & Kelly, 1977; Gadd & Mowll, 1983; Belde *et al.*, 1988), and it was concluded that $K^+$ release detected after $Cd^{2+}$ binding resulted from membrane damage (Gadd & Mowll, 1983).

The presence of $K^+$ and $Na^+$ ions lowered $Cs^+$ toxicity towards *Escherichia coli* and *Bacillus subtilis*, and also decreased overall $Cs^+$ accumulation levels (Perkins & Gadd, 1995). Similar trends were observed for $Cs^+$ accumulation by the cyanobacterium *Synechocystis* PCC 6803 (Avery, Codd & Gadd, 1991). For $Cs^+$ accumulation studies with *Chlorella emersonii*, it was concluded that, the resulting loss of $K^+$ was responsible for growth inhibition, rather than the presence of intracellular $Cs^+$ (Avery, Codd & Gadd, 1992). Uptake of $Cs^+$ into microalga *Chlorella salina* vacuoles, was correlated with a stoichiometric exchange for $K^+$, however, no loss of $K^+$ from the cell surfaces or cytoplasm was evident (Avery, Codd & Gadd, 1993), and accumulation of $Li^+$ in *Saccharomyces cerevisiae* X2180-1B occurred via an apparent stoichiometric relationship of 1:1 with $K^+$ (Perkins & Gadd, 1993b).

### 1.5.2 *$H^+$ efflux*

A membrane-induced proton motive force was found to influence the metal ion binding capacity of *Bacillus subtilis* cell walls (Urrutia Mera *et al.*, 1992). During the metabolism of living cells, a membrane-induced proton force that continuously pumped protons into the cell wall fabric was detected and such an effect was absent in non-metabolising cells. This resulted in competition between $H^+$ ions and free metal ions for binding sites on viable cells. Consequently non-living cells were found to adsorb more metal ions than actively metabolising cells. After glucose addition to a *Saccharomyces cerevisiae* suspension, progressive glucose-dependent proton efflux was observed, and was viewed as an indicator of cell metabolic activity (Karamushka & Gadd, 1994). Inhibition of $H^+$ efflux was detected at relatively low $Cu^{2+}$ additions, but such toxic

effects were controlled by the introduction of exogenous $Ca^{2+}$ and $Mg^{2+}$ ions. It was concluded that the protective effects of $Ca^{2+}$ and $Mg^{2+}$ were mediated by competitive and stabilising interactions at the cell surface.

### 1.5.3 *$H^+$, $Ca^{2+}$ and $Mg^{2+}$ displacement*

The adsorption of $Sr^{2+}$ ions by *Vaucheria* released equivalent amounts of $Ca^{2+}$ and $Mg^{2+}$ ions, and it was concluded that adsorption of alkaline earth metal ions is an ion-exchange phenomenon based on electrostatic interactions (Crist *et al.*, 1990). The adsorption of $Cu^{2+}$ ions caused a release of $Ca^{2+}$ and $Mg^{2+}$ ions, but also of $H^+$, demonstrating additional covalent bonding. Half the amount of the monovalent $H^+$ ions released plus the sum of the divalent $Ca^{2+}$ and $Mg^{2+}$ ions released equalled the total amount of $Cu^{2+}$ ions adsorbed, indicating stoichiometric exchange. Similarly, the adsorption of $Sr^{2+}$ to live *Saccharomyces cerevisiae* cells resulted in a release of $Mg^{2+}$ and $Ca^{2+}$, but also of $H^+$ (Avery & Tobin, 1992). It was considered that the pH drops recorded after $Sr^{2+}$ addition to the biomass resulted from the covalent bonding of $Sr^{2+}$ ions to surface anionic groups which including carboxylate and phosphate. The displacement of $Ca^{2+}$ and $Mg^{2+}$ ions resulted from electrostatic ion-exchange interactions and represented ionic binding. This suggested a combination of both ionic and covalent bonding, but direct stoichiometric exchanges were not apparent.

### 1.6 *Physico-chemical correlations*

Using vacuum dried *Rhizopus arrhizus* biomass, Tobin, Cooper & Neufield (1984) demonstrated metal adsorption to be directly related to ionic radii for a range of divalent and trivalent metal ions. It was concluded that all the cation adsorption sites had an affinity for all the cations tested, although, certain fractions of the adsorption sites preferentially bound particular cations (Tobin, Cooper & Neufield, 1988). Similarly, the cations $Co^{2+}$ and $Cd^{2+}$ were found to be accumulated by viable *Saccharomyces cerevisiae* via an apparently general ion uptake system with limited specificity related to ionic radii (Norris & Kelly, 1977). Competition studies demonstrated that a range of divalent ions inhibited $Co^{2+}$ uptake by viable *Saccharomyces cerevisiae*, and inhibition potential increased in the order, $Ca^{2+} < Cd^{2+} < Mn^{2+} < Mg^{2+} < Ni^{2+} < Zn^{2+}$. This series displays decreasing ionic radii as determined by Pauling (1960), demonstrating that the inhibition of $Co^{2+}$ uptake is greatest by cations of similar size. The displacement of the surface-bound cationic dyes, Janus Green, Victoria Blue B and Methyl Violet, from the gram-negative bacterium *Pseudomonas cepacia* was achieved using a range of divalent metal ions (Savvaidis *et al.*, 1990). In general, the displacement efficiencies increased in the order, $Co^{2+} < Ni^{2+} < Cu^{2+} < Cd^{2+} < Pb^{2+}$. This series was also found to be applicable to gram-positive bacteria and to yeast, and for the transition metal ions was in accordance with the Irving-Williams series.

### 1.7 *Selenium and living systems*

Selenium (Se) is in Group 16 (VIB) of the Periodic Table, and is classified as a metalloid as it exhibits chemical and physical properties that are intermediate between those of metals and non-metals (Frankenberger & Karlson, 1994; Haygrath, 1994). It has a valency of *2-* in combination with hydrogen or metals, and in oxygen compounds exists as the *4+* and *6+* oxidation states. Among the elements, selenium is ranked seventieth in order of abundance, and in the earths crust is found at concentrations of *ca.* 0.09 mg $kg^{-1}$ (see Thompson-Eagle & Frankenberger, 1991; Frankenberger & Karlson, 1994). Most seleniferous soils in the world are found in arid and semiarid regions, and the rate and extent to which selenium is mobilised depends on its chemical speciation and sediment partitioning. The most common ions found in natural waters and soils are selenate ($SeO_4^{2-}$) and selenite ($SeO_3^{2-}$), and both are considered to be potentially toxic (Frankenberger & Karlson, 1994). It is recognised as an element that is required in trace amounts by microorganisms (Atkinson *et al.*, 1990), plants and animals (Axley & Stadtman, 1989; Stadtman, 1990; Mayland, 1994; Terry & Zayed, 1994), but can be toxic at high concentrations (Olivas & Donard, 1994) and has relatively narrow boundaries between toxicity and deficiency (Haygrath, 1994). *Safe* selenium levels in water are reported not to exceed the upper limit of 10 μg $l^{-1}$ (see Mayland, 1994). Various human intake levels have been reported as:

| | |
|---|---|
| low intake levels: | 11 μg $day^{-1}$ |
| adequate intake levels: | 110 μg $day^{-1}$ |
| high intake levels: | 750 μg $day^{-1}$ |
| chronic selenosis intake levels: | 5 mg $day^{-1}$ |

(see Stadtman, 1990; Haygrath, 1994). In animal nutrition, selenium has been identified as the metal cofactor for the enzyme glutathione peroxidase (Mayland, 1994). In microorganisms, selenium-dependent enzymes include glycine reductase of *Clostridia*, and some hydrogenases and formate dehydrogenases (see Axley, 1989; Stadtman, 1990). All organisms are considered to contain Se-cysteyl-tRNAs that decode UGA, and also, selenocysteine is proposed to function as the 21$^{st}$ proteinaceuous amino acid (see Lauchli, 1993). It seems likely that the majority of selenium toxicity is related to its interference in sulphur metabolism, especially during the formation of catalytically active proteins. Selenium has many chemical properties similar to those of sulphur but slight differences can lead to altered tertiary structure and dysfunction of proteins and enzymes, if for example, selenocysteine is incorporated into proteins in place of cysteine (Lauchli, 1993). Selenium toxicity may also disrupt the methylation function of methionine. Methionine serves as a methyl donor through its reaction with ATP to form S-adenosylmethionine (SAM). SAM transfers its methyl group to a variety of metabolites, and replacement of selenium for sulphur may affect the production of SAM and therefore the efficiency of methylation (see Terry & Zayed, 1994).

### **1.7.1** *Industrial uses and sources of selenium*

The greatest source of selenium contamination in the environment comes from mine production, primarily as a by-product of copper refining. The main industrial application of selenium is in the glass industry, where it is used to give glass a red appearance, and prevent iron oxide discolouration. It is used in paint and plastic pigments, and as an antioxidant in some inks and lubricant oils. It also has electrical and semiconductor properties, and is utilised in the electronics industry.

### 1.8 *Microbial transformations of selenium compounds*

Microorganisms play an important role in the cycling of many different elements including carbon, nitrogen and sulphur, and they are also considered to be an essential component in the recycling of selenium. Various microorganisms are capable of mediating a number of transformations of inorganic selenium compounds including reduction, volatilization (Lortie *et al.*, 1992; Gadd 1993*a*, *b*; Morley *et al.*, 1995) and oxidation (Frankenberger & Karlson, 1994).

Microbial transformation of selenium oxyanions by reduction to insoluble amorphous elemental selenium ($Se^0$) by a range of microbes is well documented in the literature (Falcone & Nickerson, 1963; McReady, Campbell & Payne, 1966; Zieve *et al.*, 1985; Ramadan *et al.*, 1988; Maiers *et al.*, 1988; Bender *et al.*, 1991; Moore & Kaplan, 1992; Steinberg & Oremland, 1990; Tomei *et al.*, 1992; Macy, Lawson & DeMoll-Decker, 1993; Frankenberger & Karlson, 1994; Gharieb, Wilkinson & Gadd, 1995) and represents an important aspect of the selenium cycle by which the element is sequestered into soils and sediments (Oremland *et al.*, 1991, 1994; Gadd 1993*a*, *b*). Microscopic analysis of selenite-reducing microorganisms has revealed the intracellular biosorption of amorphous selenium within the cytoplasm (McReady *et al.*, 1966; Tomei *et al.*, 1992) as well as on the exterior of fungal hyphae and spores (Ramadan *et al.*, 1988, Gharieb *et al.*, 1995). Such containment of selenium could be exploited to enhance removal of selenite from contaminated waters/soils by harvesting selenium-laden biomass and appropriate disposal. However, *in situ* stimulation of selenite reduction may not be a suitable long term solution to selenite-contaminated waters since amorphous elemental selenium remaining in the aqueous phase may enter the food chain through bottom-feeding organisms (Lovley, 1993).

Microbial transformation of inorganic selenium compounds into volatile organic and inorganic selenium derivatives is an important link in the biogeochemical cycle of this element (Tan *et al.*, 1994), and has been reported to constitute an effective decontamination process for polluted soils, sediments and waters (Karlson & Frankenberger, 1990; Thompson-Eagle & Frankenberger, 1990*a*, *b*; Thompson-Eagle, Frankenberger & Longley, 1991). Volatilisation through methylation, is thought to be a protective mechanism used by microorganisms to detoxify their surrounding environment (Thompson-Eagle & Frankenberger, 1991). Under aerobic conditions selenium is permanently removed from seleniferous environments by this transformation and is released into the atmosphere (Atkinson *et al.*, 1990; Frankenberger & Karlson, 1994). Dimethylselenide ($[CH_3]_2Se$) is considered to be the main metabolite produced as a result of selenium volatilization by microbes (Zieve *et al.*, 1985; Frankenberger & Karlson, 1994). The methylation of inorganic selenium to dimethylselenide is postulated to consist of the reduction of $Se^0$ to the $Se^{2-}$ species and subsequent methylation to form dimethylselenide (Thompson-Eagle & Frankenberger, 1991). This alkylated derivative is excreted readily from microbial cells due to high volatility (see Karlson, Spencer & Frankenberger, 1994) and high lipid solubility in the cell membranes (see Gadd, 1993*a*) and is approximately 500-700 times less toxic to rats than aqueous selenite and selenate ions (Frankenberger & Karlson, 1994). Obligate aerobic fungi are thought to be the predominant selenium-methylating organisms among the soil microflora (Frankenberger & Karlson, 1989), whereas the principal methylating microorganisms present in pond water were determined to be aerobic bacteria (Thompson-Eagle & Frankenberger, 1991). Dimethylselenide is also the principal respiratory product of animals ingesting excess selenium (Mayland, 1994), and can be detected by a garlic like odour from the breath.

In contrast to reduction and volatilization the microbial oxidation of selenium and its compounds is not very well documented although some reduced forms of selenium have been reported to be oxidized by laboratory bacterial cultures and fungi (see Frankenberger & Karlson, 1994).

### 1.9 *Selenium reduction and accumulation/biosorption*

The reduction of selenium oxyanions to the amorphous elemental form precedes selenium accumulation/biosorption by microorganisms. Selenite reduction to elemental selenium is considered a two-step process, $Se^{4+}$ reduction to $Se^{2+}$, and then reduction to $Se^{0}$ (McCready *et al.*, 1966). The accumulation of elemental selenium is identified by a characteristic red colour of the biosorbents and a range of mechanisms are discussed below.

#### 1.9.1 *Mechanisms of selenium oxyanion reduction*

Dialysis studies using yeasts revealed, that cofactors necessary for enzymatic reduction of selenite by cell-free preparations include, a quinone, a thiol substance, a pyridine nucleotide, and an electron donor (Nickerson & Falcone, 1963). Selenite appears to be bound to proteins by thiol groups, and is released as metallic selenium after accepting four electrons (Falcone & Nickerson, 1963). The reduction of selenite was shown to be directly dependent on the metabolic activity of *Salmonella heidelberg*, and not on spontaneous chemical reductions occurring as a result of media constituents, or pH change during microbial growth (McCready *et al.*, 1966). Selenite reduction was found to be primarily associated with the lag phase of growth, presumably as a detoxification procedure preceding growth. The intermediate in the conversion of selenite to elemental

selenium was identified as the divalent selenium ion, which was more toxic than the tetravalent precursor. Optimal selenium oxyanion reduction by *Pseudomonas stutzeri* was shown to occur under aerobic conditions between pH 7.0 and 9.0 (Lortie *et al.*, 1992). No selenite or selenate reduction occurred below pH 5.5 and 6.5 respectively, and the upper limit for both was pH 9.5.

**1.9.2** *Dissimilatory reduction of selenate, selenite, sulphate and nitrate ions*

Selenate reduction to elemental selenium by anaerobic bacteria in sediments and cultures, was found to be inhibited by $O_2$, $NO_3^-$ and $MnO_2$, but not by $SO_4^{2-}$ or FeOOH (Oremland *et al.*, 1989). Similarly, an anaerobic freshwater enrichment grew with both nitrate and selenate as the electron acceptor, but when both anions were present, nitrate reduction preceded selenate reduction. For one isolate, the presence of nitrate precluded the reduction of selenate. The bacterium *Thauera selenatis* was found to respire selenate anaerobically, using acetate as the preferred electron donor (Macy *et al.*, 1993). Here the reduction of selenate to elemental selenium was not inhibited by nitrate, and both oxyanions were found to be reduced concomitantly. The biochemical reductions of selenate to selenite and nitrate to ammonium, by an obligately anaerobic selenate-respiring bacterium, were also shown to be dissimilatory and capable of sustaining anaerobic respiration (Oremland, 1994). Overall nitrate has been identified as the preferred electron acceptor for growth of freshwater selenate-respiring bacteria, and both oxyanions were shown to be capable of supporting respiration (Steinberg *et al.*, 1992).

**1.9.3** In situ *and sediment depth profiles of selenium oxyanion reduction*

Measurements of *in situ* rates of selenate removal by dissimilatory bacterial reduction in sediments, revealed that 85% of selenate reduction, and all denitrification activities were confined to the upper 4 to 8 cm of the sediment profile, whereas, 89% sulphate reduction was greatest below 8 cm (Oremland *et al.*, 1990). Depth profiles indicated that the reduction of $^{75}SeO_4^{2-}$ decreased with increasing sediment depth (Oremland *et al.*, 1991). These findings suggest, that sulphate-reducing microorganisms are not responsible for selenate reduction in sediments (Lovley, 1993). Furthermore molybate, a known inhibitor of sulphate reduction, was found not to inhibit selenate reduction (Oremland, 1989). Under laboratory conditions, mixed microbial mats, composed of stratified layers of bacteria and cyanobacteria, were successful at transforming selenate *in situ*, and were suggested as low-cost bioremediation system for water decontamination (Bender *et al.*, 1991).

**1.9.4** *Intracellular accumulation/biosorption of selenium*

Microscopic examination of a *Fusarium* species grown in the presence of sodium selenite revealed the deposition of red elemental selenium within the fungal cells, as well as on the surface of hyphae and spores (Ramadan *et al.*, 1988). The presence of selenium increased cellular carbohydrate, protein and lipid levels, and induced the biosynthesis of several low molecular weight proteins. This was interpreted as a tolerance mechanism to high levels of selenium as either an equilibrium process, or a compensationary mechanism for the replacement of metabolites damaged by selenium. Labelling studies revealed the incorporation of selenite into the amino acids, selenocysteine and selenocysteic acid.

In similar studies, cultures of *Wolinella succinogens* reduced both selenite and selenate to red amorphous elemental selenium, but only after the cultures reached the stationary phase of growth (Tomei *et al.*, 1992). Transmission electron microscopy and X-ray spectroscopy verified the intracellular deposition of electron-dense selenium granules in the vacuoles, and scanning electron microscopy revealed the presence of needle-like crystal structures of elemental selenium on the surfaces of hyphae and conidia.

### 1.10 *Selenium volatilisation*

As discussed above, the formation of volatile selenium compounds generally involves the reduction of non-volatile selenium compounds, both organic and inorganic, to the $Se^{2-}$ species, and the subsequent addition of free methyl groups to produce volatile organic selenium products. Techniques to measure and enhance this process in microorganisms are reported below.

#### 1.10.1 *Experimental protocols designed to measure volatile selenium compounds and transforming microorganisms*

Resting cell suspensions of a strain of *Corynebacterium*, isolated from soil formed dimethylselenide from selenite, selenate, elemental selenium and methaneseleninate (Doran & Alexander, 1977). Headspace gas over resting cell suspensions was periodically injected into a gas chromatography unit for the positive identification and quantification of dimethylselenide. The methylated product was formed endogenously and the greatest rate of dimethylselenide formation occurred when methaneseleninate

was the substrate. Dimethylselenide formation from selenite by cell-free extracts was achieved by the addition of *S*-adenosylmethionine which was identified as a cofactor in the transfer of methyl groups. A study on selenium volatilization using *Mortierella stylospora*, $^{75}$selenite and $^{75}$selenate (Zieve *et al.* 1985), air was periodically flushed through 250 ml conical flasks containing the growing cultures in the presence of the inorganic selenium species, and effluent gases were passed directly into 10 ml concentrated nitric acid traps for retention of volatile selenium compounds. More volatile selenium was found to be evolved from cultures supplied with selenite than with selenate, and on solid media augmented with selenite, colonies appeared pink/red indicating the deposition of elemental selenium.

A protocol for the rapid measurement of $^{75}$Se-labelled dimethylselenide evolved from soil as a result of microbial activity was developed by Karlson & Frankenberger (1988*a*). Portions of soil augmented with $^{75}$Se labelled $Na_2SeO_3$ were placed into Erlenmeyer flasks, and the headspace air saturated with water was exchanged at constant flowrates. The effluent gases were passed separately through a single trap containing 1.08 g of activated carbon, and a series of used cartridges changed at regular intervals were rinsed with a range of polar and non-polar solvents to extract bound volatile selenium compounds. Quantification of selenium compounds volatilised was achieved using a gamma counter counting for $^{75}$Se, and the main volatile product was determined to be primarily dimethylselenide by GC-mass spectrometry. It was found that solvents with low to moderate polarity were the strongest extractants, non-polar solvents were weak extractants, water was intermediate and the extraction efficiency of alcohols decreased with increasing chain length. Methanol was the preferred solvent, extracting *ca.* 95.2% of the $^{75}$Se labelled volatiles.

### 1.10.2 *Selenium biomethylation enhancement*

It is considered that since pectin and its monomer galacturonic acid have partially methylated structures, they may provide a source for direct transfer of free methyl groups from the carbohydrate to the microbial methylation pathway (Karlson & Frankenberger, 1988*b*). Fungal growth from the selenite augmented soils was promoted by the addition of complex carbon sources such as pectin and plant residues, and the predominant fungi isolated were identified as *Fusarium* and *Penicillium* species (Karlson & Frankenberger, 1988*b*). Addition of the trace elements nickel, zinc and cobalt was also found to stimulate biomethylation in the order: Ni < Zn < Co (Karlson & Frankenberger, 1988*b*). Cobalt in the form of methylcobalamin (methyl-$B_{12}$), nickel containing enzymes such as methyl-coenzyme-M reductase and zinc transferases and oxido-reductases are known to promote alkylation reactions in microbes, and most likely serve as cofactors in methylation reactions. The addition of the fungi *Acremonium falciforme*, *Penicillium citrinum* and *Ulocladium tuberculatum* to native and autoclaved soils supplemented with both $Na_2SeO_3$ and $Na_2SeO_4$ was found to enhance and restore volatilisation rates (Karlson & Frankenberger, 1989). Pectin addition was again found to accelerate alkylselenide evolution, and a minimum selenium threshold for alkylselenide production was not found.

Laboratory analysis of selenium contaminated agricultural drainage water revealed that selenium biomethylation is protein-peptide limited rather than nitrogen-, amino acid-, or carbon limited (Thompson-Eagle & Frankenberger, 1990*b*). It was concluded that the methylating active ingredient is an organic nitrogenous compound, with a level of organisation greater than that of a collection of purified amino acids.

Dialysis studies indicated that the active ingredient is likely to be a mixture of simple peptides with molecular weight less than 6000 to 8000 daltons. In selenium contaminated evaporation pond water, biomethylation was optimal when the systems were well-mixed under aerobic conditions and amended with a casein protein source (Thompson-Eagle & Frankenberger, 1990). Biomethylation rates were also found to be directly related to microbial numbers. In a study on selenium methylation by plants, the rate of volatilisation was found to depend on the chemical form of selenium available (Terry & Zayed, 1994). It was apparent that as selenate was reduced to selenite or selenomethionine, it became more readily available for volatilisation by plant metabolic processes.

**1.10.3** *Temperature, pH and salinity effects on selenium volatilisation*

The optimum pH and temperature values for selenium methylation by the fungus *Alternaria alternata* were determined to be 6.5 and 30°C respectively (Thompson-Eagle *et al.*, 1989). In selenium augmented pond water, increasing the temperature to 35°C and the addition of 1% glucose with a fungal innoculum *Alternaria alternata* together doubled dimethylselenide production (Thompson-Eagle & Frankenberger, 1990*a*). In a saline seleniferous soil, optimum dimthylselenide production was observed at pH 8.0 and a temperature of 35°C, and for every 10°C rise in temperature from 5 to 35°C, the rate of selenium biomethylation increased 2.6-fold (Frankenberger & Karlson, 1989).

In seleniferous soil sediments, temperature studies revealed that selenium leached and volatilised increased with increasing temperatures (Calderone *et al.*, 1990). Increasing temperature was considered to promote selenium mineralisation and increase

the soluble selenium fraction available for biomethylation. Similarly in selenium contaminated evaporation pond water, biomethylation increased with increasing pH as a result of the greater solubility of selenium oxyanion compounds at higher pH values, and hence their bioavailability for methylation (Thompson-Eagle & Frankenberger, 1990).

In general increased salinisation was found to reduce selenium volatilisation from soils (Karlson & Frankenberger, 1990), and the microbial volatilisation of selenium from soils was found to decrease with decreasing particle size, resulting from reductions in oxygen transfer and good ventilation conditions (Tan *et al.*, 1994).

### 1.11 *Fate of dimethylselenide in the atmosphere*

The majority of organic compounds present in the troposphere undergo photolysis and chemical reactions with hydroxyl and nitrate radicals, and ozone. Under laboratory conditions, gaseous dimethylselenide was found to be transformed chemically into more oxidised and less volatile species, but did not undergo photolysis (Atkinson *et al.*, 1990). In the atmosphere, these resultant selenium-containing products which can be either particle-associated or distributed between the gas and particle phases, are relatively unstable and may be sorbed onto submicrometer particulates such as aerosols that have relatively long residence times. By these methods dimethylselenide is dispersed and diluted by air currents directly away from contaminated areas with possible deposition occurring in selenium-deficient areas.

# CHAPTER 2

# MATERIALS AND METHODS

*Interactions of metal and metalloid ions with fungal biomass*

*PhD Research Thesis by*

*Joseph M. Brady* B.Sc.

## CHAPTER 2: MATERIALS AND METHODS

### 2.0 *Organism, culture conditions and metal analysis*

#### 2.0.1 *Rhizopus arrhizus biomass*

In 1 l Erlenmeyer flasks, *Rhizopus arrhizus,* strain CMI83711, was cultured in 500 ml of liquid medium comprising (g $l^{-1}$): bacteriological peptone (cat. no. L37, OXOID, Hampshire, England), 10; sucrose, 20; $KH_2PO_4$, 1; $NaNO_3$, 1; and $MgSO_4.7H_2O$, 0.5. Cultures were grown at 25°C on an orbital shaker at 150 rev $min^{-1}$ for 5 days. The microorganism was maintained on solid medium obtained by adding 1.5% agar (cat. no. L11, OXOID, Hampshire, England) to the above medium.

The biomass was separated from the broth by filtration and washed with distilled, deionised water. For metal ion adsorption experiments, quantities of the harvested biomass were freeze dried (Edwards Freeze Dryer, Chamber 3/Super Modulyo, Sussex, England) and oven dried (55°C for 8 h). Live non-metabolising biomass was prepared by suspending the harvested biomass in 500 ml of distilled, deionised water for 24 h in 1 l Erlenmeyer flasks, at 25°C on an orbital shaker at 150 rev $min^{-1}$. The resultant mycelium pellets were press-dried between sheets of filter paper (cat. no. 1001 090, Whatmann, Kent, England), and appropriate dry weight values were calculated.

All the biomass forms (freeze-dried, oven-dried and live non-metabolising) were considered to be non-metabolically active, and each type was homogenised using a SORVALL OMNI-MIXER (cat. no. 17106, DU POINT Instruments, Connecticut, USA), and sieved (Laboratory Test Sieves, ENDECOTTS LTD, London, England) to particle sizes not greater than 0.5 mm in diameter.

**2.0.2** *Metal analysis*

$Sr^{2+}$, $Mn^{2+}$, $Zn^{2+}$, $Cd^{2+}$, $Cu^{2+}$, $Pb^{2+}$, $Ca^{2+}$, $Mg^{2+}$ and $K^{+}$, were analysed using a Perkin-Elmer 3100 atomic absorption spectrophotometer. Standard metal stock solutions (1000 ppm) were prepared by dissolving known quantities of $Mn^{2+}$, $Zn^{2+}$, $Cd^{2+}$, $Cu^{2+}$, $Ca^{2+}$, $Mg^{2+}$ and $K^{+}$ sulphates salts, and $Sr^{2+}$ and $Pb^{2+}$ nitrate salts, in distilled, deionised water.

**2.0.3** *pH analysis*

pH values were measured using a Corning 220 pH meter fitted with a W.T.W. E56 precision glass electrode.

**2.1** ***Section one: Biosorption characterisation***

*For each of the ions $Sr^{2+}$, $Cd^{2+}$ and $Cu^{2+}$, over the concentration range 0-166.67 ppm, adsorption isotherms were determined using freeze-dried, live non-metabolising and oven-dried biomass types. Initial solution pH values were 4 and 6 for $Sr^{2+}$ and $Cd^{2+}$ systems, and 4 and 5 for $Cu^{2+}$ systems. Final solution $Ca^{2+}$, $Mg^{2+}$ and $H^{+}$ levels were also measured.*

**2.1.1** *Isotherm protocol*

For each isotherm study a series of acid-washed 250ml Erlenmeyer flasks were prepared with 100 ml of distilled, deionised water. Aliquots of a $Sr^{2+}$, $Cd^{2+}$ or $Cu^{2+}$ 1000 ppm stock solution (1, 2, 5, 10 and 20 ml), prepared from sulphate salts dissolved in distilled, deionised water, were introduced into individual flasks and resulted in series of metal solutions in the 0-166.67 ppm concentration range. The pH values were adjusted to 4 and 6 for $Sr^{2+}$ and $Cd^{2+}$ systems, and to 4 and 5 for $Cu^{2+}$ systems using dilute solutions of $HNO_3$ and NaOH, and 0.1 g portions (dry weight) of freeze-dried, live non-metabolising or oven-dried biomass were added to each flask. The metal-biomass systems were incubated at 25°C on an orbital shaker at 150 rev $min^{-1}$ for a period of 24 h (equilibrium conditions were observed after 3 h, see *sections 3.2.2* and *4.2.2*). Final pH values were then determined, samples were removed from the flasks and centrifuged (17,000 *g*, 15 s), and the biomass free supernatants were analysed for final metal concentrations as described above in section *2.0.2*.

## 2.2 *Section two: Application of the hard and soft principle*

*Two differing protocols were used to investigate the uptake of metal ions by freeze dried* Rhizopus arrhizus *biomass, and the subsequent displacement and competition effects when a second metal was introduced into the system. For the ions* $Sr^{2+}$, $Mn^{2+}$, $Zn^{2+}$, $Cd^{2+}$, $Cu^{2+}$ *and* $Pb^{2+}$, *equilibrium studies determined overall adsorption, displacement and inhibition levels for two metal combinations, and in addition final solution* $Ca^{2+}$, $Mg^{2+}$ *and* $H^{+}$ *levels were measured. Time-course studies using the ions* $Sr^{2+}$, $Cd^{2+}$ *and* $Cu^{2+}$, *examined adsorption, displacement and inhibition trends over a 6 h time period for two metal combinations.*

### 2.2.1 *Equilibrium studies*

A series of acid washed 250 ml Erlenmeyer flasks was prepared, each containing 100 ml of the relevant 300 µmol $l^{-1}$ metal stock solution ($t_0$ metals). Stocks were prepared by dissolving appropriate metal salts in distilled deionized water, with pH adjusted to 4.0 using dilute $HNO_3$. At $t_0$, 1 g $l^{-1}$ of biomass was added to each flask, and the systems agitated at 25°C on an orbital shaker at 150 rev $min^{-1}$. At $t_{180}$, 1 ml of a second metal stock solution was added to relevant flasks, resulting in $t_{180}$ metal concentrations again of 300 µmol $l^{-1}$, and the systems were agitated as before. After a further period of 3 h, the biomass was separated from the metal solutions by centrifugation (17,000 *g*, 15 s), and the supernatants were tested for final metal concentrations and pH values.

**2.2.2** *Time-course studies*

To a 2 l pyrex vessel, 1 l of distilled, deionised water was delivered, and the pH adjusted to 4.0 using dilute $HNO_3$. A 1 g $l^{-1}$ quantity of freeze dried biomass was added to the reaction vessel, and the system was stirred continuously using a magnetic stirrer for 3 h at 25°C to promote equilibrium conditions. A 5 ml sample was removed, centrifuged (17,000 *g*, 15 s) to separate the biomass, and the supernatant was retained for metal analysis. At $t_0$ 1 ml of the relevant metal stock solution was added to the stirred reaction vessel to give an overall metal concentration of 300 µmol $l^{-1}$ ($t_0$ metal). At intervals over a period of 3 h, 5 ml samples were removed, and centrifuged immediately (17,000 *g*, 15 s). All sample supernatants were retained for metal analysis. After 3 h, at $t_{180}$, 1 ml of a second metal stock solution was added to the reaction vessel to give an overall second metal concentration also of 300 µmol $l^{-1}$ ($t_{180}$ metal). Samples were removed for metal analysis as described above for a further 3 h period.

**2.3** ***Section three: Effects of biomass concentration***

*For each of the ions $Sr^{2+}$, $Cd^{2+}$ and $Cu^{2+}$, three adsorption isotherms were determined using biomass concentrations of 1, 0.5 and 0.25 g $l^{-1}$ over a set metal concentration range 0-50 ppm. As before final solution $Ca^{2+}$, $Mg^{2+}$ and $H^+$ levels were determined.*

**2.3.1** *Isotherm preparation*

Individual 100 ml aliquots of 10, 20, 30, 40 and 50 ppm stock solutions of $Sr^{2+}$, $Cd^{2+}$ and $Cu^{2+}$ were dispensed into a series of acid-washed 250ml Erlenmeyer flasks, and the pH values were adjusted to 4 using dilute solutions of $HNO_3$ and NaOH. Biomass

portions of 0.1, 0.05 and 0.025 g were contacted with all of the above metal ion concentrations, and biomass-free and metal-free flasks were prepared as controls. All flasks were agitated at 25°C on an orbital shaker at 150 rev $min^{-1}$ for a period of 24 h and final pH and metal levels were determined as previously outlined.

### 2.4 *Section four: Continuous flow systems*

*150 μmol $l^{-1}$ $Cu^{2+}$ solutions were pumped upflow into columns packed with 0.8 g of freeze-dried biomass immobilised in 40% (w/w) poly-vinyl formal (PVF), at influent flowrates ranging from 3.40-11.63 ml min-1, and breakthrough curves were evaluated. Effluent levels of $Ca^{2+}$, $Mg^{2+}$ and $H^{+}$ ions were also determined. The effect of the immobilisation procedure on the biomass biosorption characteristics was also investigated by isotherm type analysis. Resultant $Cu^{2+}$ breakthrough curves were modelled using a two parameter fixed-bed adsorption model.*

#### 2.4.1 *Biomass immobilisation and column preparation*

Freeze-dried *Rhizopus arrhizus* biomass was homogenised to particle sizes not greater than 0.5 mm in diameter and 1 g quantities were mixed with 0.67 g of PVF powder in open pyrex petri dishes. PVF was polymerised by single 15 ml aliquot additions of dichloromethane (DCM) and the mixtures were allowed to evaporate to dryness. The resultant immobilised biomass discs were reduced to particle sizes of 0.5-1.0 mm in diameter and added into 1 l of distilled, deionised water. The mixture was continuously stirred and equilibrated to pH 4 by dropwise additions of concentrated $HNO_3$ over a 3 h period. Quantities of the $H^{+}$ ion equilibrated immobilised biomass corresponding to 0.8

g of the freeze-dried fungus (dry wt) were collected and packed into polypropylene columns of 70 mm in length with an internal diameter of 14 mm. Influent 150 μmol $l^{-1}$ $Cu^{2+}$ solutions, pH balanced to 4 using $HNO_3$, were pumped in an upflow direction through the columns by peristaltic pumps, at flowrates ranging from 3.40 to 11.63 ml $min^{-1}$. Effluent volumes were collected at regular 30 min intervals in 250 ml conical flasks, solution $Cu^{2+}$, $Ca^{2+}$, $Mg^{2+}$ and $H^+$ ion levels were determined, and $Cu^{2+}$ breakthrough curves were plotted.

**2.4.2** *Isotherm procedure*

A range of test biosorbents with biomass loadings of 40, 50, 60, 70 and 80% (w/w) in PVF were prepared as outlined above. In addition a control biosorbent was prepared by treating 1 g of native freeze-dried biomass with 15 ml of DCM, and the mixture was allowed to dry by evaporation. Using quantities of the biosorbents corresponding to 0.1 g of native freeze-dried biomass, a series of $Cu^{2+}$ adsorption isotherms were prepared as in section *2.1.1*, at initial solution pH values of 4. At equilibrium, $Cu^{2+}$, $Ca^{2+}$, $Mg^{2+}$ and $H^+$ ion levels were determined.

**2.4.3** *Two parameter fixed-bed adsorption model (Belter et al. 1988)*

The two parameter fixed-bed adsorption model as described by Belter *et al.* (1988) was applied to the column breakthrough data. The model relates change in solution concentration to column residence time and is given by *equation 2.4.1*. The breakthrough curves are modelled by two parameters: a characteristic time and a standard deviation.

$$C/C_i = \tfrac{1}{2}(1 + \mathrm{erf}[t - t_{50} / \sigma t_{50}\sqrt{2}]) \qquad (2.4.1)$$

where

$C_i$ = Influent $Cu^{2+}$ concentration

$C$ = Effluent $Cu^{2+}$ concentration at time $t$

$t_{50}$ = Time when $C = \tfrac{1}{2}C_i$

$\sigma t_{50}$ represents the standard deviation, a measure of the slope of the curve. The quantity erf($x$) is the error function of $x$, values of which are given in *Appendix E*, and when $t < t_{50}$

$$\mathrm{erf}[-x] = -\mathrm{erf}[x] \qquad (2.4.2)$$

The mathematical procedure involves calculating a representative value of σ for each breakthrough curve.

## 2.5 *Section five: Selenite adsorption studies*

*Selenite adsorption isotherms were prepared with live non-metabolising fungal biomasses of Rhizopus arrhizus and a Penicillium species. Here, $K^+$ equilibrium levels were monitored in conjunction with $Ca^{2+}$, $Mg^{2+}$ and $H^+$.*

*Isotherm protocol*

Live non-metabolising biomass of a *Penicillium* species was cultured and processed under identical conditions as described above for *Rhizopus arrhizus* in section *2.0.1.* A sodium selenite stock of 1000 ppm was prepared by dissolving the appropriate weight of $Na_2SeO_3.5H_2O$ salt (Cat. No. 6607, MERCK, Darmstadt, Germany) in distilled, deionised water. Using live non-metabolising biomasses of both fungi, at an initial

solution pH values of 4, selenite isotherms were prepared as described in section *2.1.1*, and final $Ca^{2+}$, $Mg^{2+}$, $H^{+}$ and $K^{+}$ levels were determined. A suitable assay for the measurement of final selenium levels in the supernatant is described below in section *2.6.2* following.

## 2.6 *Section six: Selenite transformation studies*

*Because of the novelty of the work in this section, a brief description of the method development is included here.*

### **2.6.1** *The development of a protocol for monitoring the transformation of selenite into volatile selenium compounds*

In studies on selenium volatilization using *Mortierella stylospora*, $^{75}$selenite and $^{75}$selenate (Zieve *et al.* 1985), and soil microflora and $^{75}$selenite (Tan *et al.*, 1994), bioreactor effluent gases were flushed directly into concentrated nitric acid in order to trap volatile selenium species. It was therefore decided to apply similar trapping techniques to the initial studies in this work.

Under aseptic conditions, 50 ml glass vessels were prepared with 15 ml of malt extract agar augmented with 200-1000 µmol $l^{-1}$ of selenite. The vessels were sealed with rubber bungs, and using syringe needles and peristaltic tubing, were attached to two acid traps in series containing 2 ml aliquots of 6*M* $HNO_3$ in polypropylene test tubes. Circular layers of sterile dialysis tubing were spread over the top of the solidified media, and were inoculated with 5 mm agar plugs of a *Fusarium* species. The dialysis tubing was used to facilitate the isolation of biomass from the media. Vacuum pumps were

attached to the second acid trap in each series, and sterile filter ports, attached to syringe needles were opened on the bioreactors. Air was flushed through the systems, and exhaust gases were flushed directly into the acid traps. This procedure was repeated on a daily basis over 2 wk periods. Using atomic adsorption spectrophotometery, a selenium assay with a linear range up to 400 μmol $l^{-1}$ was developed. A 1000 ppm selenium stock was prepared by dissolving the approriate weight of $Na_2SeO_3.5H_2O$ in 5 ml of concentrated $HNO_3$, and diluting to 1 l in a volumetric flask with distilled, deionised water. Standard curves were prepared by dilution with distilled, deionised water, and acid trap samples were analysed for selenium compounds. With this experimental design no selenium compounds were detected in the acid traps. This was attributed to the low quantities of selenium initially present in the systems and the relatively large linear range of the selenium assay.

In order to increase selenium levels for atomic adsorption spectrophotometery optimisation, bioreactors with 5 l quantities of growth media (media components as described for section *2.6.2*) supplemented with 1000 μmol $l^{-1}$ of selenite were prepared. The solutions were inoculated with the *Fusarium* species, and constantly aerated at a temperature of 25°C for 4 wk. Exhaust gases were flushed into two acid traps in series each containing 10 ml aliquots of 6M $HNO_3$ in glass test tubes. Condensers were installed on the bioreactors and acid traps to minimise solution evaporation and contamination of the trap contents by evaporated selenite enriched media. However, growth of the *Fusarium* species in the presence of selenite was slow, reaching only a maximum value of *ca.* 1 g $l^{-1}$, and no selenium compounds were detected in the acid traps after 4 wk. The work was repeated with a *Penicilium* species isolated as described

in section *2.6.2*, but although biomass levels reached *ca.* 6.0 g $l^{-1}$, no appreciable levels of selenium compounds were detected in the acid aliquots after 2-4 wk periods. A more sensitive method of selenium detection in the form of inverse polaragraphy that can detect selenium at 1 µmol $l^{-1}$ levels using a 2*M* $CH_3COOH$:2*M* $CH_3COONH_4$ buffer solution was then adopted. Nevertheless, analysis of acid from traps exposed to exhaust gases of the *Penicillium* species cultured in selenite still did not reveal the presence of selenium compounds. Consequently an alternative form of a trapping agent had to be considered.

In an earlier study, charcoal was successfully used to retain volatile $^{75}Se$-radiolabelled dimethylselenide (Karlson & Frankenberger, 1988*a*), and it was decided to use a series of two activated charcoal traps, each containing 2 g of charcoal in a polypropylene cartridges, in place of the acid traps. After a 4 wk period, known quantities of charcoal from the traps were rinsed in the 2*M* $CH_3COOH$:2*M* $CH_3COONH_4$ buffer, and introduced into the polaragraph reaction chamber. The presence of selenium compounds evolved from the actively metabolising *Penicillium* species was detected. It was concluded that the *Penicillium* species was capable of volatilising inorganic sodium selenite into volatile selenium compounds, and decided that the next step was to quantify the transformations.

Inverse polarography was considered to be ion species specific, so atomic adsorption spectrophotometery was chosen as the best method for selenium analysis. A suitable protocol for the extraction of volatile selenium compounds retained by activated charcoal (extraction protocol as described for section *2.6.2*) was devised based on the technique devised by Karlson & Frankenberger (1988*a*) for the extraction of $^{75}Se$-

labelled dimethylselenide from activated charcoal. From a range of organic and inorganic solutions, methanol was identified as the optimum solvent, extracting *ca.* 95.2% of the $^{75}Se$ labelled volatiles. In order to optimise the selenium assay by atomic absorption spectrophotometery it was found necessary to transform organic selenium species extracted in the methanol into inorganic species. This was achieved by dissolving these volatiles in hot concentrated acid solutions and diluting appropriately (sampling processing as in section *2.6.2*).

### 2.6.2 *Protocol for the measurement of selenite volatilisation*

*Bioreactors with working volumes of 5 l and sodium selenite concentrations of 1000 μmol $l^{-1}$ were inoculated with a Penicillium species and continuously aerated over two week periods. Selenium in the aqueous phase and associated with the biomass as well as volatile selenium compounds were determined. In addition pH and biomass concentrations were monitored. Biomass-free and selenite-free control bioreactors were also set up and monitored for two week periods to assess any physico-chemical changes which may have occurred. The design and operation of these bioreactors are described below and all processes were performed in triplicate.*

#### 2.6.2.1 *Organism and media preparation*

For experimental purposes, the *Penicillum* species was grown in liquid medium comprising (g $l^{-1}$): glucose, 20; $(NH_4)_2SO_4$, 5.0; $KH_2PO_4$, 0.5; $MgSO_4.7H_2O$, 0.2; $CaCl_2.6H_20$, 0.05; NaCl, 0.1; $FeCl_3.6H_2O$, 0.0025; $ZnSO_4.7H_2O$, 0.004; $MnSO_4.4H_2O$, 0.004; and $CuSO_4.5H_2O$, 0.004. Stock solutions of glucose and the above salts were

prepared in distilled, deionised water and sterilised separately by autoclaving (121°C, 1.5 bar, 20 min). Stock solutions (0.5 mol $l^{-1}$) of $Na_2SeO_3.5H_2O$ (Cat. No. 6607, MERCK, Darmstadt, Germany) were prepared in distilled, deionised water and sterilized by membrane filtration (cellulose nitrate, pore size 0.45 µm, Cat. No. 7184-002, Whatman, Kent, England).

**2.6.2.2** *Microorganism isolation and identification*

The fungus used in this study was originally isolated from the atmosphere in open Erlenmeyer shake flasks (25°C, 150 rev $min^{-1}$) containing the above liquid culture medium augmented with 1000 µmol $l^{-1}$ of sodium selenite and exposed to the laboratory air for 7 days. The organism was purified by successive screening on sodium selenite enriched (1000 µmol $l^{-1}$) malt extract agar plates (Cat. No. CM59, Oxoid, Hampshire, England) and in preliminary work was found to transform selenite in solution. Fungal inocula were prepared by loop inoculation of spores from these plates into 0.5 l of liquid culture medium in shake flasks, and incubation at 25°C for 5 days at 150 rev $min^{-1}$. In the broth media the fungus grew as finely suspended pale-white mycelium pellets, thereby facilitating the removal of representative biomass samples.

Under a light microscope, spore-bearing structures characteristic to *Penicillium* species from the class Deuteromycotina (fungi imperfecti), *i.e.* conidia formed from flask-shaped cells (phialides) on branched ("penicillates") conidiophores (Deacon, 1980; Stanier *et al.*, 1988) were observed, and thus the fungi was classified as a *Penicillium*.

**2.6.2.3** *Bioreactor configuration*

The fermentations were performed in 7 l cylindrical pyrex culture vessels (140 mm i.d. x 450 mm) as part of a New Brunswick Scientific (New Jersey, U.S.A.) Fermentor Drive Assembly (Model no. FS-607). The temperature of the bioreactors were maintained at 25°C for the duration of the experiments. Initially bioreactors contained 4.5 l of sterile liquid culture medium, 1 ml of sterile silicone antifoaming agent (Cat. No. 33151 2K, BDH, Poole, England) and 10 ml aliquot of sterile 0.5 mol $l^{-1}$ $NaSeO_3.5H_2O$ stock solution. At $t_0$ (day 1) 0.5 l of inocula were added to each bioreactor culture vessel resulting in final media volumes of 5 l, initial biomass concentrations of approximately 0.6 g $l^{-1}$ (dry weight) and initial sodium selenite concentrations of 1000 µmol $l^{-1}$. For biomass-free controls, 0.5 l of sterile distilled, deionized water was added to the reactors instead of the *Penicillium* inocula.

Bioreactor contents were stirred at impeller speeds of 250 rev $min^{-1}$ and aerated using air pumps (cat. no. XP-990, Penn-Plax, New Tork, U.S.A.) fitted with sterile filters (HEPA-VENT, cat. no. 6723-5000, Whatman, Kent, England) delivering air at rates of approximately 4 l $min^{-1}$. The exhaust gases were passed through water-cooled condensers in order to minimise medium evaporation and into a series of three activated charcoal traps each consisting of 2 g of activated charcoal (14-60 mesh, cat. no. C-3014, SIGMA, St. Louis, MO, U.S.A.) contained in polypropylene tubes (i.d. 14mm X 76mm). Each series of charcoal traps were replaced every 7 days and the final weights of used charcoal were recorded.

At the start of each process, the culture vessels, liquid culture media, air filters, air inlet and exhaust lines (silicone tubing i.d. 4.8mm) and water cooled condensers were all sterilized by autoclaving (121°C, 1.5 bar, 20 min). A diagram of the working apparatus is exhibited in *Figure 2.6.1.*

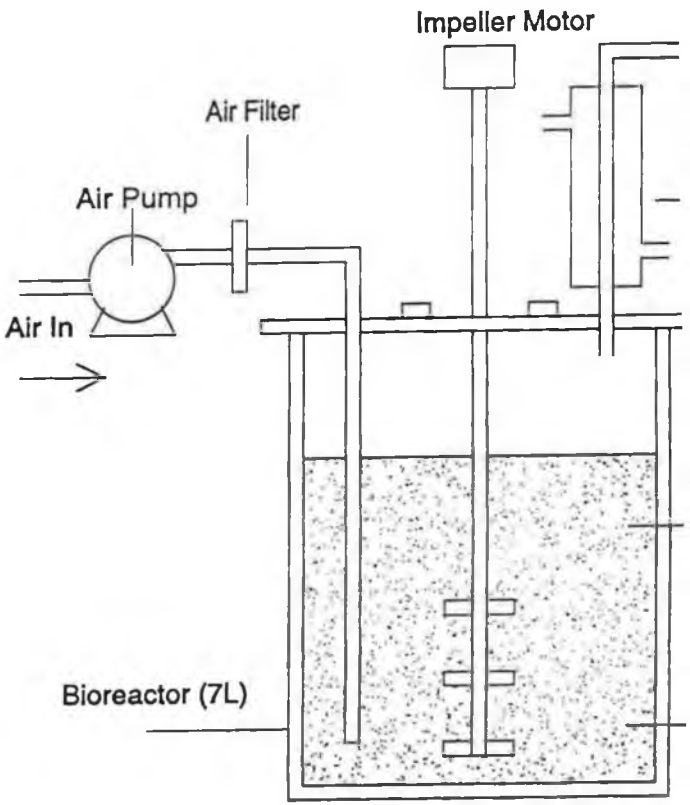
Impeller Motor
Air Filter
Air Pump
Air In
Bioreactor (7L)

**Figure 2.6.1:** Selenium volatilisation by a *Penicillium* species: bioreactor design.

**2.6.2.4** *Sample processing*

At 1-2 day intervals, four 10 ml sample aliquots were aseptically removed from each culture vessel. Two aliquots were centrifuged (17,000 *g*, 15 s) to separate fungal biomass from solution and the supernatants were retained. The biomass pellets were washed twice with 5 ml of distilled, deionized water, acid digested in 2 ml of 6M HCl:3M $HNO_3$ solution (90°C, 1 h) and diluted to 10 ml with distilled, deionized water. To 4 ml of the resultant biomass-free supernatants, 1 ml aliquots of 6*M* HCl:3*M* $HNO_3$ solution were added. For further dilutions of these biomass and supernatant preparations a 1.2*M* HCl:0.6*M* $HNO_3$ diluent was used. The remaining samples were filtered through pre-weighed filters (Cat. no. 1001 090, Whatman, Kent, England) and the filtrates were discarded. The filter papers plus retentates were oven-dried at 55°C for 24 h and biomass dry weights were calculated after weighing. Total selenium in solution was determined using a Perkin-Elmer 3100 atomic absorption spectrophotometer with reference to appropriate standards of $Na_2SeO_3.5H_2O$ prepared in 1.2*M* HCl:0.6*M* $HNO_3$ solution.

**2.6.2.5** *Recovery of volatilised selenium compounds*

Recovery of volatilised selenium compounds from the activated charcoal traps was achieved by solvent extraction using 100% methanol. For each trap, a 2 ml aliquot of 6*M* HCL:3*M* $HNO_3$ solution was heated to boiling in a polypropylene test tube immersed in a vessel of boiling water. A representative 0.5 g quantity of trap charcoal was introduced into a 250 ml conical flask followed by a 5 ml aliquot of 100% methanol and the flask was appropriately sealed. The methanol/charcoal mixture was

stirred and heated to dryness on a hot plate magnetic stirrer and the vapourised compounds evolved were passed through a glass tube directly into the boiling acid solution contained in the polypropylene test tube. This technique is illustrated in *Figure 2.6.2.* A second and third 5 ml aliquot of 100% methanol were added into the 250 ml conical flask and again evaporated to dryness as before. As the boiling point of the acid solution was above that of methanol, the volumes in the polypropylene test tubes remained at 2 ml after the extraction processes with no detectable changes and final volumes were made up to 10 ml with distilled, deionized water. Where necessary dilutions were prepared using a 1.2*M* HCl:0.6*M* $HNO_3$ diluent and total selenium in solution was determined as before.

### 2.7 *Section seven: Transformation enhancement studies*

*Using the same bioreactor design as outlined above, enhancement of selenium accumulation/biosorption and biomethylation was investigated by adding Dulbecco's Modified Eagle Medium (DMEM) to the reactor media.*

*Operating procedure*

Three bioreactors (a), (b) and (c), were augmented with 1000 µmol $l^{-1}$ of selenite, inoculated with the *Penicillium* species, and continuously stirred under aerobic conditions for 2 wk periods at 25°C as previously described in section *2.6.2.* Each system was augmented with a total of 50 ml of Dulbecco's Modified Eagle Medium 10X (cat. no. 042-02501, GibcoBrl), with aliquots introduced at different time interals. For reactor (a), 50 ml was added at $t_0$, for reactor (b), 25 ml was added both at $t_0$ and on day 7, and for reactor (c), 50 ml was added on day 7. DMEM additions made available a range of components to the actively metabolising fungus including amino acids, vitamins

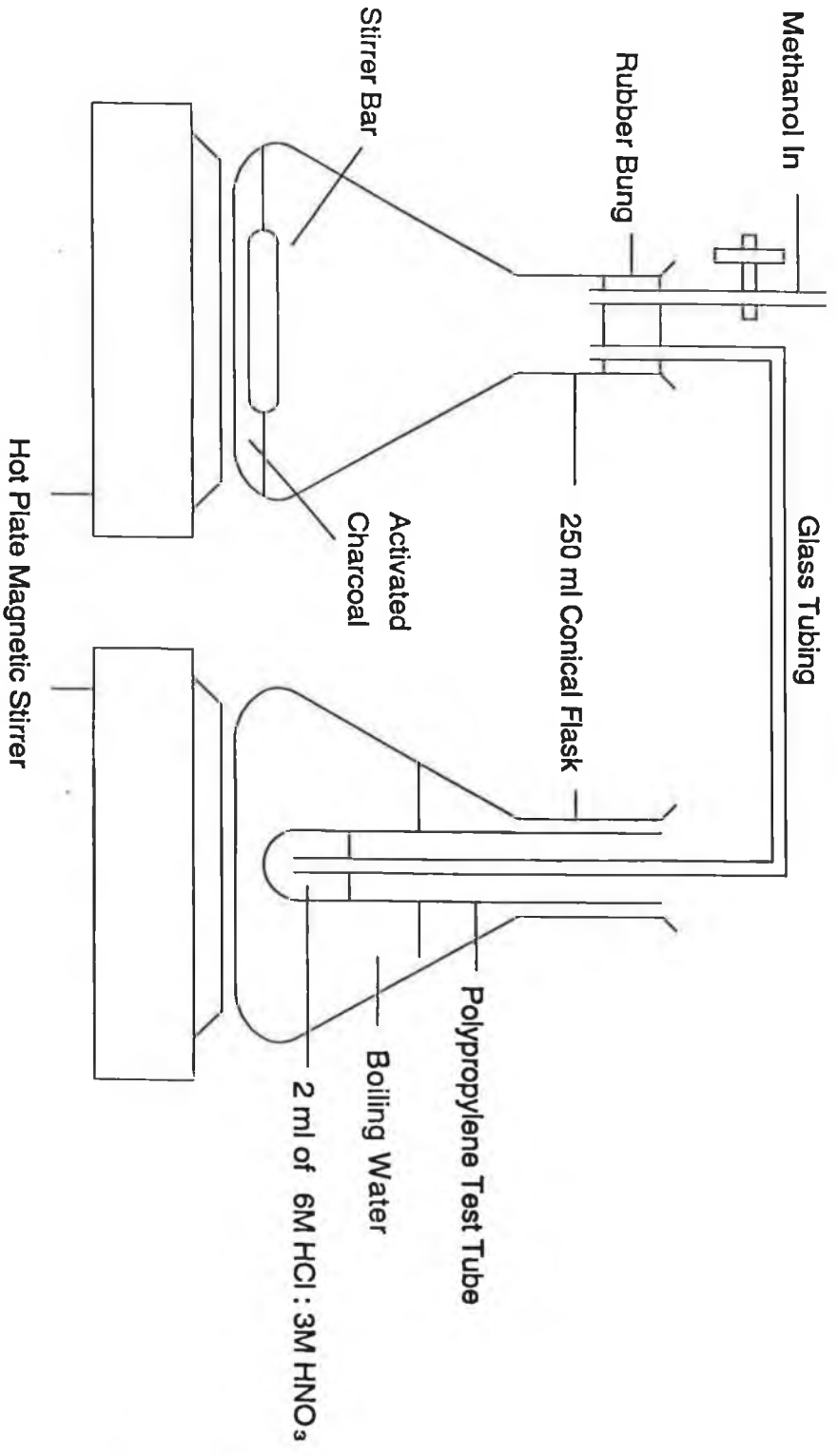


**Figure 2.6.2:** Extraction of volatile selenium compounds from activated charcoal: apparatus.

and inorganic salts, and final concentrations after addition are outlined in *Table 2.7.1*. When DMEM additions are taken into account, glucose was supplied to the media at overall concentrations of 20 g $l^{-1}$. Activated charcoal traps, four in series, were changed at weekly intervals, and as before, selenium in the aqueous phase, selenium associated with the biomass, volatile selenium compounds, pH and biomass concentrations were all monitored over time.

**Table 2.7.1**: Final concentration of components supplied to fungal media by Dulbecco's Modified Eagle Medium 10X after addition.

| *INORGANIC SALTS* | mg $l^{-1}$ | *AMINO ACIDS* | mg $l^{-1}$ |
|---|---|---|---|
| $CaCl_2.2H_2O$ | 26.40 | L-Arginine.HCl | 8.40 |
| $Fe(NO)_3.9H_2O$ | 0.01 | L-Cystine | 4.80 |
| KCL | 40.00 | Glycl-L-Glutamine | 80.60 |
| $MgSO_4.7H_2O$ | 20.00 | Glycine | 3.00 |
| NaCl | 640.00 | L-Histidine HCl.H2O | 4.20 |
| $NaHCO_3$ | 370.00 | L-Isoleucine | 10.50 |
| $NaH_2PO_4.2H_2O$ | 14.10 | L-Leucine | 10.50 |
| | | L-Lysine.HCl | 14.60 |
| | | L-Methionine | 3.00 |
| | | L-Phenylalanine | 6.60 |
| | | L-Serine | 4.20 |
| | | L-Threonine | 9.50 |
| | | L-Tryptophan | 1.60 |
| | | L-Tyrosine | 7.20 |
| | | L-Valine | 9.40 |

| *VITAMINS* | mg $l^{-1}$ | *OTHER COMPONENTS* | mg $l^{-1}$ |
|---|---|---|---|
| D-Ca pantothenate | 0.40 | D-Glucose | 450.00 |
| Choline Chloride | 0.40 | Phenol Red | 1.50 |
| Folic Acid | 0.40 | | |
| i-Inositol | 0.72 | | |
| Nicotinamide | 0.40 | | |
| Pyridoxal HCl | 0.40 | | |
| Riboflavin | 0.40 | | |
| Thiamine HCl | 0.40 | | |

# CHAPTER 3

# RESULTS

*Interactions of metal and metalloid ions with fungal biomass*

*PhD Research Thesis by*

*Joseph M. Brady* B.Sc.

## CHAPTER 3: RESULTS

### 3.1 *Biosorption characterisation: results*

#### 3.1.1 *Adsorption isotherm analysis*

At the pH values investigated, each of the biomass types (freeze-dried, oven-dried and live non-metabolising) exhibited uptake of $Sr^{2+}$, $Cd^{2+}$ and $Cu^{2+}$ ions. In each case, the amount of metal adsorbed increased with increasing solution concentration until adsorbent saturation. The uptake data, $q$, when plotted against final solution concentrations, $C_f$, yield adsorption isotherms concave towards the abscissa in all cases reflecting favourable adsorption (Weber, 1972). Isotherms for $Sr^{2+}$, $Cd^{2+}$ and $Cu^{2+}$ uptake by freeze-dried, live non-metabolising and oven-dried biomass at pH 4 are shown in *Figure 3.1.1*. The maximum equilibrium uptake values observed for each system over the pH range are tabulated in *Table 3.1.1*. Of the three ions, $Cu^{2+}$ was adsorbed to the highest levels with freeze dried biomass displaying a maximum loading of 441 μmol $g^{-1}$. $Cd^{2+}$ was adsorbed to intermediate levels ranging from 220 to 286 μmol $g^{-1}$, and $Sr^{2+}$ exhibited both the lowest uptake of 165 μmol $g^{-1}$ for live non-metabolising biomass, and the least variation between the biomass types (165-200 μmol $g^{-1}$). The pH values selected for each system were chosen to preclude hydroysis of the metal ions and to conform to reported optimum values for metal binding. The data obtained at the differing pH values agree to within limits of 5%.

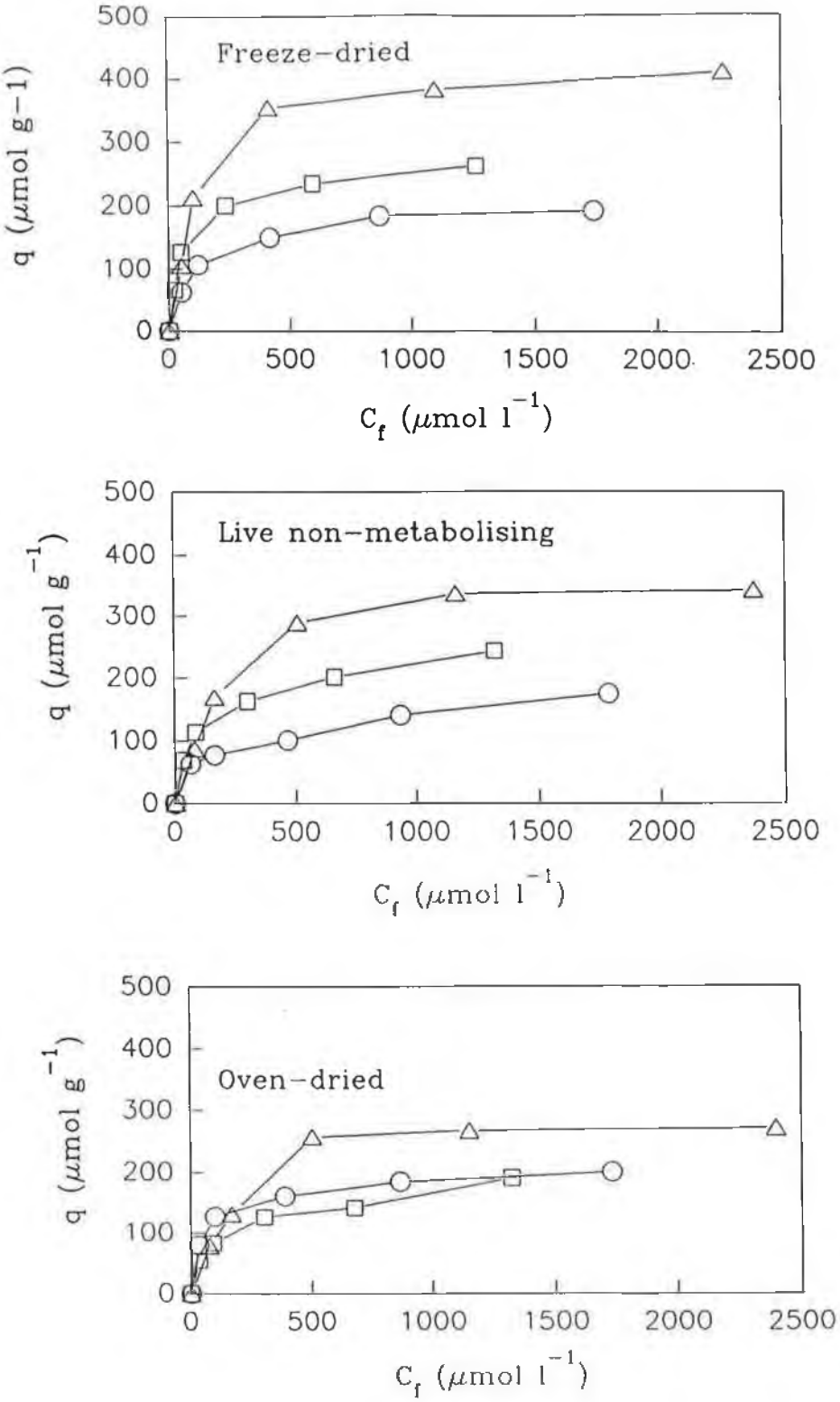


**Figure 3.1.1:** Equilibrium adsorption isotherms for freeze-dried, oven-dried and live non-metabolising *Rhizopus arrhizus* biomass at initial solution pH values of 4.
$Sr^{2+}$ ( ○ ), $Cd^{2+}$ ( □ ) and $Cu^{2+}$ ( △ ).

### 3.1.2 *Biomass pretreatment effects*

The effects of biomass pretreatment were found to vary for each metal ion. For $Sr^{2+}$ freeze dried and oven dried biomass adsorbed generally equivalent levels (*ca.* 190 μmol $g^{-1}$), whereas the uptake level for live non-metabolising biomass, was marginally lower at *ca.* 170 μmol $g^{-1}$. In contrast, $Cu^{2+}$ was bound to the highest level by freeze dried biomass (*ca.* 440 μmol $g^{-1}$), followed in order by live non-metabolising and oven dried biomasses, with uptake values of *ca.* 70% and 60% of the freeze dried value respectively. For $Cd^{2+}$, the same trend is apparent: freeze dried biomass demonstrating a maximum uptake value of *ca.* 270 μmol $g^{-1}$, followed by live non-metabolising and oven dried biomasses, with values of 90% and 70% of the freeze dried value, respectively.

**Table 3.1.1**: Maximum metal uptake values for metal-biomass systems in initial solutions of pH 4 and 6.

| Metal ion | Biomass type | pH | Metal uptake (μmol $g^{-1}$) | (mg $g^{-1}$) |
|---|---|---|---|---|
| $Sr^{2+}$ | Freeze-dried | 4 | 191 | 16.74 |
| | | 6 | 200 | 17.52 |
| | Live | 4 | 165 | 14.46 |
| | | 6 | 174 | 15.25 |
| | Oven-dried | 4 | 190 | 16.65 |
| | | 6 | 191 | 16.74 |
| $Cd^{2+}$ | Freeze-dried | 4 | 262 | 29.45 |
| | | 6 | 286 | 32.15 |
| | Live | 4 | 243 | 27.32 |
| | | 6 | 246 | 27.65 |
| | Oven-dried | 4 | 220 | 24.73 |
| | | 6 | 228 | 25.63 |
| $Cu^{2+}$ | Freeze-dried | 4 | 424 | 26.94 |
| | | 5 | 441 | 28.02 |
| | Live | 4 | 342 | 21.73 |
| | | 5 | 357 | 22.69 |
| | Oven-dried | 4 | 271 | 17.22 |
| | | 5 | 278 | 17.67 |

### 3.1.3 *$Ca^{2+}$ and $Mg^{2+}$ ion displacement*

Displacement of both $Ca^{2+}$ and $Mg^{2+}$ ions occurred as a result of test ion adsorption to biomass. As illustrated in *Figure 3.1.2* for the pH 4 systems, displacement was found to increase with increasing test ion adsorption until saturation levels were reached. Using standard regression analysis, the ratios of $Ca^{2+}$ and $Mg^{2+}$ displaced to test ions adsorbed were calculated, and are presented in *Table 3.1.2*. Maximum $Ca^{2+}$ and $Mg^{2+}$ ions displacement by $Sr^{2+}$, $Cd^{2+}$ and $Cu^{2+}$ were constant at *ca.* 20 and 110 μmol $g^{-1}$ respectively, and did not vary either with biomass type or pH.

### 3.1.4 *$H^+$ ion displacement/competition*

For each metal-microbial system, the pH of the metal-free controls increased to neutrality on addition of the biomass. The relationship between final solution pH and test ion adsorption levels are illustrated in *Figure 3.1.3* for pH 4 systems. For the $Sr^{2+}$ systems, the final solution pH was independent of the degree of uptake, and at maximum uptake levels remained at neutrality. For the $Cd^{2+}$ and $Cu^{2+}$ systems final solution pH values decreased linearly with increasing metal uptake to minimum values of *ca.* 5.5 and 4.0 respectively. Overall, for $Sr^{2+}$ uptake, no $H^+$ displacement was detected. At maximum uptake of $Cd^{2+}$ and $Cu^{2+}$, $H^+$ displacement was *ca.* 2.2 and 120 μmol $g^{-1}$ respectively. These trends were identical for each biomass type to within limits of 5%. When $H^+$ ion displacement was plotted against metal uptake ($q$) for $Cd^{2+}$ and $Cu^{2+}$ systems at pH 4, curved relationships were evident as illustrated in *Figure 3.1.4* and *3.1.5* respectively.

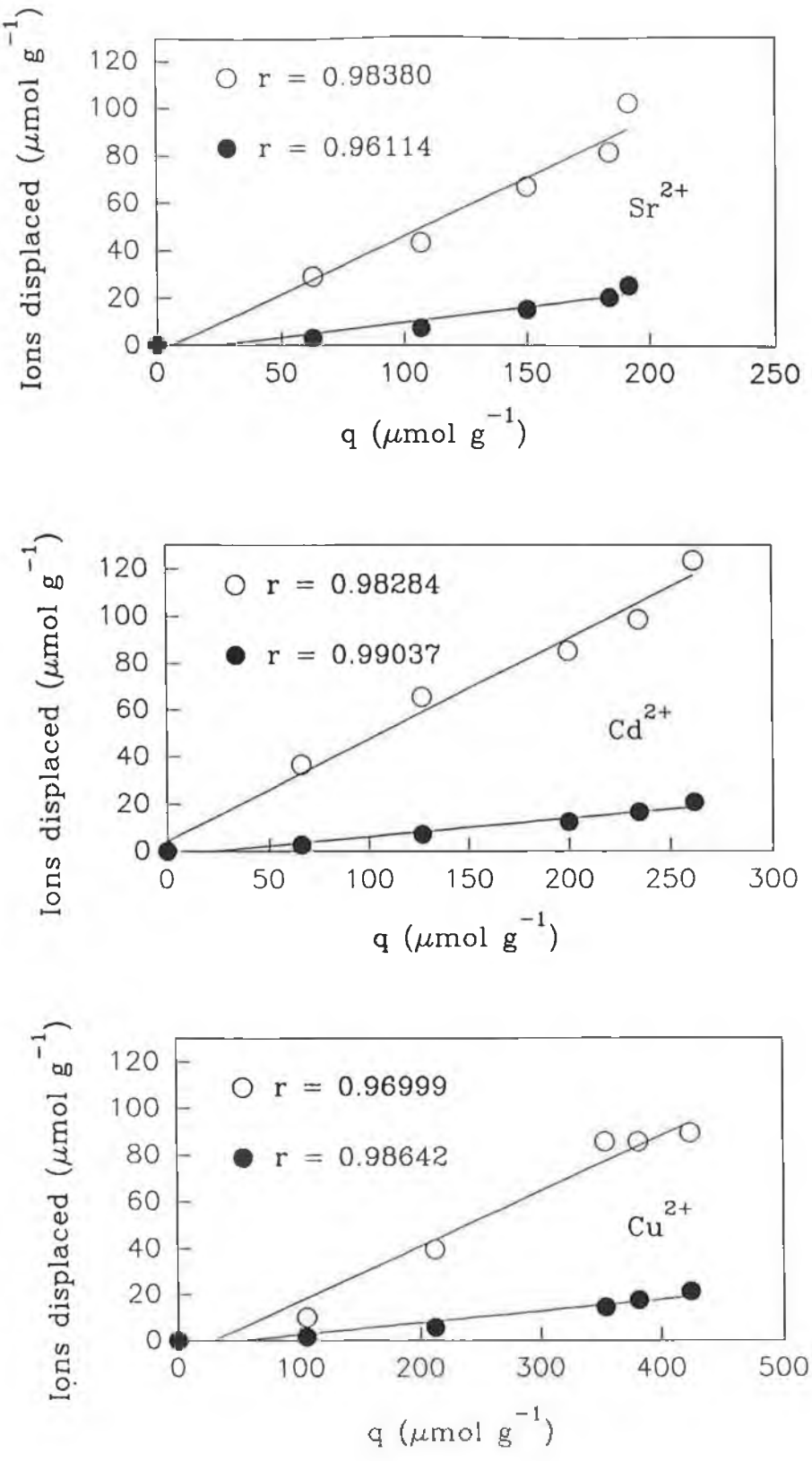


**Figure 3.1.2:** Equilibrium $Ca^{2+}$ and $Mg^{2+}$ ion displacement from *Rhizopus arrhizus* biosorbents as a consequence of $Sr^{2+}$, $Cd^{2+}$ and $Cu^{2+}$ adsorption, versus metal uptake ($q$) at initial solution pH values of 4.
$Ca^{2+}$ ( ● ) and $Mg^{2+}$ ( ○ ).

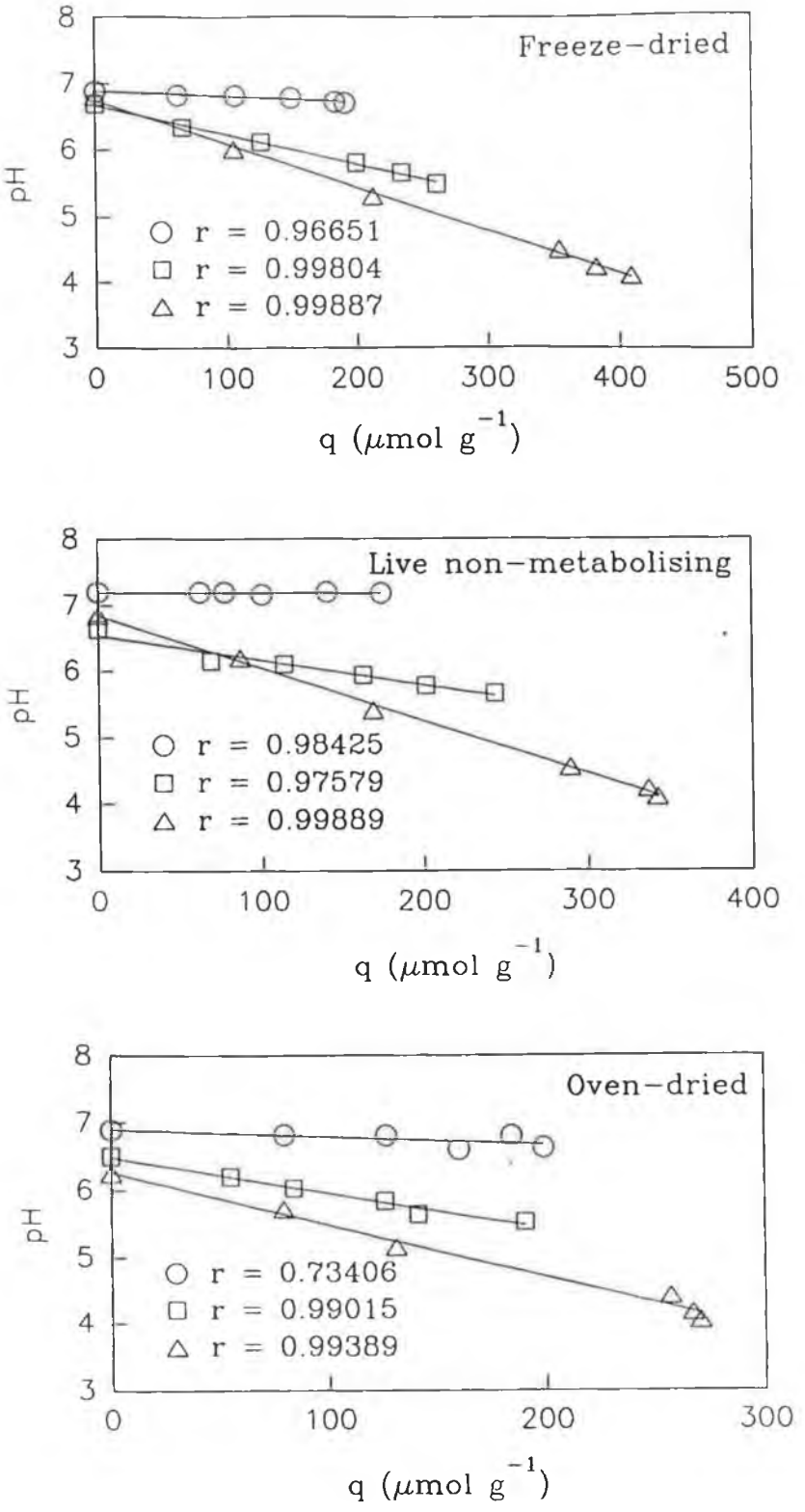


**Figure 3.1.3:** Final pH values at equilibrium versus metal uptake (*q*) for freeze-dried, oven-dried and live non-metabolising *Rhizopus arrhizus* biomass at initial solution pH values of 4.
$Sr^{2+}$ ( ○ ), $Cd^{2+}$ ( □ ) and $Cu^{2+}$ ( △ ).

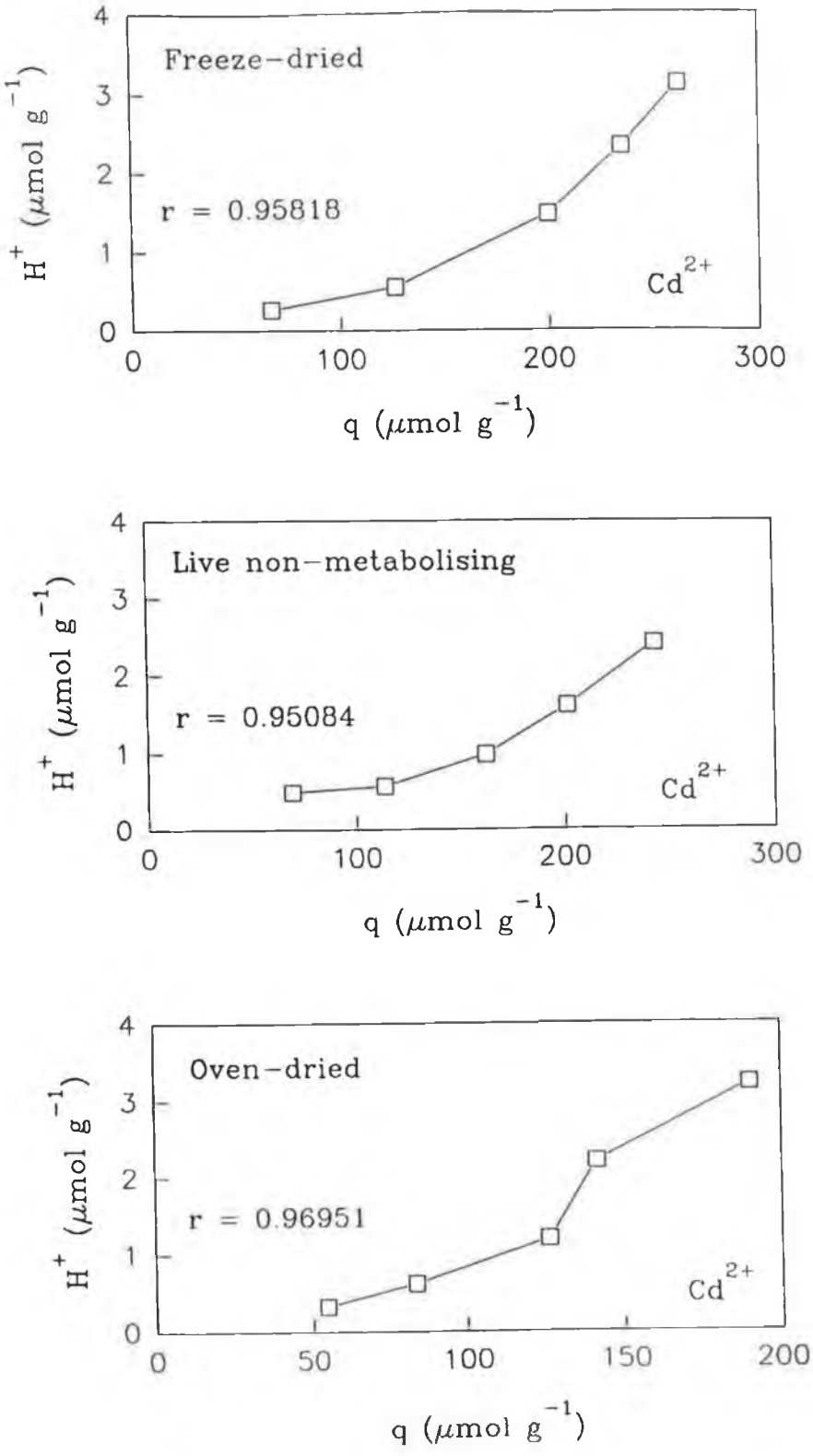


**Figure 3.1.4:** Equilibrium $H^+$ ion displacement from freeze-dried, oven-dried and live non-metabolising *Rhizopus arrhizus* biomass as a consequence of $Cd^{2+}$ adsorption, versus metal uptake ($q$) at initial solution pH values of 4.

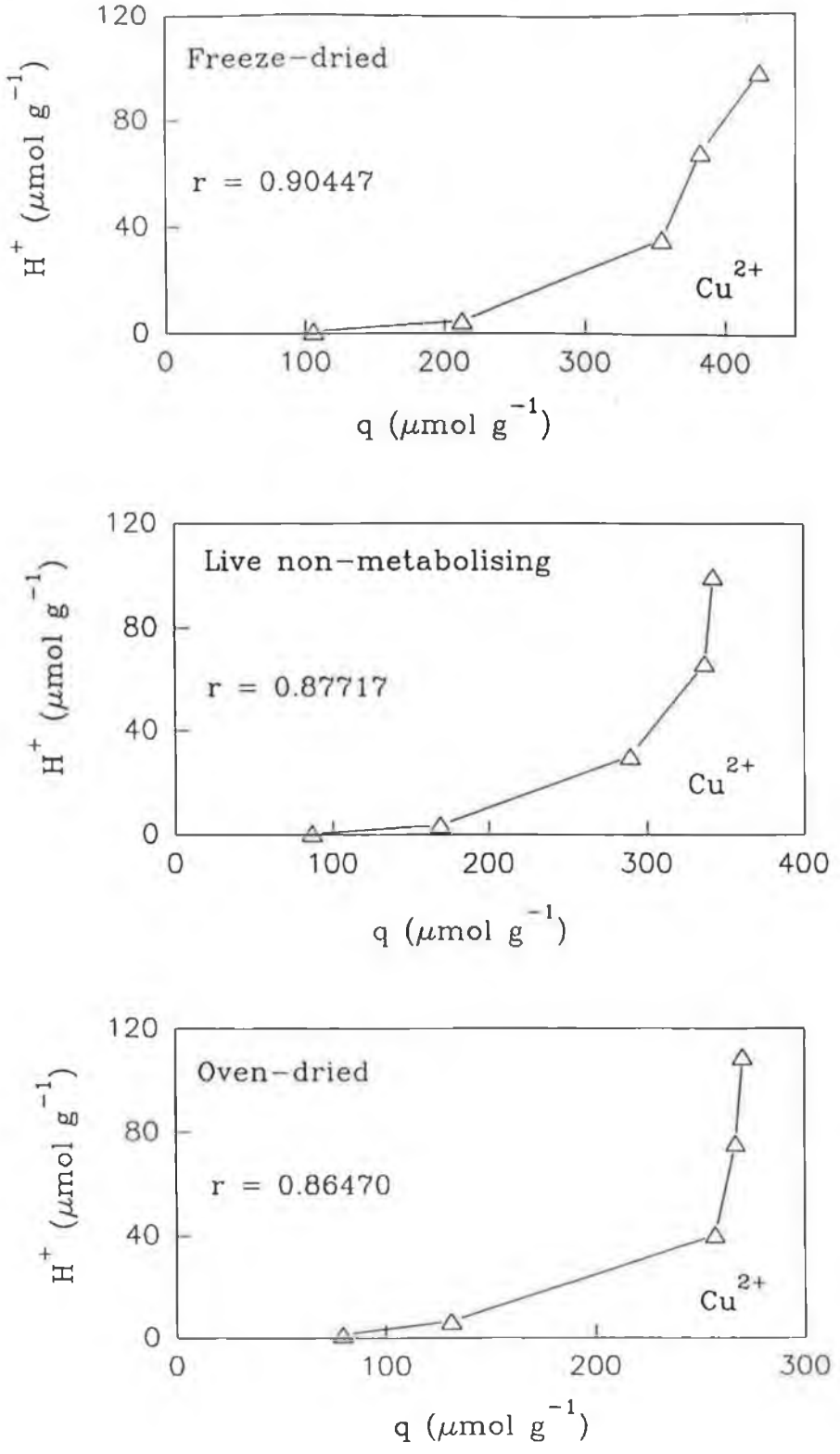


**Figure 3.1.5:** Equilibrium $H^+$ ion displacement from freeze-dried, oven-dried and live non-metabolising *Rhizopus arrhizus* biomass as a consequence of $Cu^{2+}$ adsorption, versus metal uptake ($q$) at initial solution pH values of 4.

**Table 3.1.2**: Molar ratios of $Ca^{2+}$ and $Mg^{2+}$ ions displaced to test ions adsorbed at initial solution pH values of 4.

| | | | |
|---|---|---|---|
| **Freeze-dried biomass systems** | | | |
| | $Sr^{2+}$ | $Cd^{2+}$ | $Cu^{2+}$ |
| $Ca^{2+}$ | 0.17 | 0.09 | 0.06 |
| $Mg^{2+}$ | 0.53 | 0.50 | 0.28 |
| $Ca^{2+}$ + $Mg^{2+}$ | 0.70 | 0.59 | 0.34 |
| **Live biomass systems** | | | |
| | $Sr^{2+}$ | $Cd^{2+}$ | $Cu^{2+}$ |
| $Ca^{2+}$ | 0.19 | 0.10 | 0.07 |
| $Mg^{2+}$ | 0.58 | 0.58 | 0.34 |
| $Ca^{2+}$ + $Mg^{2+}$ | 0.77 | 0.68 | 0.41 |
| **Oven-dried biomass systems** | | | |
| | $Sr^{2+}$ | $Cd^{2+}$ | $Cu^{2+}$ |
| $Ca^{2+}$ | 0.18 | 0.11 | 0.09 |
| $Mg^{2+}$ | 0.55 | 0.60 | 0.42 |
| $Ca^{2+}$ + $Mg^{2+}$ | 0.73 | 0.71 | 0.51 |

### 3.1.5 *Modelling of adsorption data*

The Langmuir, BET and Freundlich models were applied to the adsorption data, and plotted in the following forms:

| | |
|---|---|
| $q_e^{-1}$ versus $C_f^{-1}$ | (Langmuir model) |
| $C_f/(C_s - C)q_e$ versus $C_f/C_s$ | (BET model) |
| log $q_e$ versus log $C_f$ | (Freundlich model) |

The term $C_s$ is the the saturation concentration of the adsorbate. Conformity to each model was confirmed if linear plots were returned, curved plots suggested non-conformity. The Scatchard transformation model was further fitted to the adsorption data and represented as plots of $q_e/C_f$ versus $q_e$.

The type of plots observed for each metal-biomass system, whether curved or linear, and corresponding correlation coefficient $r$ values, are all presented in *Table 3.1.3*.

**Table 3.1.3**: Type of plots obtained from the application of Scatchard transformation analysis and the Langmuir, BET and Freundlich models to the adsorption data.

| | Langmuir | BET | Freundlich | Scatchard |
|---|---|---|---|---|
| **$Sr^{2+}$ (pH 4)** | | | | |
| Freeze | + | - | - | + |
| -dried | r= 0.99 | r= 0.93 | r= 0.95 | r= 0.98 |
| Live | - | - | + | @ |
| | r= 0.92 | r= 0.98 | r= 0.99 | r= 0.82 |
| Oven | + | - | - | + |
| -dried | r= 1.00 | r= 0.93 | r= 0.97 | r= 0.98 |
| **$Sr^{2+}$ (pH 6)** | | | | |
| Freeze | + | - | - | + |
| -dried | r= 0.99 | r= 0.93 | r= 0.95 | r= 0.98 |
| Live | - | - | + | @ |
| | r= 0.97 | r= 0.94 | r= 0.99 | r= 0.91 |
| Oven | + | - | - | + |
| -dried | r= 1.00 | r= 0.93 | r= 0.95 | r= 1.00 |
| **$Cd^{2+}$ (pH 4)** | | | | |
| Freeze | + | - | - | + |
| -dried | r= 1.00 | r= 0.96 | r= 0.95 | r= 0.98 |
| Live | + | - | + | @ |
| | r= 0.99 | r= 0.96 | r= 0.99 | r= 0.96 |
| Oven | + | - | + | @ |
| -dried | r= 0.99 | r= 0.96 | r= 0.99 | r= 0.92 |
| **$Cd^{2+}$ (pH 6)** | | | | |
| Freeze | + | - | - | + |
| -dried | r= 1.00 | r= 0.95 | r= 0.95 | r= 1.00 |
| Live | + | - | - | + |
| | r= 1.00 | r= 0.95 | r= 0.95 | r= 1.00 |
| Oven | - | - | + | @ |
| -dried | r= 0.98 | r= 0.94 | r= 0.99 | r= 0.96 |
| **$Cu^{2+}$ (pH 4)** | | | | |
| Freeze | + | - | - | * |
| -dried | r= 0.98 | r= 0.94 | r= 0.92 | r= 0.95 |
| Live | + | - | - | * |
| | r= 0.99 | r= 0.91 | r= 0.93 | r= 0.96 |
| Oven | + | - | - | * |
| -dried | r= 1.00 | r= 0.91 | r= 0.93 | r= 0.94 |
| **$Cu^{2+}$ (pH 5)** | | | | |
| Freeze | + | - | - | * |
| -dried | r= 0.99 | r= 0.94 | r= 0.92 | r= 0.95 |
| Live | + | - | - | * |
| | r= 0.99 | r= 0.91 | r= 0.94 | r= 0.96 |
| Oven | + | - | - | * |
| -dried | r= 0.99 | r= 0.91 | r= 0.91 | r= 0.93 |

+ Linear plot @ Curved plot convex to the origin
- Non-linear plot * Curved plot concave to the origin
*r = correlation coefficient*

Representative curved and linear plots for each model type are presented in *Figures 3.1.6*, *3.1.7*, *3.1.8* and *3.1.9*. General trends and observations include:

(a) For all $Cu^{2+}$ systems, Langmuir plots were linear, BET and Freundlich plots were curved, and Scatchard plots were curved concave to the origin.

(b) When both Langmuir and Scatchard plots were linear, Freundlich and BET plots were curved.

(c) When Freundlich plots were linear, BET and Scatchard plots were curved. Scatchard plots in this case were convex to the origin.

### **3.1.6** *Error analysis*

Duplicate experiments were performed in all cases, and the results were all found to agree to within limits of 1%. Six replicate $Cu^{2+}$ ion uptake experiments using oven dried biomass at an initial solution pH of 4, were performed for the purpose of statistical analysis. The standard deviation was found to be less than 4%, and these trends are consistent with previously reported error analyses (Tobin *et al.*, 1990).

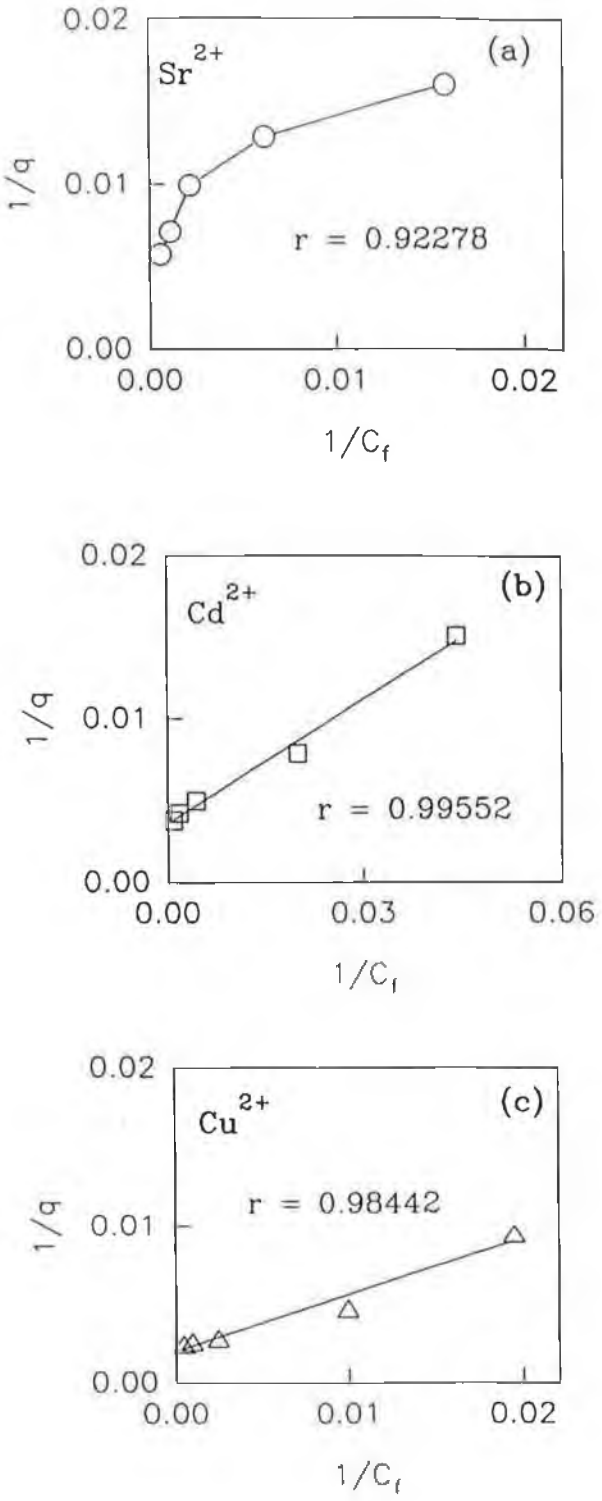


**Figure 3.1.6:** Representative Langmuir plots for *Rhizopus arrhizus* biosorbents at initial solution pH values of 4. Curved plot for $Sr^{2+}$ and live non-metabolising biomass (a), and linear plots for $Cd^{2+}$ and $Cu^{2+}$ freeze-dried biomass systems (b) and (C).

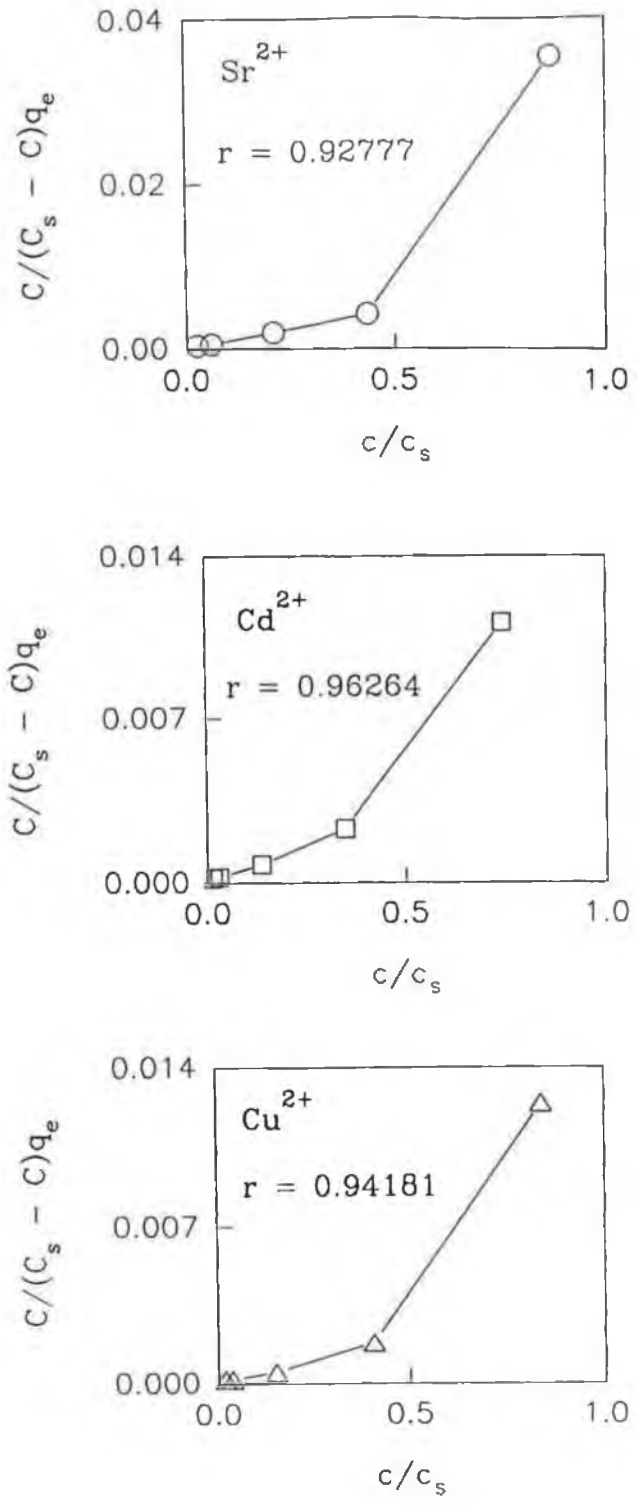


**Figure 3.1.7:** Representative curved BET plots for freeze-dried *Rhizopus arrhizus* biosorbent systems at initial solution pH values of 4.

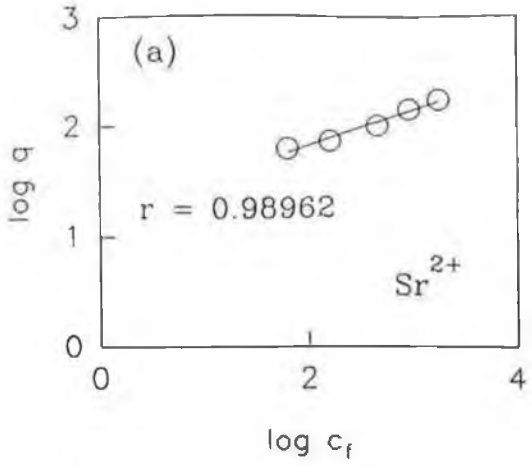


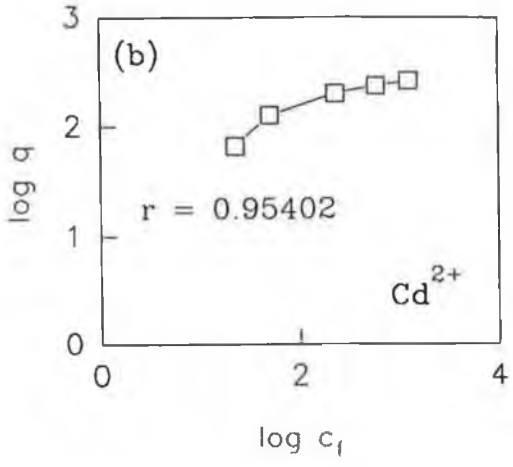


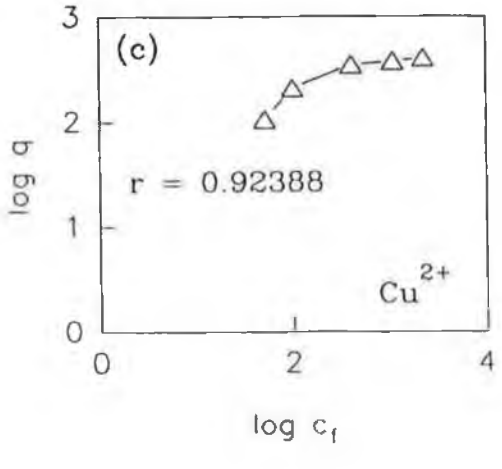


Figure 4.1.7

**Figure 3.1.8:** Representative Freundlich plots for *Rhizopus arrhizus* biosorbents at initial solution pH values of 4. Linear plot for $Sr^{2+}$ and live non-metabolising biomass (a), and curved plots for $Cd^{2+}$ and $Cu^{2+}$ freeze-dried biomass systems (b) and (C).

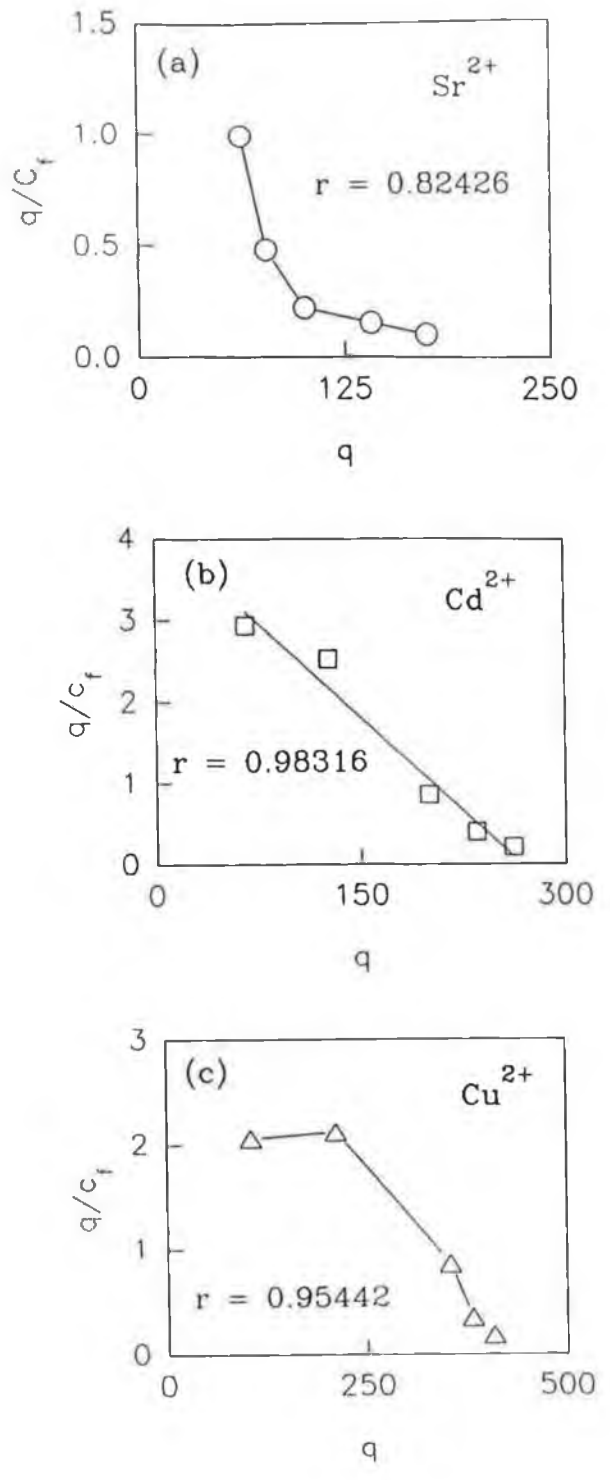


**Figure 3.1.9:** Representative Scatchard transformation plots for *Rhizopus arrhizus* biosorbents at initial solution pH values of 4.
Curved plot convex to the origin for $Sr^{2+}$ and live non-metabolising biomass (a), linear plot for $Cd^{2+}$ and freeze-dried biomass (b), and curved plot concave to the origin for $Cu^{2+}$ and freeze-dried biomass (C).

### 3.2 *Application of hard and soft principle: results*

#### 3.2.1 *Equilibrium studies*

Maximum equilibrium uptake levels varied considerably for different ions, as reported in *Table 3.2.1*. $Sr^{2+}$ exhibited the lowest uptake at 75.31 μmol $g^{-1}$ while $Pb^{2+}$ was taken up to levels of 250.98 μmol $g^{-1}$. $Ca^{2+}$, $Mg^{2+}$ and $H^{+}$ ions were found to be displaced from the biomass ligands as a consequence of test ion adsorption. $Ca^{2+}$ displacement was constant for $Sr^{2+}$, $Mn^{2+}$ and $Zn^{2+}$ at 3.35 μmol $g^{-1}$, but increased in order for $Cd^{2+}$, $Cu^{2+}$ and $Pb^{2+}$. $H^{+}$ ion displacement from the biomass varied from 0 μmol $g^{-1}$ for $Sr^{2+}$ to 9.84 μmol $g^{-1}$ for $Cu^{2+}$, and increased in the order: $Sr^{2+} < Mn^{2+} < Zn^{2+} < Cd^{2+} < Pb^{2+} < Cu^{2+}$. $Mg^{2+}$ displacement from the biomass was constant for all the test ions at ca. 72 μmol $g^{-1}$.

**Table 3.2.1**: Metal uptake values ($q$) and $Ca^{2+}$, $Mg^{2+}$ and $H^{+}$ displacement values for $t_0$ metals at equilibrium.

| Metal | q (μmol $g^{-1}$) | $Ca^{2+}$ (μmol $g^{-1}$) | $Mg^{2+}$ (μmol $g^{-1}$) | $H^{+}$ (μmol $g^{-1}$) |
|---|---|---|---|---|
| $Sr^{2+}$ | 75.31 | 3.35 | 72.00 | 0 |
| $Mn^{2+}$ | 121.77 | 3.35 | 72.00 | 0.87 |
| $Zn^{2+}$ | 142.14 | 3.35 | 72.00 | 1.39 |
| $Cd^{2+}$ | 190.30 | 4.01 | 72.00 | 1.90 |
| $Cu^{2+}$ | 224.09 | 5.52 | 72.00 | 9.84 |
| $Pb^{2+}$ | 250.98 | 7.87 | 72.00 | 3.98 |

In the majority of cases and on a molar basis, addition of $t_{180}$ metals caused displacement of $t_0$ metals as illustrated in *Table 3.2.2*. The most marked displacement was caused by $Pb^{2+}$ which completely displaced preloaded $Sr^{2+}$. Conversely, addition of $Sr^{2+}$, $Mn^{2+}$ and $Zn^{2+}$ had no effect on the levels of preloaded $Cu^{2+}$ or $Pb^{2+}$. With the exception of $Sr^{2+}$ preloaded systems, the displacement potential of the ions increased in the order: $Sr^{2+} < Mn^{2+} < Zn^{2+} < Cd^{2+} < Cu^{2+} < Pb^{2+}$. For $Sr^{2+}$ preloaded biomass, the displacement potential order was $Cu^{2+} < Cd^{2+} < Zn^{2+} < Mn^{2+} < Pb^{2+}$.

**Table 3.2.2**: Percentage of $t_0$ metals displaced by the addition of $t_{180}$ metals for *equilibrium studies*.

| | $t_{180}$ displacing metals | | | | | |
|---|---|---|---|---|---|---|
| | $Sr^{2+}$ (1.020)* | $Mn^{2+}$ (1.990) | $Zn^{2+}$ (2.128) | $Cd^{2+}$ (2.713) | $Cu^{2+}$ (2.979) | $Pb^{2+}$ (3.287) |
| $t_0$ metal | | | | | | |
| $Sr^{2+}$ | -- | 52 | 42 | 36 | 28 | **100** |
| $Mn^{2+}$ | 14 | -- | 31 | 43 | 45 | 45 |
| $Zn^{2+}$ | 8 | 28 | -- | 44 | 58 | 60 |
| $Cd^{2+}$ | 8 | 20 | 24 | -- | 58 | 59 |
| $Cu^{2+}$ | 0 | 0 | 0 | 5 | -- | 16 |
| $Pb^{2+}$ | 0 | 0 | 0 | 12 | 33 | -- |

* Covalent Index values (see *Appendix B*).

Preloading the biomass with $t_0$ metal ions generally resulted in uptake inhibition of $t_{180}$ metals. For $Pb^{2+}$ systems however, preloaded $Sr^{2+}$, $Mn^{2+}$ and $Zn^{2+}$ ions exerted no inhibitory effects. Inhibition uptake levels of $t_{180}$ metals are presented in *Table 3.2.3*.

**Table 3.2.3**: Percentage uptake inhibition of $t_{180}$ metals caused by preloaded $t_0$ metals for *equilibrium studies*.

| | Preloaded $t_0$ metals | | | | | |
|---|---|---|---|---|---|---|
| | $Sr^{2+}$ (1.020)* | $Mn^{2+}$ (1.990) | $Zn^{2+}$ (2.128) | $Cd^{2+}$ (2.713) | $Cu^{2+}$ (2.979) | $Pb^{2+}$ (3.287) |
| $t_{180}$ metal | | | | | | |
| $Sr^{2+}$ | -- | 72 | 49 | 44 | 39 | **100** |
| $Mn^{2+}$ | 19 | -- | 36 | 50 | 51 | 57 |
| $Zn^{2+}$ | 17 | 25 | -- | 51 | 53 | 63 |
| $Cd^{2+}$ | 5 | 20 | 44 | -- | 58 | 65 |
| $Cu^{2+}$ | 3 | 5 | 7 | 8 | -- | 23 |
| $Pb^{2+}$ | 0 | 0 | 0 | 12 | 38 | -- |

* Covalent Index values (see *Appendix B*).

The most marked effect was again exhibited by $Pb^{2+}$, which completely inhibited $Sr^{2+}$ uptake. Similar to above, the inhibition potential of the metal ions followed the order: $Sr^{2+} < Mn^{2+} < Zn^{2+} < Cd^{2+} < Cu^{2+} < Pb^{2+}$, except for $Sr^{2+}$ $t_{180}$ systems. Where $Sr^{2+}$ was the $t_{180}$ ion, the order was $Cu^{2+} < Cd^{2+} < Zn^{2+} < Mn^{2+} < Pb^{2+}$.

### 3.2.2 *Time-course studies*

Equilibrium conditions were reached within 3 h of metal-biomass contact, with 95% saturation occurring within the first 5 min. As illustrated in *Figure 3.2.1*, maximum equilibrium adsorption levels for $Sr^{2+}$, $Cd^{2+}$ and $Cu^{2+}$ were 80, 180 and 210 μmol $g^{-1}$ respectively. On the introduction of $t_{180}$ metals, displacement of preloaded $t_0$ metals was observed for $Cd^{2+}$ and $Cu^{2+}$ additions only. $Cu^{2+}$ displaced $Sr^{2+}$ and $Cd^{2+}$ preloaded levels by 15 and 53% respectively, $Cd^{2+}$ reduced $Sr^{2+}$ and $Cu^{2+}$ levels by 45 and 6%, and $Sr^{2+}$ had no displacing effect on either $Cu^{2+}$ or $Cd^{2+}$. These results are summarised in *Table 3.2.4*.

**Table 3.2.4**: Percentage of $t_0$ metals displaced by the addition of $t_{180}$ metals for *time-course studies*.

| | $t_{180}$ displacing metals | | |
|---|---|---|---|
| | $Sr^{2+}$ | $Cd^{2+}$ | $Cu^{2+}$ |
| * | (1.020) | (2.713) | (2.979) |
| $t_0$ metals | | | |
| $Sr^{2+}$ | -- | 45 | 15 |
| $Cd^{2+}$ | 0 | -- | 54 |
| $Cu^{2+}$ | 0 | 6 | -- |

* Covalent Index values (see *Appendix B*).

As a consequence of preloading the biomass with $t_0$ metals, uptake inhibition of $t_{180}$ metals was detected for all dual metal systems. $Cu^{2+}$ inhibited $Sr^{2+}$ and $Cd^{2+}$ uptake values by 50 and 60% respectively, $Cd^{2+}$ inhibited $Sr^{2+}$ and $Cu^{2+}$ levels by 50 and 10%, and $Sr^{2+}$ inhibited $Cd^{2+}$ and $Cu^{2+}$ by 15% and 4%. These results are summarised in *Table 3.2.5*.

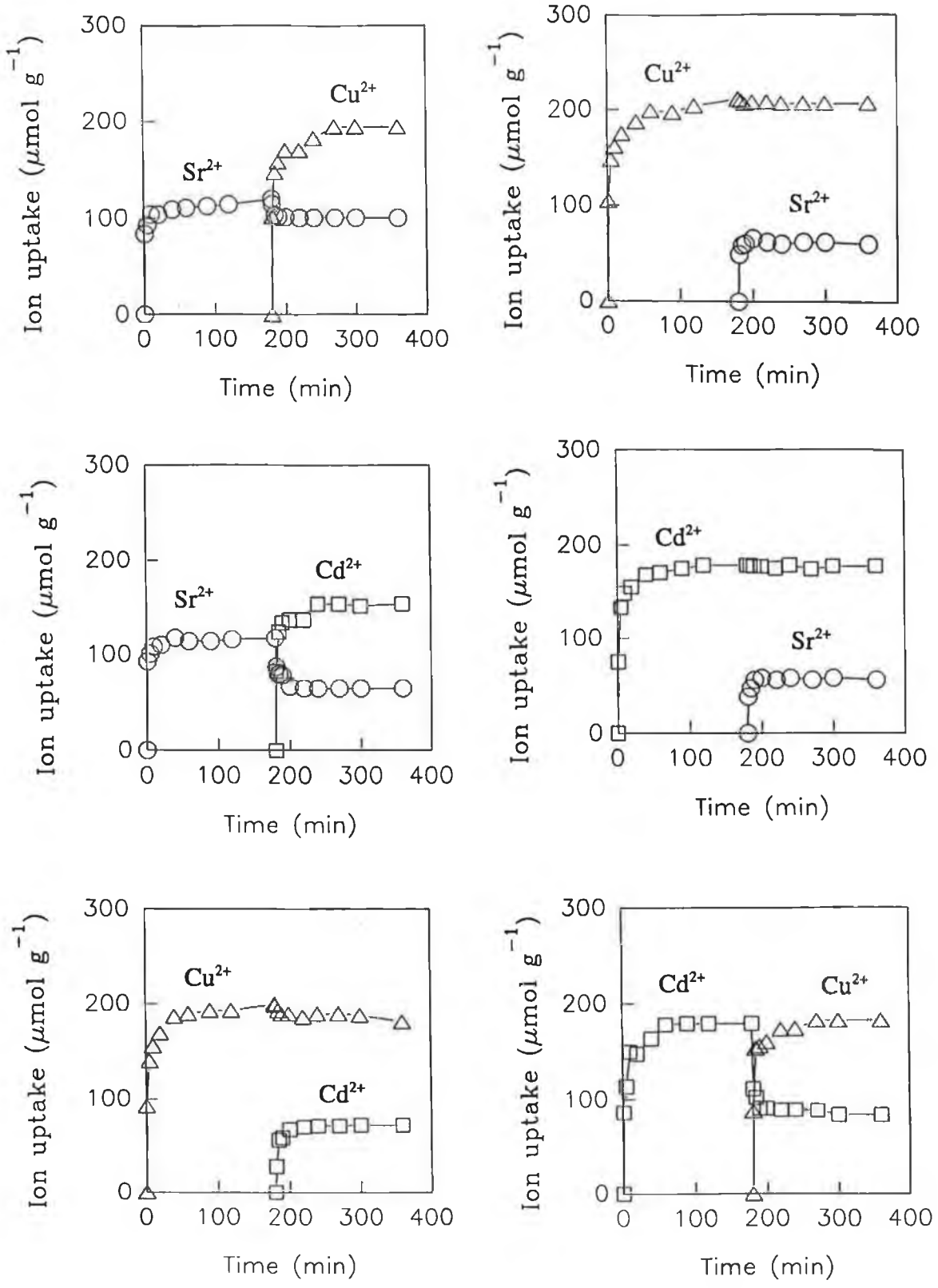


**Figure 3.2.1:** Time profiles of the adsorption of $Sr^{2+}$, $Cd^{2+}$ and $Cu^{2+}$ ions by freeze-dried *Rhizopus arrhizus* biomass, and of the subsequent displacement and inhibition effects when a second metal is introduced into the systems at $t_{180}$. $Sr^{2+}$ ( ○ ), $Cd^{2+}$ ( □ ) and $Cu^{2+}$ ( △ ).

**Table 3.2.5**: Percentage uptake inhibition of $t_{180}$ metals caused by preloaded $t_0$ metals for *time-course studies*.

| | Preloaded $t_0$ metals | | |
|---|---|---|---|
| | $Sr^{2+}$ (1.020) | $Cd^{2+}$ (2.713) | $Cu^{2+}$ (2.979) |
| $t_{180}$ metals | | | |
| $Sr^{2+}$ | -- | 50 | 50 |
| $Cd^{2+}$ | 15 | -- | 60 |
| $Cu^{2+}$ | 4 | 10 | -- |

* Covalent Index values (see *Appendix B*).

Similar to adsorption, displacement and inhibition equilibrium conditions occurred within 3 h of metal-biomass contact, with 95% of the reactions occuring within 5 min.

### 3.2.3 *Error analysis*

Duplicate experiments were performed in all cases, and the results were all found to agree to within limits of 3%.

## 3.3 *Effects of biomass concentration: results*

### 3.3.1 *Isotherm analysis*

The shape of adsorption isotherm curves appear to be independent of solution biomass concentration for $Sr^{2+}$, $Cd^{2+}$ and $Cu^{2+}$. Isotherms determined at biosorbent levels of 0.25, 0.5 and 1 g $l^{-1}$ are combined for each test ion as illustrated in *Figure 3.3.1*, and it is clear that such curves are superimposed. The adsorption data was linearised using the Langmuir adsorption model as illustrated in *Figure 3.3.2*. For each test ion system, the transformed isotherm data determined at the three biomass levels show good fit to a single regression line.

Biosorbent saturation is apparent especially at the lowest biomass concentrations, with $Cu^{2+}$ bound to the highest degree displaying a maximum loading of *ca.* 400 µmol $g^{-1}$ (*Figure 3.3.1*), followed in order by $Cd^{2+}$ and $Sr^{2+}$, with maximum loadings of *ca.* 280 and 130 µmol $g^{-1}$ respectively.

### 3.3.2 *$Ca^{2+}$ and $Mg^{2+}$ release*

For each test ion ($Sr^{2+}$, $Cd^{2+}$ and $Cu^{2+}$) adsorption resulted in the release of $Ca^{2+}$ and $Mg^{2+}$ ions from the fungal biomass, and displacement increased with increasing test ion uptake as illustrated in *Figure 3.3.3* and *Figure 3.3.4* respectively. These two figures show that at all three biosorbent levels, $Ca^{2+}$ and $Mg^{2+}$ displacement plots compiled separately for each test ion appear to be identical. Maximum $Ca^{2+}$ release was constant for each of the test ions at a level of *ca.* 20 µmol $g^{-1}$, whereas maximum $Mg^{2+}$ release was *ca.* 70, 90 and 110 µmol $g^{-1}$ for $Sr^{2+}$, $Cd^{2+}$ and $Cu^{2+}$ respectively.

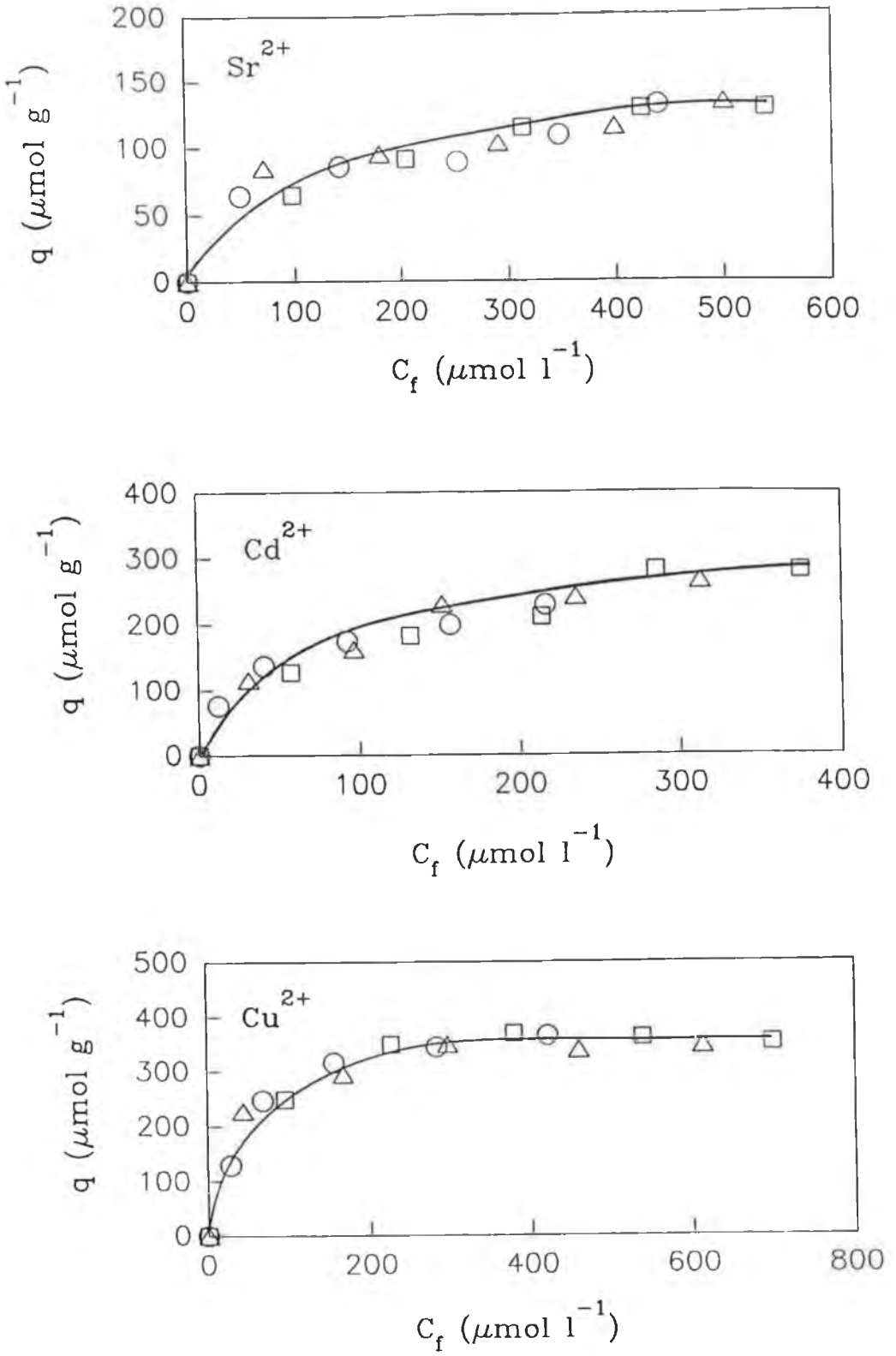


**Figure 3.3.1:** Equilibrium adsorption isotherms for $Sr^{2+}$, $Cd^{2+}$ and $Cu^{2+}$ ions with freeze-dried *Rhizopus arrhizus* biomass. Biomass concentration: 1 $gl^{-1}$ ( ○ ), 0.5 g $l^{-1}$ ( △ ) and 0.25 $gl^{-1}$ ( □ ).

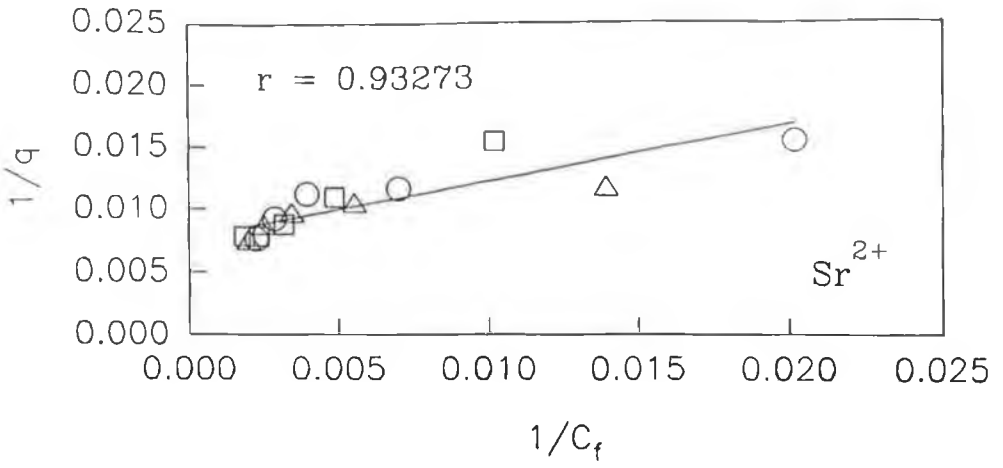


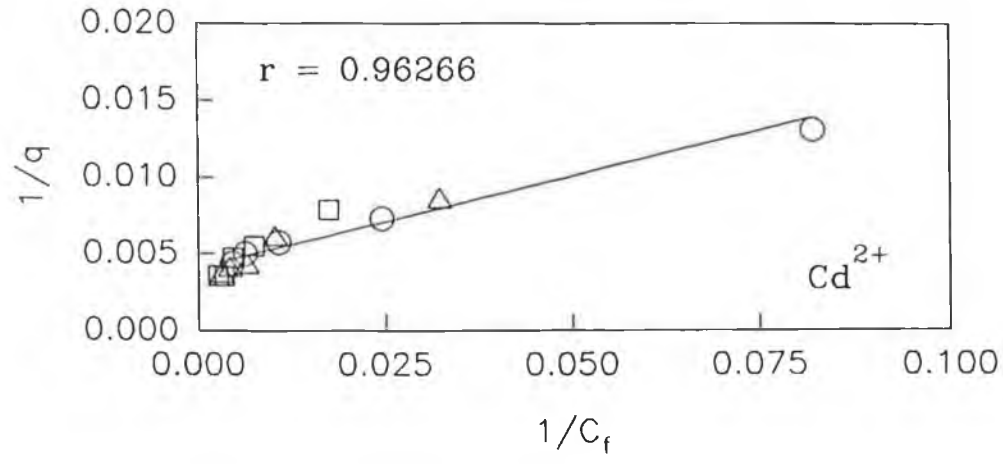


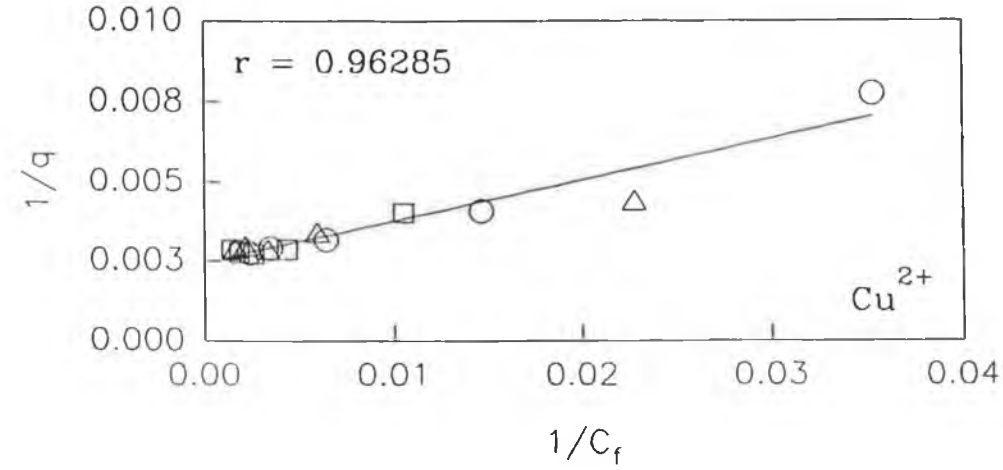


**Figure 3.3.2:** Reciprocal Langmuir plots of $Sr^{2+}$, $Cd^{2+}$ and $Cu^{2+}$ equilibrium adsorption isotherms with freeze-dried *Rhizopus arrhizus* biomass.
Biomass concentration: 1 $gl^{-1}$ ( ○ ), 0.5 g $l^{-1}$ ( △ ) and 0.25 $gl^{-1}$ ( □ ).

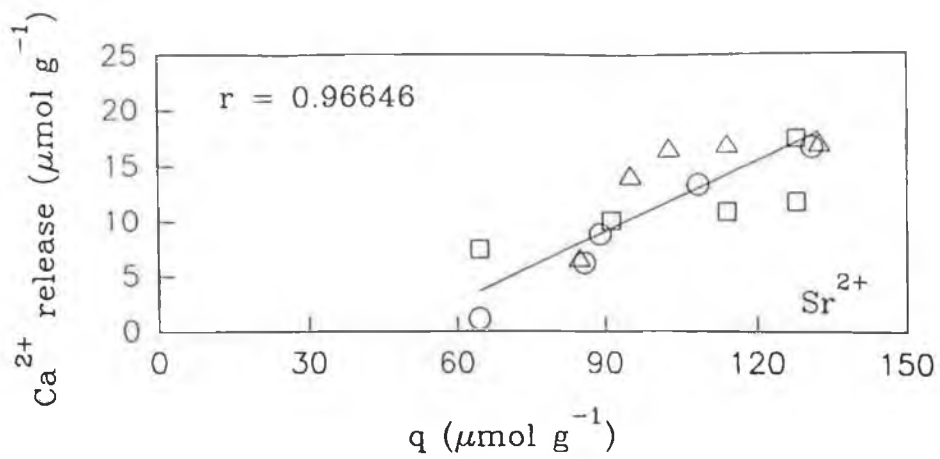


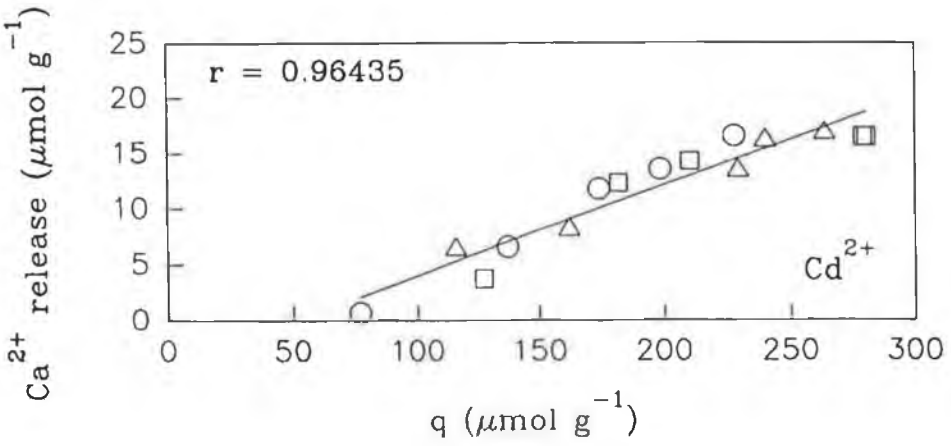


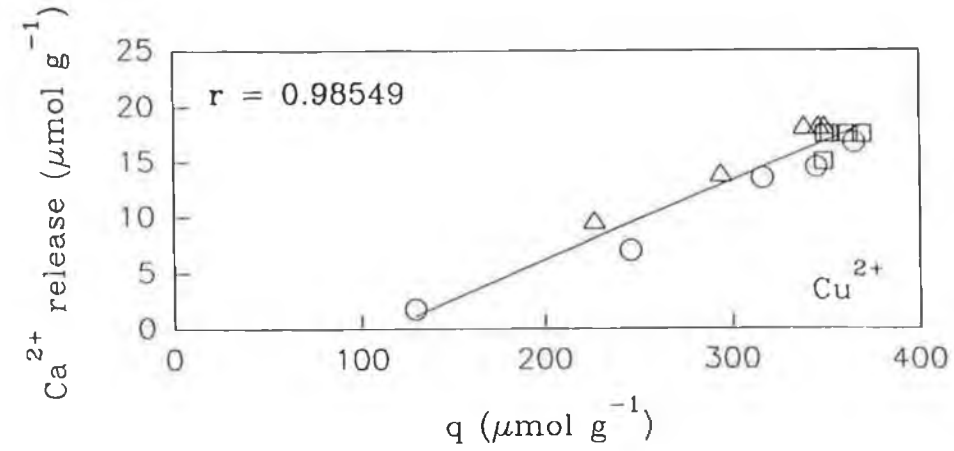


**Figure 3.3.3:** Equilibrium $Ca^{2+}$ ion displacement from freeze-dried *Rhizopus arrhizus* biomass as a consequence of $Sr^{2+}$, $Cd^{2+}$ and $Cu^{2+}$ adsorption, versus metal uptake ($q$).
Biomass concentration: 1 $gl^{-1}$ ( ○ ), 0.5 g $l^{-1}$ ( △ ) and 0.25 $gl^{-1}$ ( □ ).

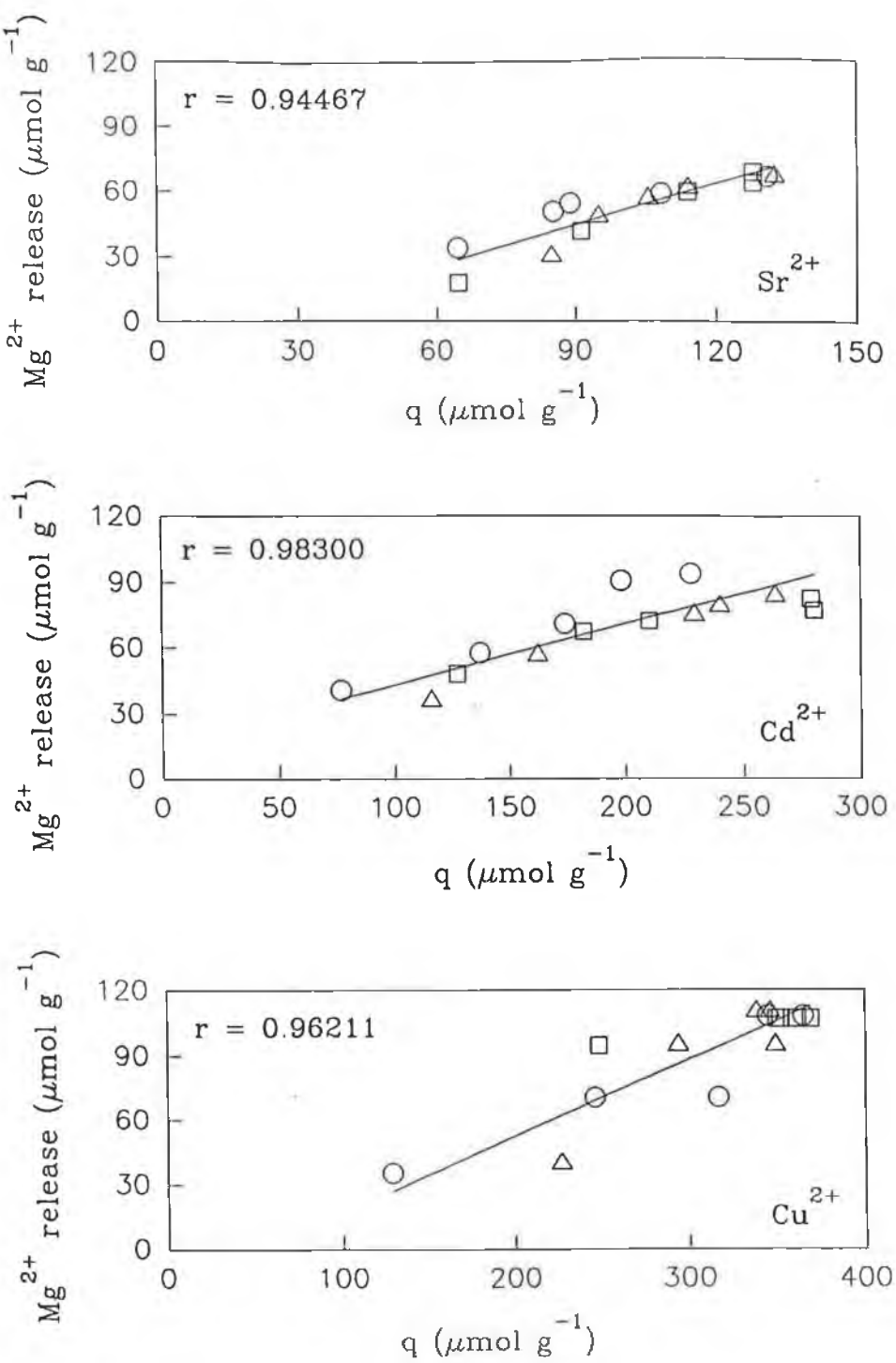


**Figure 3.3.4:** Equilibrium $Mg^{2+}$ ion displacement from freeze-dried *Rhizopus arrhizus* biomass as a consequence of $Sr^{2+}$, $Cd^{2+}$ and $Cu^{2+}$ adsorption, versus metal uptake ($q$).
Biomass concentration: 1 $gl^{-1}$ ( ○ ), 0.5 g $l^{-1}$ ( △ ) and 0.25 $gl^{-1}$ ( □ ).

### 3.3.3 *pH and $H^+$ release*

For $Cd^{2+}$ and $Cu^{2+}$ systems final solution pH values decreased with increasing metal uptake ($q_{uptake}$) as exhibited in *Figure 3.3.5*. Initially all metal solutions were pH balanced to 4, but on introduction of biomass to the metal-free controls, final equilibrium pH values increased to 6.3, 5.9 and 5.4, for 1, 0.5 and 0.25 g $l^{-1}$ additions respectively. At equilibrium these values decreased with $q_{uptake}$, and the lowest values of 5.1 and 4.2 were observed at the lowest biomass concentration of 0.25 g $l^{-1}$ for $Cd^{2+}$ and $Cu^{2+}$ respectively. The pH data was transformed into corresponding $H^+$ ion concentration values, and by subtracting the metal-free control figures, plots of $H^+$ release versus $q_{uptake}$ for $Cd^{2+}$ and $Cu^{2+}$ were made as shown in *Figure 3.3.6*. Generally the graphs exhibit linear increases of $H^+$ displacement with increasing uptake, with maximum $H^+$ release observed at the lowest biomass levels. With decreasing biosorbent levels, maximum displacement values for $Cd^{2+}$ and $Cu^{2+}$ systems were, 2.19, 7.73 and 33.09 $\mu molg^{-1}$, and 49.59, 125.01 and 280.40 $\mu molg^{-1}$, respectively.

Such pH trends were not observed for the $Sr^{2+}$ systems. As before, introduction of biomass to the metal-free controls resulted in final equilibrium pH values of 6.3, 5.9 and 5.4, for 1, 0.5 and 0.25 g $l^{-1}$ additions respectively. This values were found to remain constant with increasing $q_{uptake}$ and did not appear to vary. Hence, no plots of $H^+$ displacement versus $q_{uptake}$ were made since no $H^+$ ions were found to be released.

### 3.3.4 *Error analysis*

Triplicate experiments were performed in all cases, and the results were all found to agree to within limits of 4%.

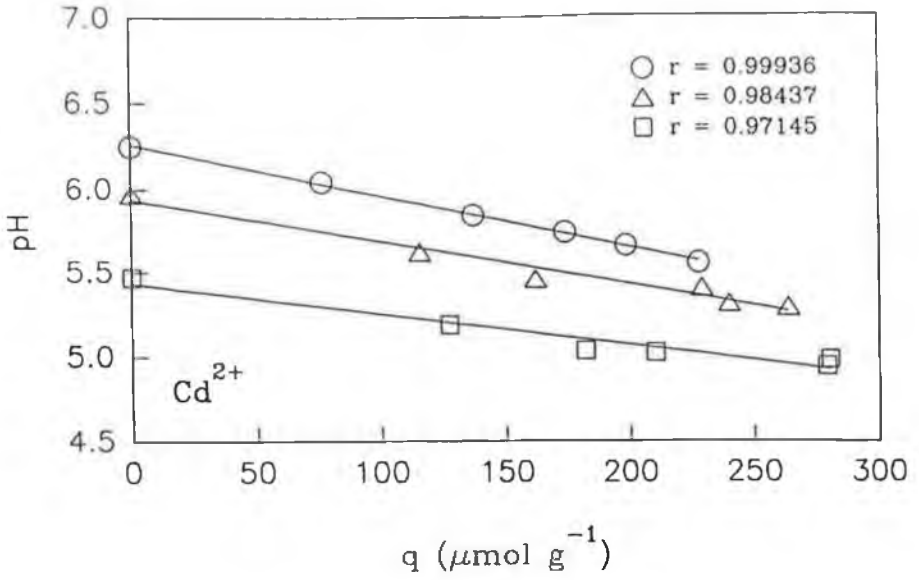


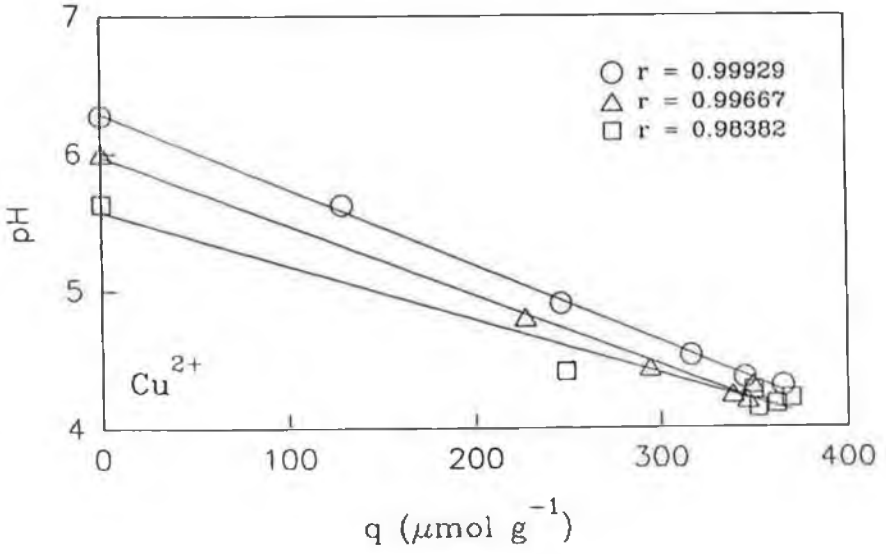


**Figure 3.3.5:** Final pH values at equilibrium versus metal uptake ($q$) for $Cd^{2+}$ and $Cu^{2+}$ freeze-dried *Rhizopus arrhizus* biomass systems.
Biomass concentration: 1 $gl^{-1}$ ( ○ ), 0.5 g $l^{-1}$ ( △ ) and 0.25 $gl^{-1}$ ( □ ).

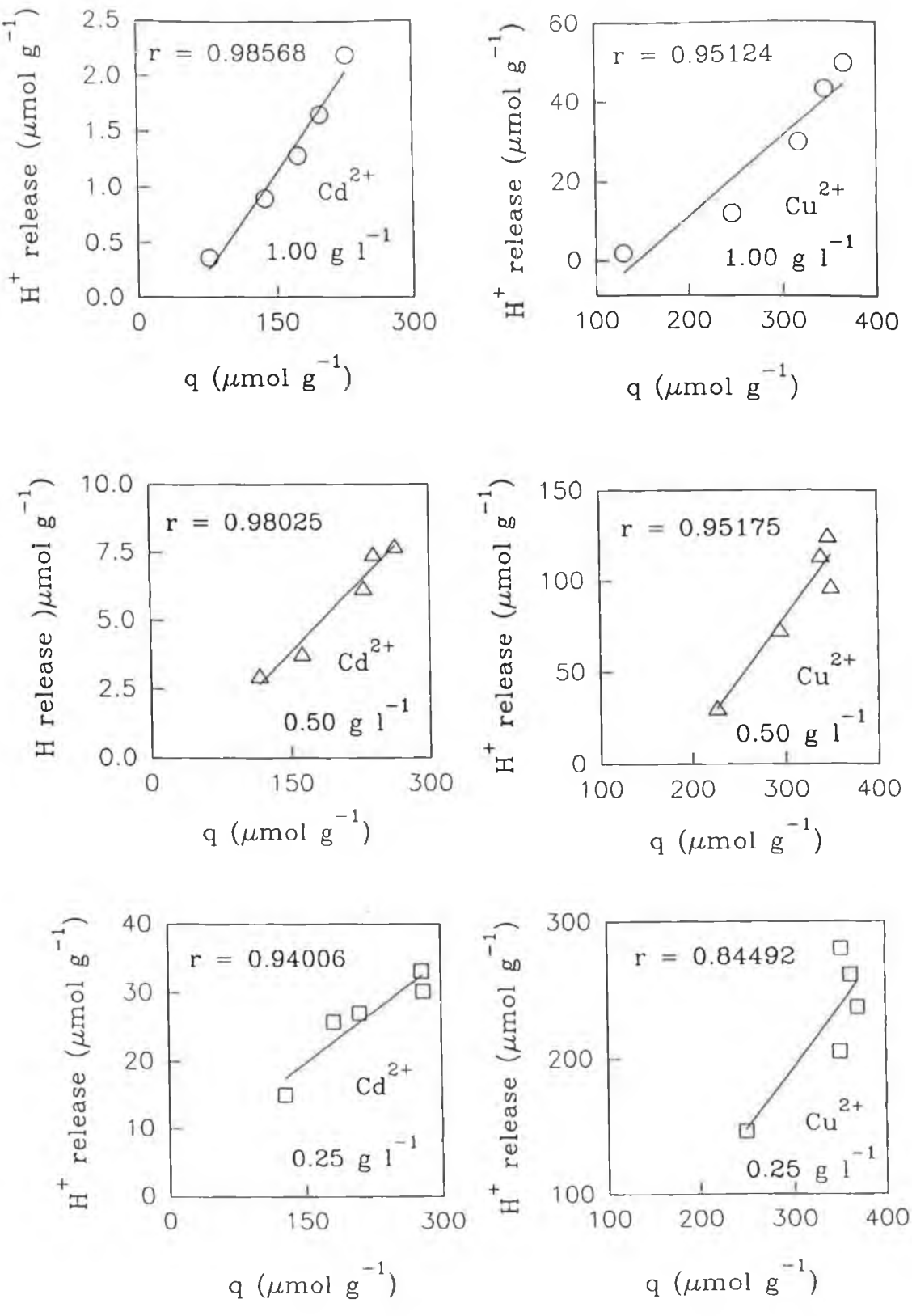


**Figure 3.3.6:** Equilibrium $H^+$ ion displacement from freeze-dried *Rhizopus arrhizus* biomass as a consequence of $Cd^{2+}$ and $Cu^{2+}$ adsorption, versus metal uptake (*q*).
Biomass concentration: 1 $gl^{-1}$ ( ○ ), 0.5 g $l^{-1}$ ( △ ) and 0.25 $gl^{-1}$ ( □ ).

### 3.4 *Continuous flow systems: results*

#### 3.4.1 *Effect of DCM on the biosorbent*

The solvent DCM was found to have no effect on the biosorptive capacity of native freeze-dried *Rhizopus arrhizus* biomass for $Cu^{2+}$ ions, and the $Ca^{2+}$, $Mg^{2+}$ and $H^+$ ion displacement potential of $Cu^{2+}$ was also unaffected. For native and DCM treated freeze-dried *Rhizopus arrhizus* biomass, $Cu^{2+}$ uptake, and corresponding $Ca^{2+}$, $Mg^{2+}$ and $H^+$ release data are tabulated with respect to initial $Cu^{2+}$ concentrations in solution in *Table 3.4.1* and *Table 3.4.2* respectively.

**Table 3.4.1**: $Cu^{2+}$ ion uptake values ($q$) and consequent $Ca^{2+}$, $Mg^{2+}$ and $H^+$ ion displacement at equilibrium using untreated freeze-dried biomass.

| $C_i$ (μmol $l^{-1}$) | 156 | 309 | 749 | 1098 | 1431 | 2623 |
|---|---|---|---|---|---|---|
| $q$ (μmol $g^{-1}$) | 124 | 233 | 329 | 370 | 419 | 430 |
| $Ca^{2+}$ (μmol $g^{-1}$) | 14 | 19 | 24 | 25 | 27 | 28 |
| $Mg^{2+}$ (μmol $g^{-1}$) | 51 | 63 | 99 | 100 | 116 | 123 |
| $H^+$ (μmol $g^{-1}$) | 3 | 18 | 79 | 98 | 112 | 138 |

**Table 3.4.2**: $Cu^{2+}$ ion uptake values ($q$) and consequent $Ca^{2+}$, $Mg^{2+}$ and $H^+$ ion displacement at equilibrium using freeze-dried biomass treated with DCM.

| $C_i$ (μmol $l^{-1}$) | 156 | 309 | 749 | 1098 | 1431 | 2623 |
|---|---|---|---|---|---|---|
| $q$ (μmol $g^{-1}$) | 126 | 234 | 329 | 353 | 400 | 419 |
| $Ca^{2+}$ (μmol $g^{-1}$) | 13 | 16 | 21 | 23 | 25 | 27 |
| $Mg^{2+}$ (μmol $g^{-1}$) | 53 | 62 | 94 | 100 | 116 | 124 |
| $H^+$ (μmol $g^{-1}$) | 3 | 23 | 91 | 110 | 126 | 140 |

Similar results are observed in all cases, with both $q_{uptake}$ and ion release values increasing over the $Cu^{2+}$ range. Overall for both systems, maximum $q_{uptake}$ was the order of *ca.* 425 µmol $g^{-1}$, and maximum $Ca^{2+}$, $Mg^{2+}$ and $H^+$ displacement was *ca.* 28, 124 and 139 µmol $g^{-1}$ respectively.

### **3.4.2** *Effect of PVF immobilisation on the biosorbent*

As with DCM, PVF immobilisation was also observed to have no effect on the biosorptive capacity of native freeze-dried *Rhizopus arrhizus* biomass for $Cu^{2+}$ ions, and the $Ca^{2+}$, $Mg^{2+}$ and $H^+$ ion displacement potential of $Cu^{2+}$ again was unaffected. *Table 3.4.3* shows $Cu^{2+}$ uptake for PVF immobilised freeze-dried *Rhizopus arrhizus* biomass of biosorbent loadings, 40, 50, 60, 70 and 80%, against initial $Cu^{2+}$ ion levels in solution.

**Table 3.4.3:** $Cu^{2+}$ ion uptake values ($q$) at equilibrium using freeze-dried biomass immobilised in PVF, with biomass loading values of 40, 50, 60, 70 and 80%.

| $C_i$ (µmol $l^{-1}$) | 156 | 309 | 749 | 1098 | 1431 | 2623 |
|---|---|---|---|---|---|---|
| $q_{40\%}$ (µmol $g^{-1}$) | 58 | 183 | 231 | 314 | 328 | 413 |
| $q_{50\%}$ (µmol $g^{-1}$) | 112 | 201 | 251 | 314 | 338 | 427 |
| $q_{60\%}$ (µmol $g^{-1}$) | 124 | 218 | 330 | 352 | 372 | 441 |
| $q_{70\%}$ (µmol $g^{-1}$) | 123 | 231 | 320 | 372 | 376 | 441 |
| $q_{80\%}$ (µmol $g^{-1}$) | 127 | 236 | 320 | 371 | 376 | 441 |

Similarly, corresponding $Ca^{2+}$, $Mg^{2+}$ and $H^+$ release data are tabulated in *Tables 3.4.4*, *3.4.5* and *3.4.6* respectively. Over the initial $Cu^{2+}$ concentration range almost identical trends are observed for each loading, $q_{uptake}$ increases to a maximum adsorption levels of *ca.* 440 µmol $g^{-1}$, and $Ca^{2+}$, $Mg^{2+}$ and $H^+$ displacement values increased to maximum values of *ca.* 20, 124 and 109 µmol $g^{-1}$ respectively.

**Table 3.4.4**: Equilibrium $Ca^{2+}$ ion displacement from freeze-dried *Rhizopus arrhizus* biomass immobilised in PVF, with biosorbent loadings of 40, 50, 60, 70 and 80%.

| $C_i$ (µmol $l^{-1}$) | 156 | 309 | 749 | 1098 | 1431 | 2623 |
|---|---|---|---|---|---|---|
| $Ca^{2+}_{40\%}$ (µmol $g^{-1}$) | 0 | 4 | 10 | 14 | 16 | 20 |
| $Ca^{2+}_{50\%}$ (µmol $g^{-1}$) | 0 | 3 | 9 | 13 | 13 | 20 |
| $Ca^{2+}_{60\%}$ (µmol $g^{-1}$) | 0 | 3 | 12 | 15 | 16 | 18 |
| $Ca^{2+}_{70\%}$ (µmol $g^{-1}$) | 0 | 7 | 14 | 14 | 16 | 22 |
| $Ca^{2+}_{80\%}$ (µmol $g^{-1}$) | 0 | 4 | 10 | 14 | 16 | 21 |

**Table 3.4.5**: Equilibrium $Mg^{2+}$ ion displacement from freeze-dried *Rhizopus arrhius* biomass immobilised in PVF, with biomsorbent loadings of 40, 50, 60, 70 and 80%.

| $C_i$ (µmol $l^{-1}$) | 156 | 309 | 749 | 1098 | 1431 | 2623 |
|---|---|---|---|---|---|---|
| $Mg^{2+}_{40\%}$ (µmol $g^{-1}$) | 35 | 49 | 67 | 109 | 103 | 116 |
| $Mg^{2+}_{50\%}$ (µmol $g^{-1}$) | 24 | 59 | 60 | 112 | 133 | 111 |
| $Mg^{2+}_{60\%}$ (µmol $g^{-1}$) | 45 | 70 | 66 | 119 | 130 | 124 |
| $Mg^{2+}_{70\%}$ (µmol $g^{-1}$) | 38 | 84 | 124 | 124 | 135 | 125 |
| $Mg^{2+}_{80\%}$ (µmol $g^{-1}$) | 33 | 82 | 105 | 118 | 130 | 140 |

**Table 3.4.6**: Equilibrium $H^+$ ion displacement from freeze-dried *Rhizopus arrhizus* biomass immobilised in PVF, with biosorbent loadings of 40, 50, 60, 70 and 80%.

| $C_i$ (µmol $l^{-1}$) | 156 | 309 | 749 | 1098 | 1431 | 2623 |
|---|---|---|---|---|---|---|
| $H^+_{40\%}$ (µmol $g^{-1}$) | 6 | 18 | 40 | 56 | 70 | 97 |
| $H^+_{50\%}$ (µmol $g^{-1}$) | 2 | 13 | 43 | 60 | 72 | 106 |
| $H^+_{60\%}$ (µmol $g^{-1}$) | 1 | 13 | 43 | 61 | 74 | 109 |
| $H^+_{70\%}$ (µmol $g^{-1}$) | 2 | 10 | 46 | 66 | 75 | 106 |
| $H^+_{80\%}$ (µmol $g^{-1}$) | 1 | 13 | 51 | 64 | 79 | 114 |

**3.4.3** *Continuous elution of $Cu^{2+}$ ions by PVF immobilised biosorbents*

Effluent $Cu^{2+}$ levels were plotted in the form of breakthrough curves for influent flowrates in the range 3.40-11.63 ml $min^{-1}$. As expected, *Figure 3.4.1*a (breakthrough curves on a time basis) demonstrate that the time required for effluent $Cu^{2+}$ concentrations to equal influent levels (complete breakthrough), increases with decreasing flowrate. Curves plotted with respect to effluent volume as illustrated in *Figure 3.4.1*b are generally similar, and in all cases influent volume required for complete breakthrough was *ca.* 1.4 l. For all columns, displacement of both $Ca^{2+}$ and $Mg^{2+}$ ions was observed to begin immediately upon $Cu^{2+}$ flow, but as cumulative influent volumes increased, ion release values decreased completely to zero. Representative plots of effluent $Ca^{2+}$ and $Mg^{2+}$ levels with respect to volume at 5.88 ml $min^{-1}$ flowrate are illustrated in *Figure 3.4.2*.

By integration of areas under the curves, maximum biosorbent levels of $Cu^{2+}$ uptake and $Ca^{2+}$ and $Mg^{2+}$ displacement were calculated and values tabulated in *Table 3.4.7*.

**Table 3.4.7**: Overall column $Cu^{2+}$ uptake values ($q$) and consequent $Ca^{2+}$ and $Mg^{2+}$ ion displacement over the influent flowrate range 3.40-11.63 ml $min^{-1}$.

| Q ml $min^{-1}$ | q µmol $g^{-1}$ | $Ca^{2+}$ µmol $g^{-1}$ | $Mg^{2+}$ µmol $g^{-1}$ | $Ca^{2+}+Mg^{2+}/q$ |
|---|---|---|---|---|
| 3.40 | 200 | 6 | 34 | 0.20 |
| 5.88 | 201 | 7 | 35 | 0.21 |
| 6.80 | 204 | 10 | 38 | 0.24 |
| 7.25 | 204 | 8 | 46 | 0.26 |
| 10.00 | 211 | 9 | 35 | 0.21 |
| 11.63 | 211 | 10 | 45 | 0.26 |

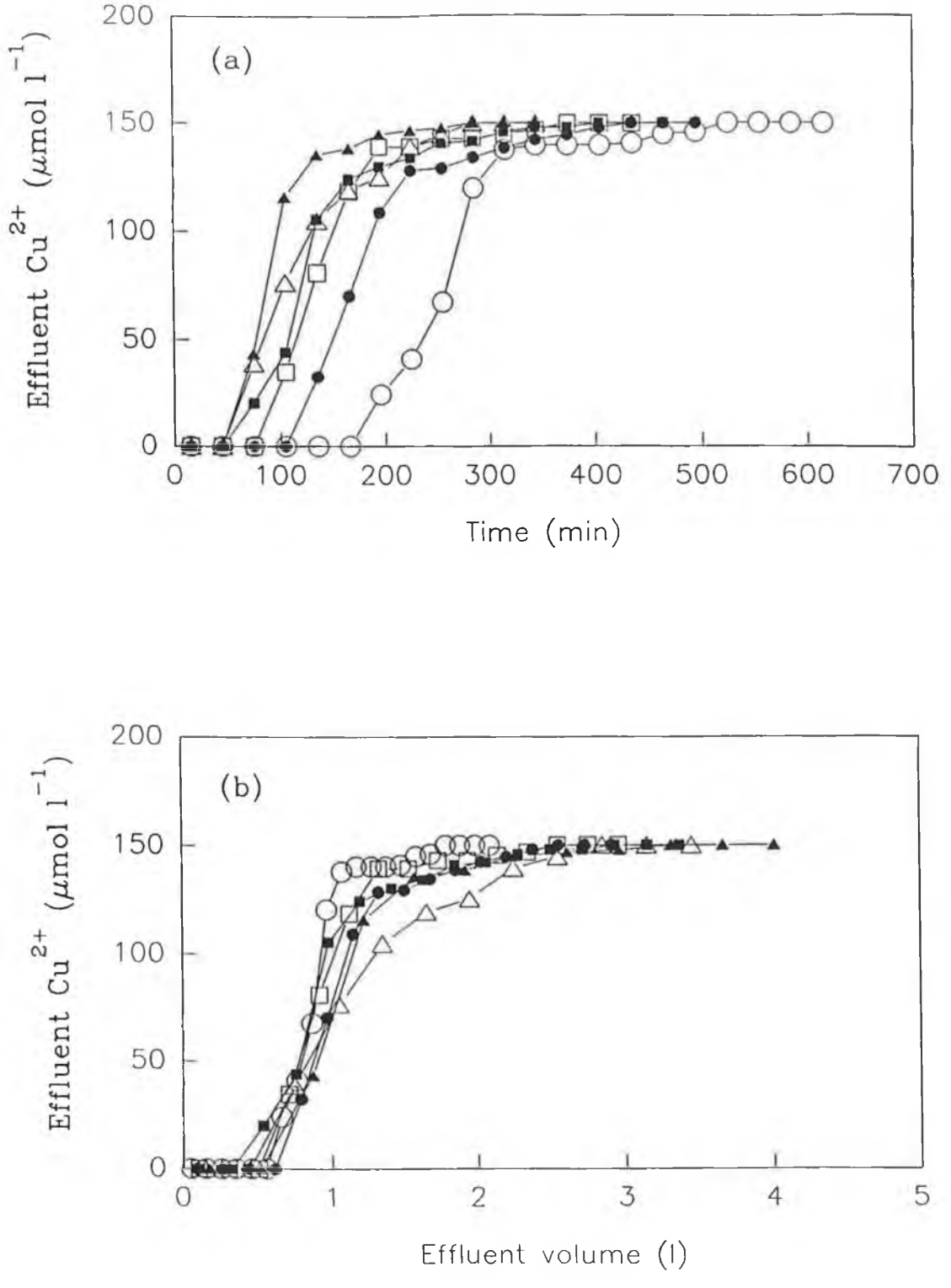


**Figure 3.4.1:** Experimental column breakthrough curves for PVF immobilised *Rhizopus arrhizus* biomass. Effluent $Cu^{2+}$ concentration versus time (a), and effluent $Cu^{2+}$ concentration versus effluent volume (b).
Flowrates (ml $min^{-1}$): 3.40 ( ○ ), 5.88 ( ● ), 6.80 ( □ ), 7.25 ( ■ ), 10.00 ( △ ) and 11.63 ( ▲ ).

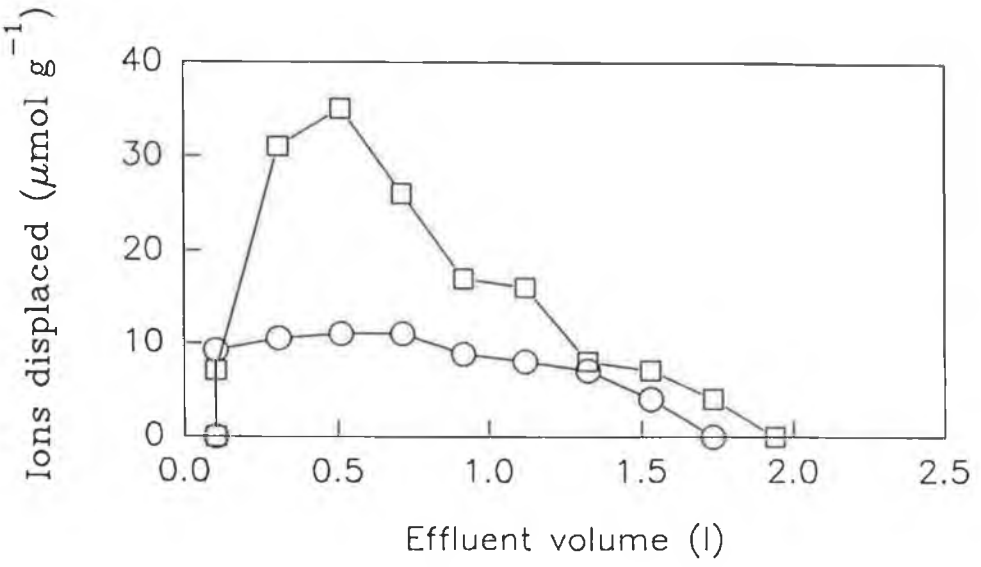


**Figure 3.4.2:** Representative $Ca^{2+}$ and $Mg^{2+}$ ion displacement plots versus effluent volume for PVF immobilised *Rhizopus arrhizus* biomass at an influent flowrate of 5.88 ml $min^{-1}$. $Ca^{2+}$ ( ○ ) and $Mg^{2+}$ ( □ ).

Uptake and displacement data were similar for each of the six columns, and average values were *ca.* 204, 9 and 39 μmol $g^{-1}$ for $Cu^{2+}$ adsorption, and $Ca^{2+}$ and $Mg^{2+}$ release respectively. In all cases, the effluent pH was constant at the influent value of 4. Since no differences in pH were detected, no $H^+$ ion displacement as a result of $Cu^{2+}$ adsorption was evident from any of the column biosorbents.

**3.4.4** *Application of mathematical model to breakthrough curves*

Using the model described in *section 2.4.3*, values of σ were calculated for each breakthrough curve. The quantity $\sigma^2$ was found to be proportional to $Q$ / $L$, where $Q$ is the flowrate, and $L$ is the column length. Since $L$ remained constant for each of the columns, a direct relationship between $\sigma^2$ and $Q$ was observed as illustrated in *Figure 3.4.3*a, and is represented mathematically by *equation 3.4.1.*

$$\sigma^2 = k_1 Q \qquad (3.4.1)$$

where $k_1$ is a constant.

According to Belter *et al.* (1988), this demonstrates that both dispersion and the kinetics of adsorption are the rate controlling steps.

A direct relationship between $t_{50}$ and $Q^{-1}$ was also found, as shown in *Figure 3.4.3*b, and is represented mathematically by *equation 3.4.2.*

$$t_{50} = k_2 / Q \qquad (3.4.2)$$

where $k_2$ is a constant value.

Using the constants $k_1$ and $k_2$ calculated from *equation 3.4.1* and *equation 3.4.2*, theoretical values of σ and $t_{50}$ were calculated for each experimental plot. Effluent $Cu^{2+}$ concentration values ($C$) were then determined and theoretical curves were plotted as

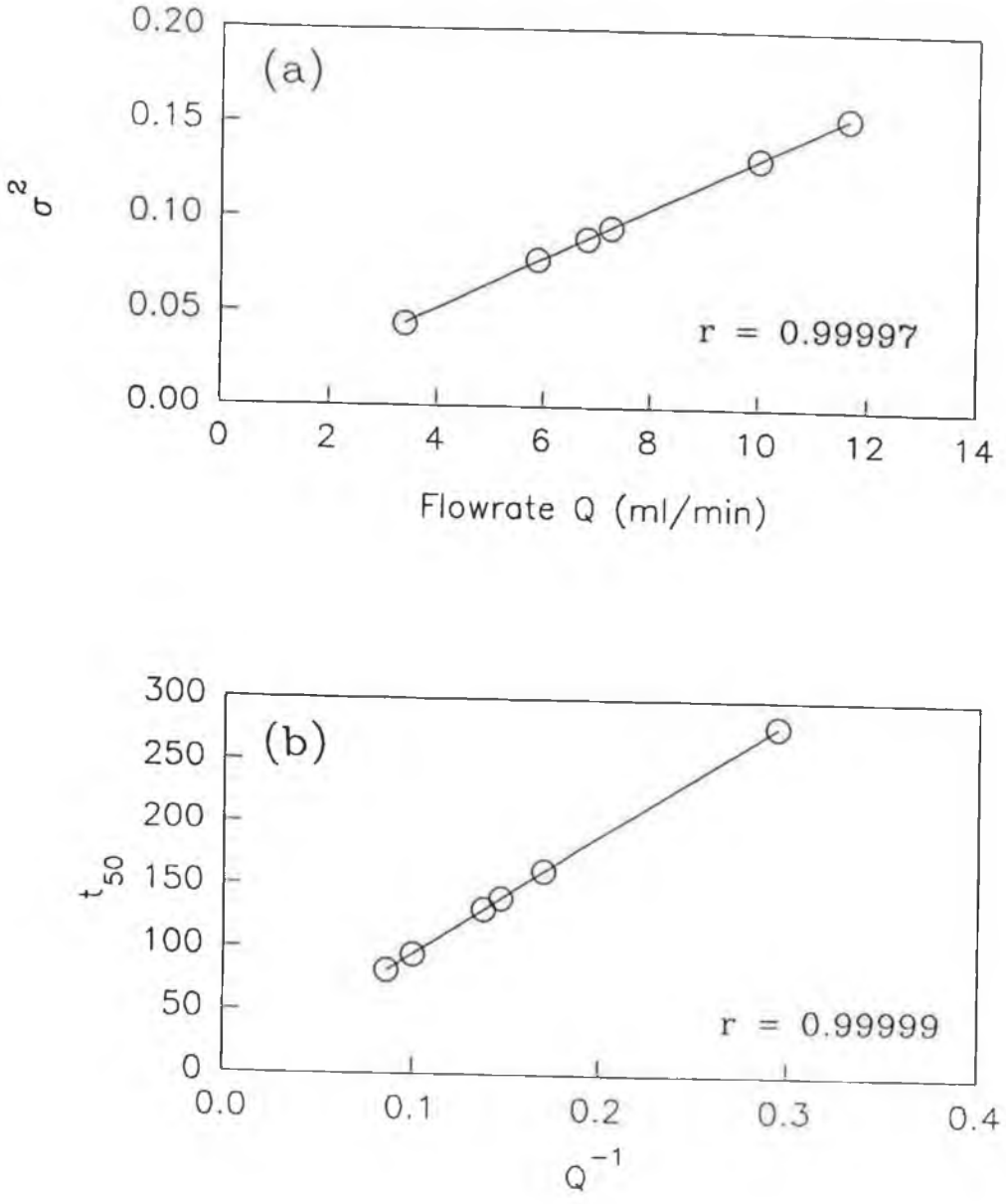


**Figure 3.4.3:** (a) Plots of $\sigma^2$ versus Q (influent flowrate), and (b) $t_{50}$ versus $Q^{-1}$, for PVF immobilised *Rhizopus arrhizus* biomass over the column influent flowrate range 3.40-11.63 ml $min^{-1}$.

illustrated in *Figure 3.4.4*. The theoretical curves (closed circles) predicted by this two parameter fixed-bed adsorption model are in close agreement with the corresponding experimental plots (open circles).

As with the experimentally determined breakthrough curves (*Figure 3.4.1*a), theoretical plots on a time basis demonstrate that complete breakthrough times (when $C = C_i$) decrease with increasing flowrate as shown in *Figure 3.4.5*a. Theoretical curves plotted with respect to volume appear to be superimposed as illustrated *Figure 3.4.5*b, and similar to *Figure 3.4.1*b, influent volumes required for complete breakthrough was *ca.* 1.4 l in all cases.

### **3.4.5** *Error analysis*

Duplicate experiments were performed in all cases, and the results were all found to agree to within limits of 6%.

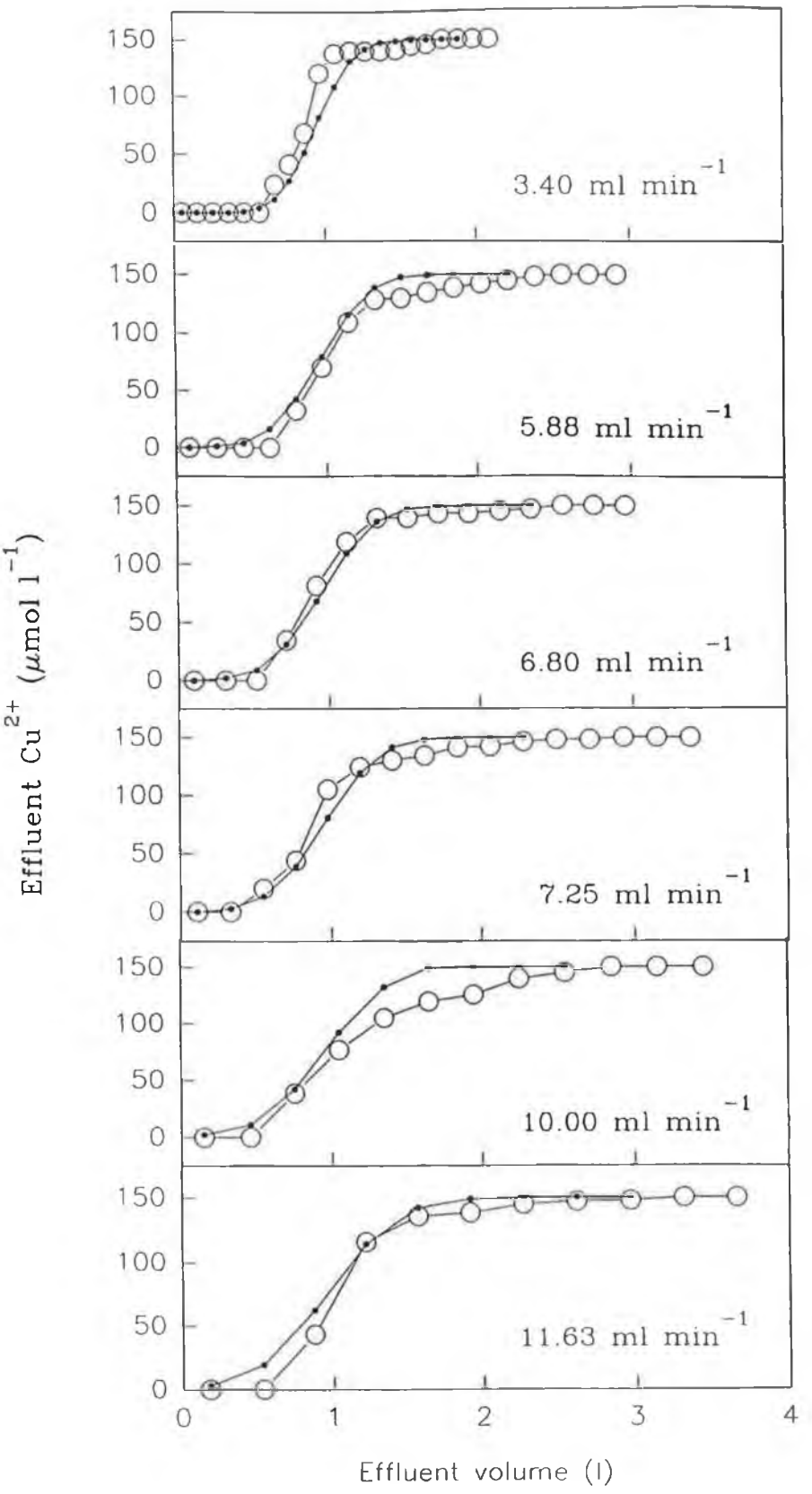


**Figure 3.4.4:** Mathematically predicted (*two parameter fixed-bed adsorption model*) and experimental column breakthrough curves ($Cu^{2+}$ effluent concentrations versus effluent volumes).
Mathematically predicted ( ● ) and experimental ( ○ ).

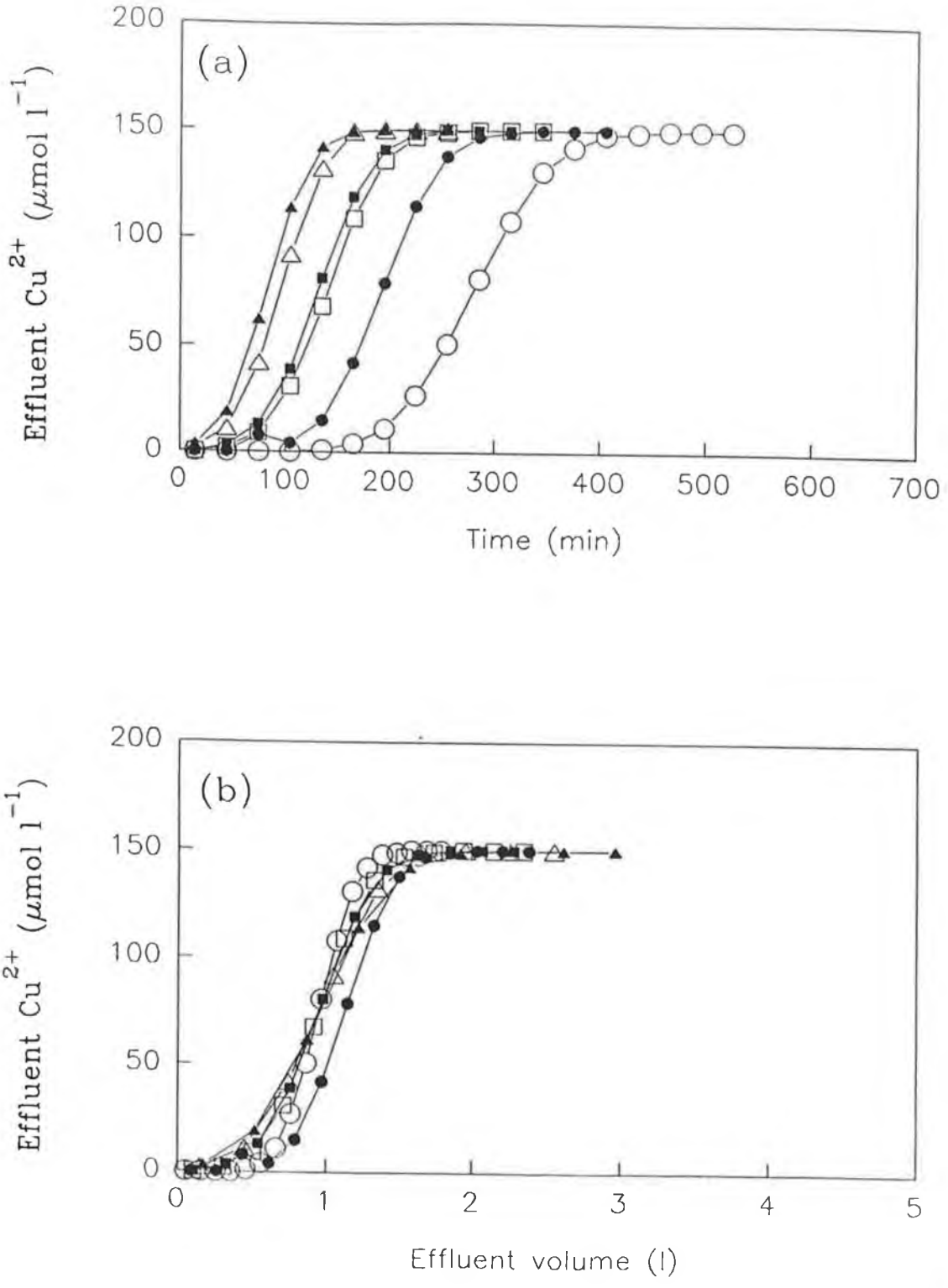


**Figure 3.4.5:** Mathematically predicted (*two parameter fixed-bed adsorption model*) column breakthrough curves for PVF immobilised *Rhizopus arrhizus* biomass. Effluent $Cu^{2+}$ concentration versus time (a), and effluent $Cu^{2+}$ concentration versus effluent volume (b).
Flowrates (ml $min^{-1}$): 3.40 ( ○ ), 5.88 ( ● ), 6.80 ( □ ), 7.25 ( ■ ), 10.00 ( △ ) and 11.63 ( ▲ ).

### 3.5 *Selenite adsorption studies: results*

#### 3.5.1 *Isotherm type analysis*

Selenite was not adsorbed to any detectable levels by live non-metabolising biomasses of *Rhizopus arrhizus* and a *Penicillium* species, but appreciable quantities of $Ca^{2+}$, $Mg^{2+}$, $H^+$ and $K^+$ ions were released into the aqueous environments. Isothermal type data, in the form of $q_{uptake}$ and $Ca^{2+}$, $Mg^{2+}$, $H^+$ and $K^+$ displacement (µmol $g^{-1}$), are tabulated with respect to an increasing external selenite concentration range 125-2111 µmol $l^{-1}$ for both fungi in *Table 3.5.1* and *Table 3.5.2*.

**Table 3.5.1**: $Ca^{2+}$, $Mg^{2+}$, $H^+$ and $K^+$ ion release at equilibrium following selenite-microbe contact with live non-metabolising *Rhizopus arrhizus* biomass.

| $C_i$ (µmol $l^{-1}$) | 125 | 248 | 603 | 1151 | 2111 |
|---|---|---|---|---|---|
| q (µmol $g^{-1}$) | 0 | 0 | 0 | 0 | 0 |
| $Ca^{2+}$ (µmol $g^{-1}$) | 1 | 2 | 4 | 6 | 10 |
| $Mg^{2+}$ (µmol $g^{-1}$) | 24 | 36 | 72 | 72 | 77 |
| $H^+$ (µmol $g^{-1}$) | 3 | 7 | 12 | 19 | 27 |
| $K^+$ (µmol $g^{-1}$) | 22 | 40 | 52 | 63 | 73 |

**Table 3.5.2**: $Ca^{2+}$, $Mg^{2+}$, $H^+$ and $K^+$ ion release at equilibrium following selenite-microbe contact with live non-metabolising biomass of a *Penicillium* species.

| $C_i$ (µmol $l^{-1}$) | 125 | 248 | 603 | 1151 | 2111 |
|---|---|---|---|---|---|
| q (µmol $g^{-1}$) | 0 | 0 | 0 | 0 | 0 |
| $Ca^{2+}$ (µmol $g^{-1}$) | 8 | 11 | 35 | 47 | 45 |
| $Mg^{2+}$ (µmol $g^{-1}$) | 1 | 4 | 44 | 53 | 60 |
| $H^+$ (µmol $g^{-1}$) | 1 | 1 | 27 | 45 | 66 |
| $K^+$ (µmol $g^{-1}$) | 86 | 155 | 297 | 302 | 364 |

Selenite uptake was not detected over the metalloid oxyanion concentration range with $q$ values remaining at zero, but $Ca^{2+}$, $Mg^{2+}$, $H^+$ and $K^+$ ion release increased with increasing selenite levels. Maximum release values for $Ca^{2+}$, $Mg^{2+}$, $H^+$ and $K^+$ were *ca.* 10, 77 27 and 73 μmol $g^{-1}$ respectively for *Rhizopus arrhizus*, and *ca.* 45, 60, 66 and 364 μmol $g^{-1}$ for the *Penicillium* species.

### **3.5.2** *Error analysis*

Duplicate experiments were performed in all cases, and the results were all found to agree to within limits of 3%.

### 3.6 *Selenite transformation studies: results*

#### 3.6.1 *Growth of the* Penicillium *species in the absence of selenite*

For the *Penicillium* species grown in the absence of selenite, no background selenium was detected either in the aqueous phase or associated with the biomass, and no volatile selenium compounds were isolated from the activated charcoal traps. The pattern of growth is illustrated in *Figure 3.6.1*. After inoculum addition growth immediately entered an approximately linear growth phase which continued to day 10 resulting in a maximum biomass dry weight of *ca.* 5.9 g $l^{-1}$. A stationary growth phase was observed from days 10-12 and thereafter growth appeared to enter a decline phase. After day 14 maximum biomass dry weight was of the order *ca.* 5.4 g $l^{-1}$ (*Figure 3.6.1*a). The initial pH of the medium was 4.20 and decreased to 3.09 on addition of the inoculum. The pH decreased steadily with time to a value of 1.89 during the growth phase and remained constant during the stationary phase. After day 12 the pH slowly increased to a final value of 1.94 on day 14 (*Figure 3.6.1*b). Results are from one of three experiments, all of which were in agreement to within limits of 4%.

#### 3.6.2 *Growth of the* Penicillium *species in the presence of selenite*

A total of *ca.* 440 μmol of volatile selenium compounds were isolated from activated charcoal traps exposed to exhaust gases of the *Penicillium* species grown in the presence of selenite by the methanol extraction technique described in section *2.6.2.4*. Total selenium extracted from each trap is tabulated in *Table 3.6.1*. Average values of 184 and 256 μmol of selenium were isolated from the first and second series of activated charcoal traps extracted after weeks 1 and 2 respectively.

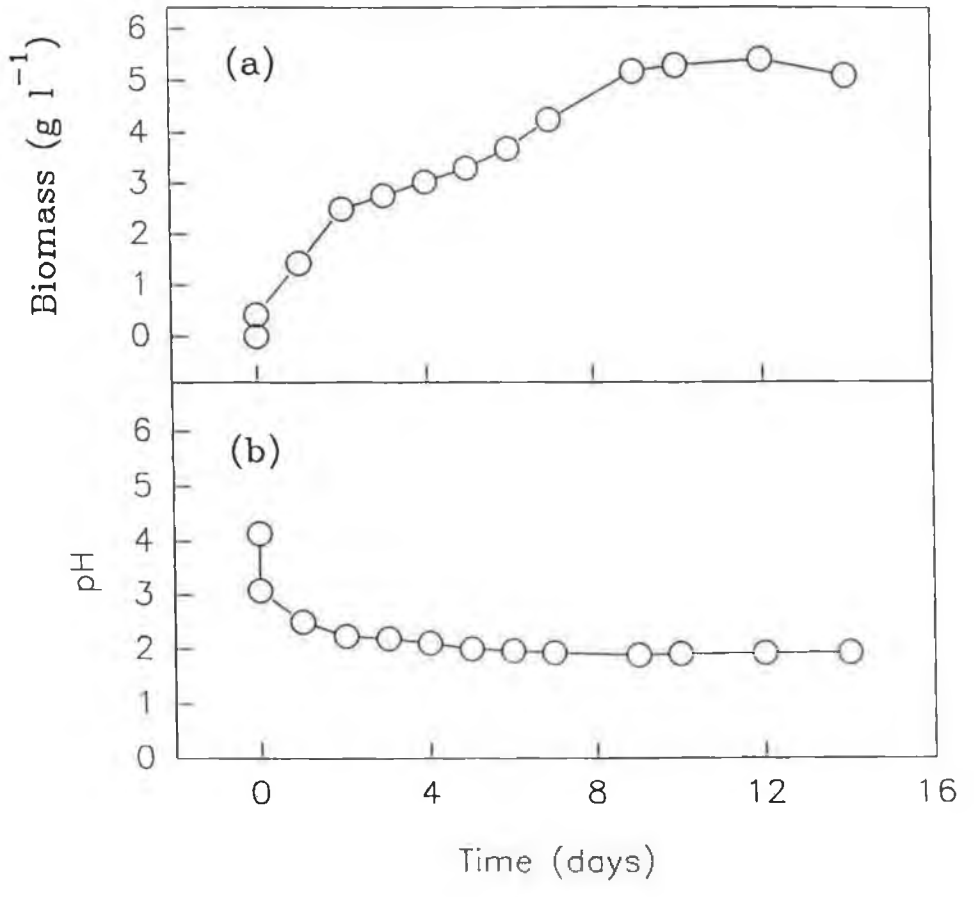


**Figure 3.6.1:** Growth of the *Penicillium* species in the absence of selenite. Biomass growth is shown in (a) and the pH change in the culture medium is shown in (b). Typical results from one of three experiments are shown all of which gave similar results: experimental points are averages of two determinations. Vertical error bars representing standard error of the mean (SEM) are smaller than the dimensions of the symbols and are subsequently not shown.

**Table 3.6.1**: Volatile selenium compounds recovered from activated charcoal traps during growth of the *Penicillium* species in a bioreactor containing 5000 µmol of sodium selenite. The first and second series of traps were harvested for analysis after weeks 1 and 2 respectively, and three traps in series were used for each week. Typical results from one of three experiments are shown all of which gave similar results. Quoted values are averages of two determinations that agreed to within limits of 5%.

| Series | Trap | Selenium Recovered (µmol) | Total (µmol) |
|---|---|---|---|
| First | 1 | 73 | |
| | 2 | 61 | |
| | 3 | 50 | 184 |
| Second | 1 | 119 | |
| | 2 | 96 | |
| | 3 | 41 | 256 |
| Overall total | | | 440 |

Fungal growth in the presence of 1000 µmol $l^{-1}$ of selenite is illustrated in *Figure 3.6.2*. A slight lag phase was noticeable from days 0-1 with growth commencing on day 2. Again a linear growth phase was observed and this continued until day 10. Growth began to level off at this point and entered a stationary phase resulting in an overall maximum biomass concentration of *ca.* 6.0 g $l^{-1}$. On day 11 a decline phase commenced and a final biomass concentration of *ca.* 5.5 g $l^{-1}$ was recorded on day 14 (*Figure 3.6.2*a). It is noteworthy that the colour of the bioreactor contents were identical to the selenite-free reactors up until day 11, but from days 11-14 a red colour prevailed.

The initial pH of the selenite rich medium was 6.10, but this rapidly decreased to pH 3.00 on addition of the inoculum. The pH decreased steadily during the linear growth phase to a minimum value of 2.02 on day 11 and increased slightly to a final value of 2.09 on day 14 (*Figure 3.6.2*b).

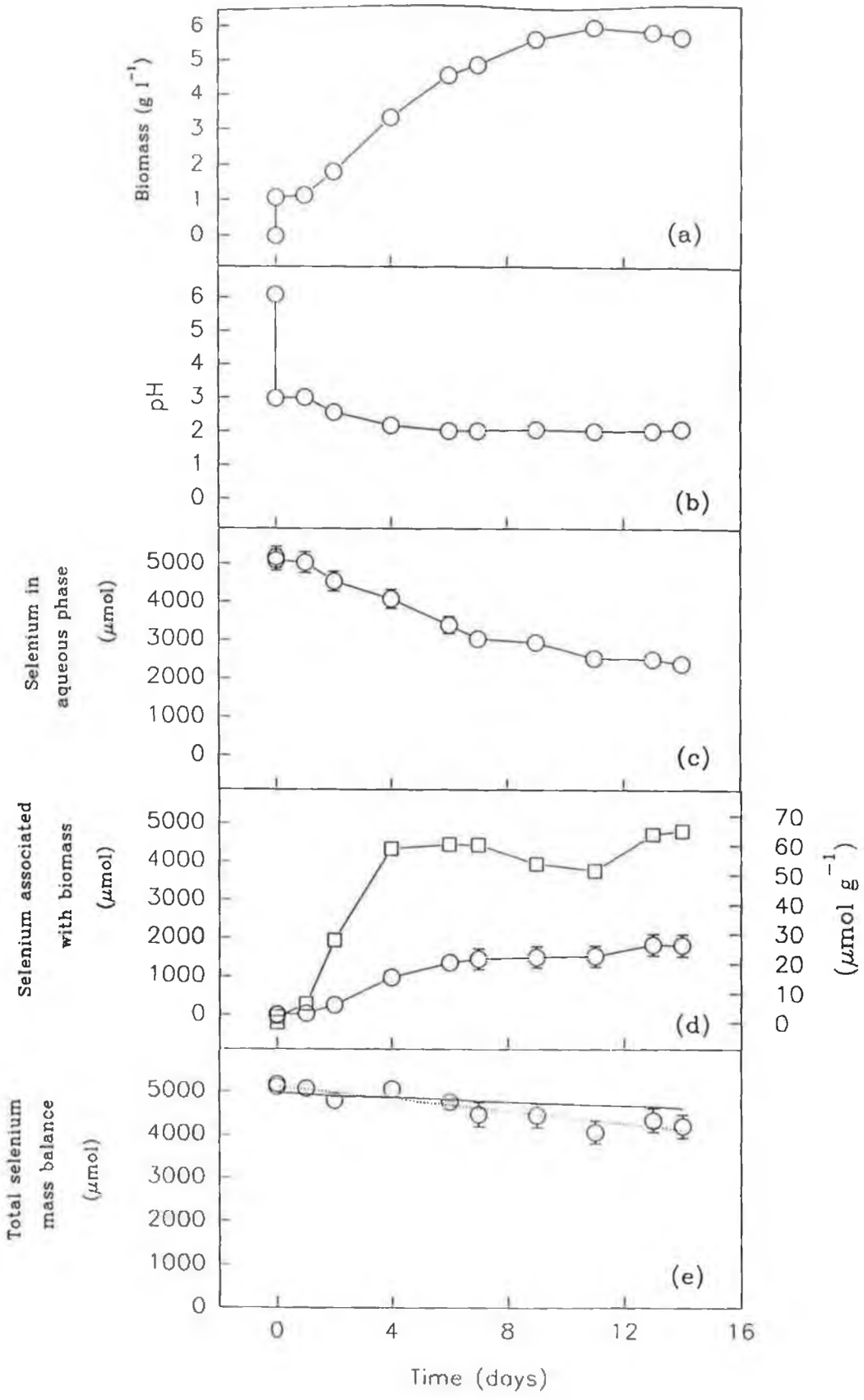


**Figure 3.6.2:** Growth of the *Penicillium* species in the presence of 1000 $\mu$mol $l^{-1}$ sodium selenite (complete legend on the following page).

**Figure 3.6.2:** Growth of the *Penicillium* species in the presence of 1000 $\mu$mol $l^{-1}$ sodium selenite. Biomass growth is shown in (a) and the changes in the pH of culture medium is shown in (b). Total selenium remaining in the aqueous phase is shown in (c). In (d) total selenium associated with the biomass (*open circles*) and selenium per unit biomass dry weight (*open squares*) are profiled. The total selenium mass balance is plotted in (e). The continuous line represents the total selenium theoretically present in the bioreactor allowing for selenium loss in sample volumes. The open circles represent total selenium experimentally determined in the aqueous phase together with that associated with the biomass regressed with a best fit line (dash line). The differences between these two lines represent loss of selenium from the system by volatilisation. Typical results from one of three experiments are shown all of which gave similar results: experimental points are averages of two determinations. Vertical error bars represent standard error of the mean (SEM) shown when these exceed dimensions of the symbols.

From an initial value of *ca.* 5000 µmol of selenium present in each bioreactor total selenium in solution decreased to *ca.* 2540 µmol during the rapid growth phase and further declined steadily to a final value of *ca.* 2510 µmol on day 14 (*Figure 3.6.2*c). Total selenium associated with the fungal biomass increased with increasing biomass concentrations to *ca.* 1530 µmol during the rapid growth phase. During the decline phase total selenium associated with the biomass continued to increase to a final value of *ca.* 1830 µmol on day 14. On a dry weight basis, selenium accumulation by the *Penicillium* species was most rapid during the phase of fastest growth and increased to a level of *ca.* 60 µmol (g dry weight)$^{-1}$ after 4 days (*Figure 3.6-2*d).

On day 14 total selenium in the aqueous phase and associated with the biomass was calculated at *ca.* 4340 µmol. Since *ca.* 5000 µmol of selenium were present initially in the reactor, *ca.* 660 µmol were lost over the 2 wk period. A total of *ca.* 440 µmol of selenium in the form of volatiles were isolated from the activated charcoal traps leaving *ca.* 220 µmol unaccounted for. The sum of selenium associated with the biomass and in the aqueous phase decreased with respect to time reflecting the selenium loss from the system, and this loss was gradual over the 2 wk period as illustrated in *Figure 3.6.2e*. As above, results are from one of three experiments, all of which were in agreement to within limits of 6%.

**3.6.3** *Biomass-free controls*

No volatile selenium compounds were isolated from activated charcoal traps exposed to biomass-free reactor exhaust gases, and reactor contents remained clear with no formation of a red colour. Total selenium in the aqueous phase was constant at 1000 µmol l$^{-1}$, and the pH after introduction of selenite remained at 6.60.

### 3.7 *Transformation enhancement studies: results*

#### 3.7.1 *Selenite volatilisation enhancement*

The transformation of selenite to volatile selenium compounds was not enhanced by single 50 ml DMEM additions, either at $t_0$ or on day 7. However two 25 ml DMEM additions, one at $t_0$ and the other on day 7, appeared to stimulate volatilisation significantly. Quantities of volatile selenium compounds extracted from activated charcoal traps are displayed in *Table 3.7.1*. For the case of a single DMEM addition at $t_0$, a total of 421 µmol of selenium were isolated, 202 µmol between $t_0$ and day 7, and 219 µmol betweens days 7-14. During the same time period for the bioreactor amended with two DMEM aliquots, 303 and 313 µmol were extracted respectively, totalling 616 µmol. For a single DMEM amendment at day 7, a total of 442 µmol were detected, 202 and 240 before and after addition respectively.

#### 3.7.2 *Effects of DMEM on biomass growth and pH*

A single 50 ml DMEM addition at $t_0$ appeared to have an inhibitory effect on the growth of the *Penicillium* species for the first 7 days, but from day 8 to day 14, biomass levels increased rapidly. For two 25 ml DMEM additions, one at $t_0$ and the other on day 7, biomass growth was linear over the 2 wk period. For the case of a single 50 ml DMEM addition on day 7, biomass growth was linear from $t_0$ to day 7, but from day 7 to day 14, growth appeared to enter into a decline phase. Maximum biomass levels were observed for systems amended with a single 50 ml DMEM addition at $t_0$.

**Table 3.7.1**: Volatile selenium compounds recovered from activated charcoal traps during growth of a *Penicillium* species in 5 l of media amended with 50 ml of DMEM and 5000 µmol of sodium selenite. The first and second series of traps were harvested for analysis after weeks 1 and 2 respectively, and four traps in series were used for each week. Quoted values are averages of two determinations that agreed to within limits of 5%.

| Series | Trap | Selenium Recovered (µmol) | Total (µmol) |
|---|---|---|---|
| **50 ml DMEM addition at $t_0$** | | | |
| First | 1 | 62 | |
| | 2 | 48 | |
| | 3 | 46 | |
| | 4 | 46 | 202 |
| Second | 1 | 61 | |
| | 2 | 58 | |
| | 3 | 52 | |
| | 4 | 48 | 219 |
| Overall total | | | 421 |
| **25 ml DMEM additions at $t_0$ and day 7** | | | |
| First | 1 | 115 | |
| | 2 | 68 | |
| | 3 | 68 | |
| | 4 | 52 | 303 |
| Second | 1 | 92 | |
| | 2 | 85 | |
| | 3 | 75 | |
| | 4 | 61 | 313 |
| Overall total | | | 616 |
| **50 ml DMEM addition at day 7** | | | |
| First | 1 | 53 | |
| | 2 | 50 | |
| | 3 | 50 | |
| | 4 | 49 | 202 |
| Second | 1 | 69 | |
| | 2 | 65 | |
| | 3 | 53 | |
| | 4 | 53 | 240 |
| Overall total | | | 442 |

For a 50 ml DMEM addition at $t_0$, biomass growth was slow from days 0-7, increasing from *ca.* 0.6 g $l^{-1}$ to 2.0 g $l^{-1}$ (*Figure 3.7.1*a). From days 7-10, growth increased rapidly to *ca.* 6.8 g $l^{-1}$, and advanced to 7.5 g $l^{-1}$ on day 14. The pH of the inoculated media decreased steadily from 3.30 to 1.90 over the 14 day period (*Figure 3.7.2*a). For two 25 ml DMEM additions, the first at $t_0$ and the second on day 7, biomass increased almost in a straight line, from *ca.* 0.6 g $l^{-1}$ at $t_0$, to *ca.* 3.0 g $l^{-1}$ on day 7, and to *ca.* 6.0 g $l^{-1}$ on day 14 (*Figure 3.7.1*b). The pH decreased from 3.30 to 1.95 over the test period (*Figure 3.7.2*b), and the second 25 ml aliquot addition of DMEM on day 7 did not noticeably affect the pH profile. For a 50 ml addition on day 7, biomass growth was linear from *ca.* 0.6 g $l^{-1}$ at $t_0$, to a maximum value of *ca.* 5.8 g $l^{-1}$ on day 7 (*Figure 3.7.1*c). From days 7-14, a decline phase was observed, and the biomass level decreased to a minimum value of *ca.* 4.9 g $l^{-1}$. The pH decresed slowly from 3.80 at $t_0$ to a final value of 1.98 on day 14.

**3.7.3** *Selenium in the aqueous phase and associated with the biomass: DMEM effects*

Selenite remaining in the aquous phase and associated with the biomass were constant after the 2 wk periods in all cases of DMEM additions. Upon fungal inoculation at $t_0$, selenite in the aqueous phase immediately decreased from a total of *ca.* 5000 to *ca.* 3750 µmol for both cases where DMEM was present (*Figure 3.7.3*a,b). In contrast in the absence of DMEM an immediate decrease to *ca.* 4300 µmol was observed (*Figure 3.7.3*c). Corresponding selenium accumulation levels by the fungal cells at $t_0$ were *ca.* 1250 and 700 µmol respectively (*Figure 3.7.4*). Selenite in the aqueous phase further decreased in all cases to final levels of *ca.* 1250 µmol on day 14 in a linear manner.

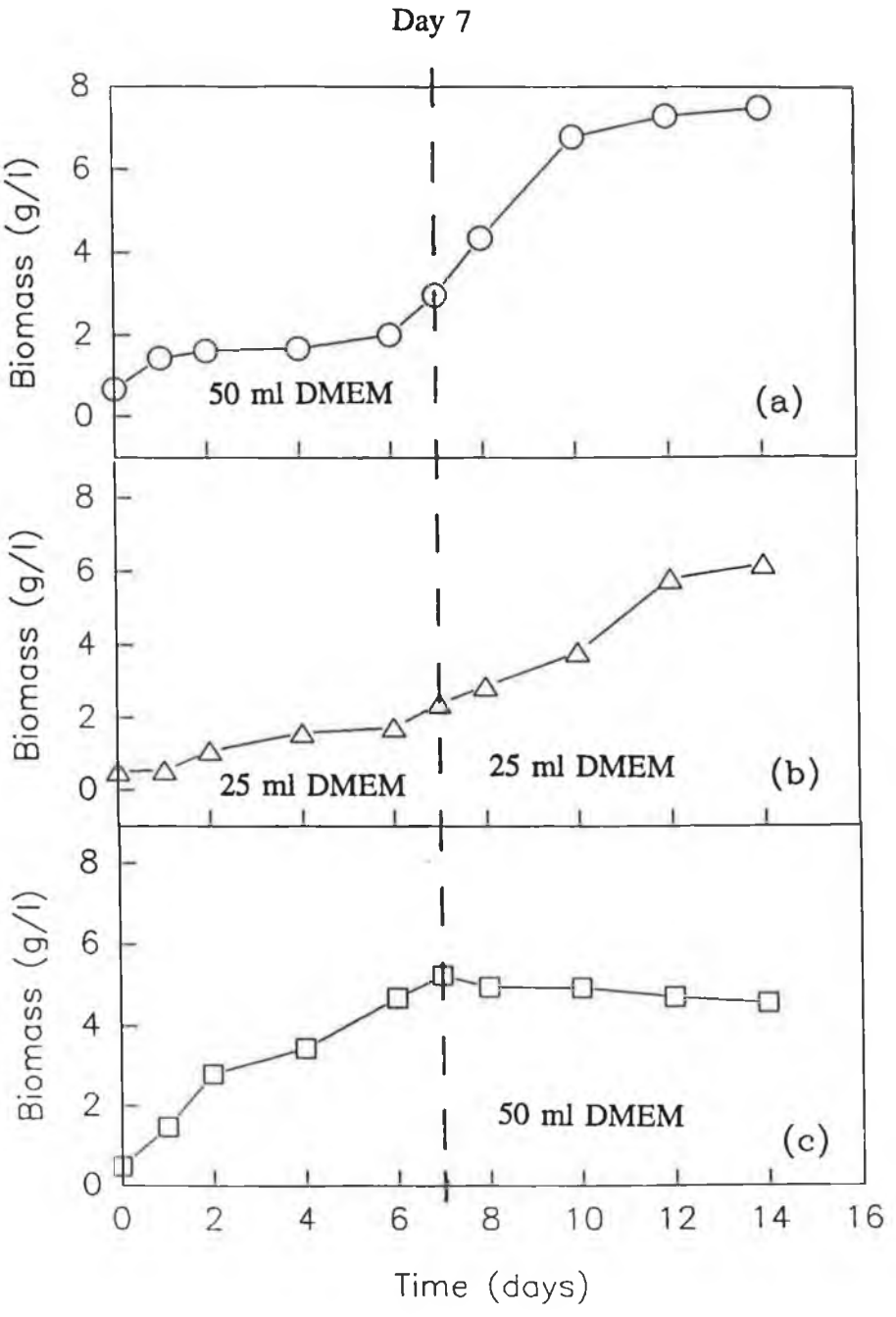


**Figure 3.7.1:** Growth of the *Penicillium* species in the presence of 1000 $\mu$mol $l^{-1}$ sodium selenite and 50 ml additions of DMEM in 5 l of media. (a) 50 ml DMEM addition at $t_0$, (b) two 25 ml DMEM additions at $t_0$ and on day 7, (c) 50 ml DMEM addition on day 7. Experimental points are averages of two determinations that agreed to within limits of 6%.

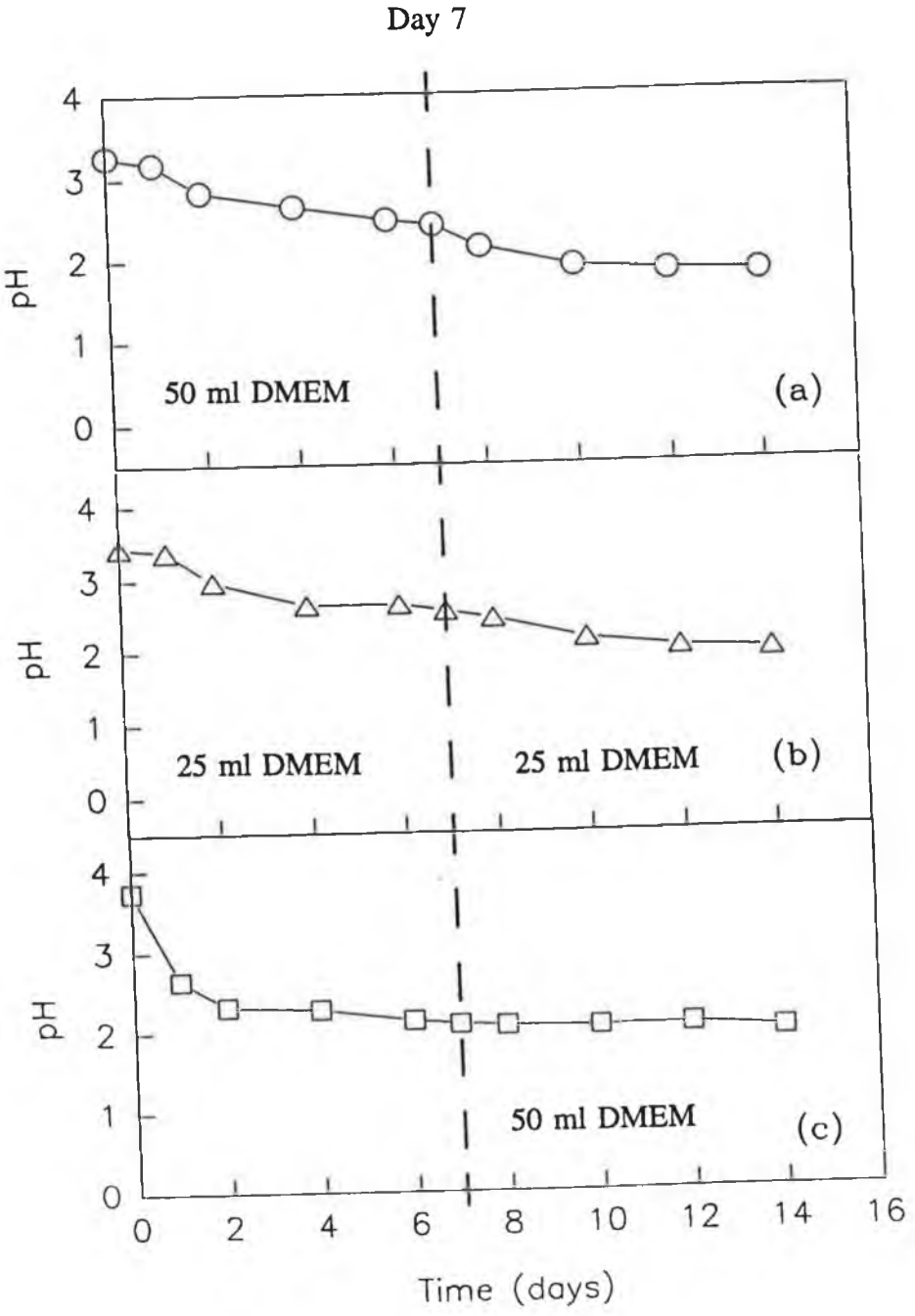


**Figure 3.7.2:** Media pH profiles of *Penicillium* species growth in the presence of 1000 $\mu$mol $l^{-1}$ sodium selenite and 50 ml additions of DMEM in 5 l of media. (a) 50 ml DMEM addition at $t_0$, (b) two 25 ml DMEM additions at $t_0$ and on day 7, (c) 50 ml DMEM addition on day 7. Experimental points are averages of two determinations that agreed to within limits of 6%.

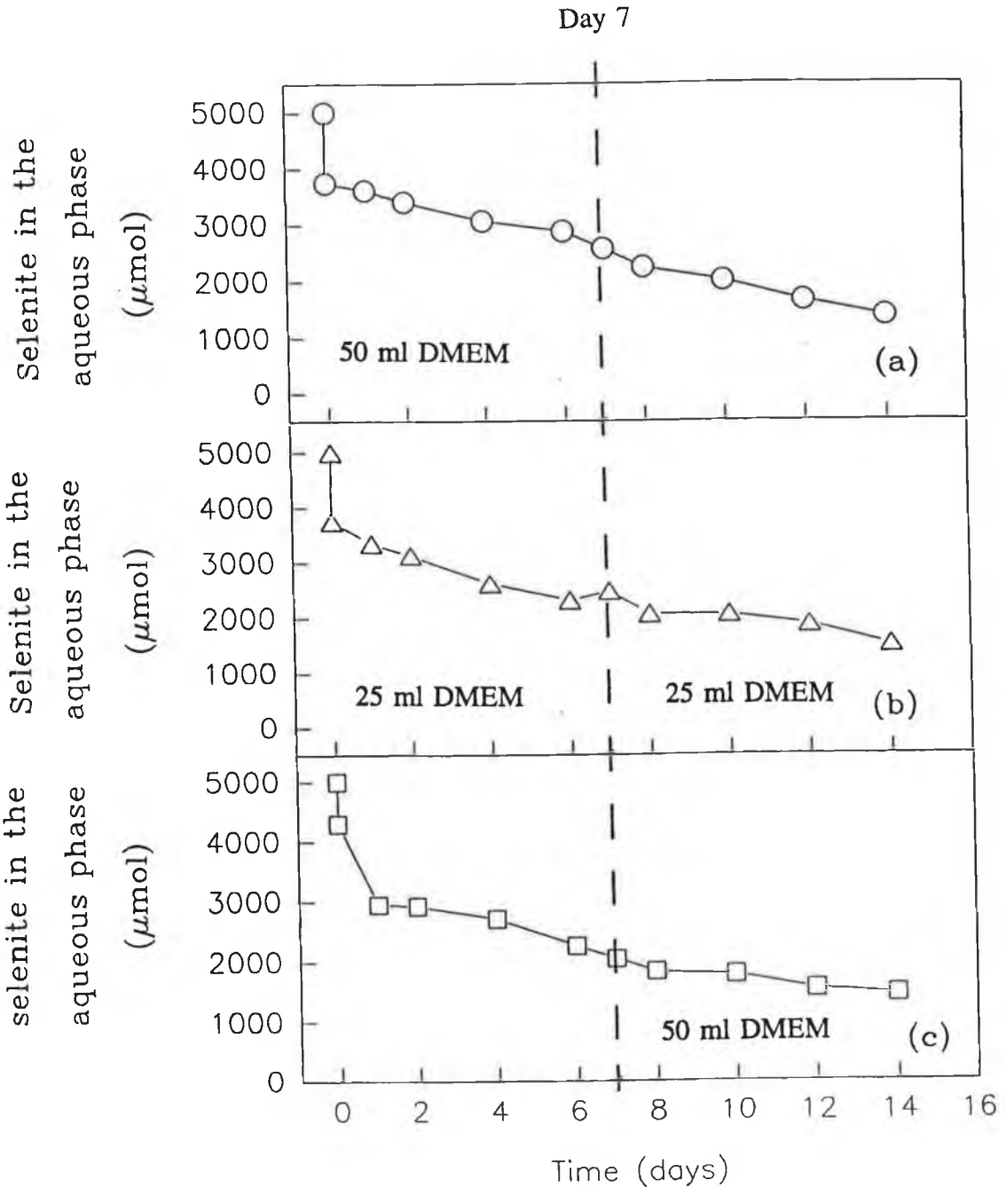


**Figure 3.7.3:** Selenium remaining in the aqueous phase as a result of *Penicillium* species growth in the presence of 1000 $\mu$mol $l^{-1}$ sodium selenite and 50 ml additions of DMEM in 5 l of media. (a) 50 ml DMEM addition at $t_0$, (b) two 25 ml DMEM additions at $t_0$ and on day 7, (c) 50 ml DMEM addition on day 7. Experimental points are averages of two determinations that agreed to within limits of 6%.

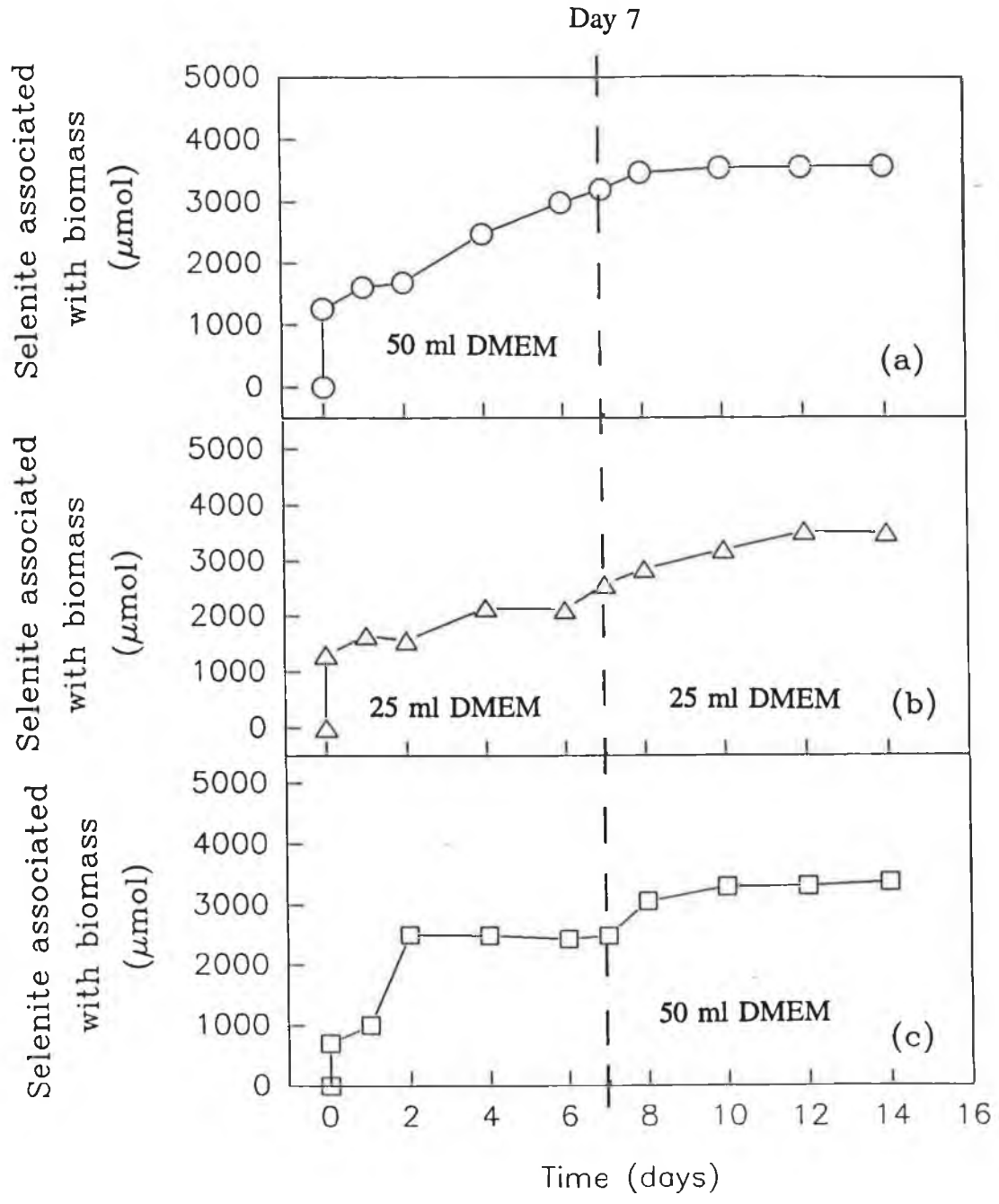


**Figure 3.7.4:** Selenium associated with the *Penicillium* species biomass grown in the presence of 1000 μmol $l^{-1}$ sodium selenite and 50 ml additions of DMEM in 5 l of media. (a) 50 ml DMEM addition at $t_0$, (b) two 25 ml DMEM additions at $t_0$ and on day 7, (c) 50 ml DMEM addition on day 7. Experimental points are averages of two determinations that agreed to within limits of 6%.

In the case of a single 50 ml aliquot addition at $t_0$, selenium associated with the biomass increased slowly from the initial accumulated level to *ca.* 3000 and 3600 µmol on day 7 and 12 respectively, and remained constant thereafter (*Figure 3.7.4*a). Biomass selenium loadings at $t_0$, and on days 7 and 14 were *ca.* 417, 215 and 96 µmol $g^{-1}$ (dry wt) respectively (*Figure 3.7.5*a). The bioreactor contents changed from a pale white colour to red on day 2, and well defined large red spherical mycelium particles developed as distinct from the finely suspended nature of the inocula.

In the systems involving two 25 ml DMEM additions, selenite accumulation was linear over the 2 wk period (*Figure 3.7.4*b). From $t_0$ to day 7 and days 7-14, selenium associated with the biomass increased to *ca.* 2160 and 3500 µmol respectively. Biomass selenium loadings decreased from *ca.* 417 µmol $g^{-1}$ at $t_0$, to *ca.* 213 and 113 µmol $g^{-1}$ on days 7 and 14 respectively (*Figure 3.7.5*b). The bioreactor contents changed again from the pale white consistency of the inocula, to the distinctive red colour of the well defined mycelium particles on day 2.

In the systems involving one 50 ml DMEM addition on day 7, selenite accumulation increased rapidly to *ca.* 2500 µmol on day 2, and from day 2 to day 14 steadily increased to *ca.* 3375 µmol on day 14 (*Figure 3.7.4*c). Overall selenite loadings were 233, 94 and 148 µmol $g^{-1}$ (dry wt), at $t_0$ and on days 7 and 14 respectively (*Figure 3.7.5*c). Biomass growth had the same pale white turbid consistency of the inocula for the first 7 days, but after the addition of DMEM the formation of spherical red mycelium pellets was observed after day 8.

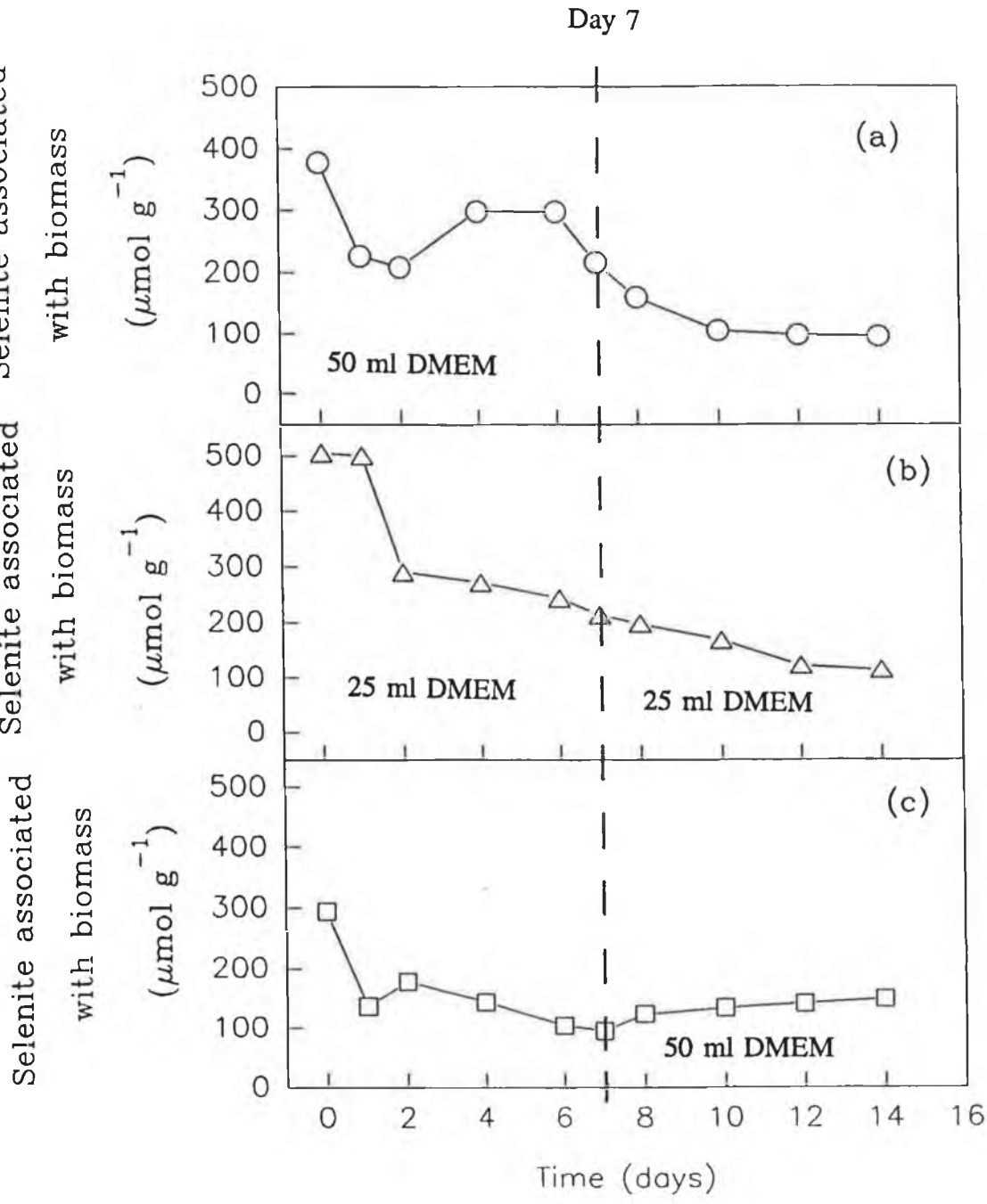


**Figure 3.7.5:** Selenium per unit dry weight associated with the *Penicillium* species biomass grown in the presence of 1000 $\mu$mol $l^{-1}$ sodium selenite and 50 ml additions of DMEM in 5 l of media. (a) 50 ml DMEM addition at $t_0$, (b) two 25 ml DMEM additions at $t_0$ and on day 7, (c) 50 ml DMEM addition on day 7. Experimental points are averages of two determinations that agreed to within limits of 6%.

# CHAPTER 4

# DISCUSSION

*Interactions of metal and metalloid ions with fungal biomass*

*PhD Research Thesis by*

*Joseph M. Brady* **B.Sc.**

## CHAPTER 4: DISCUSSION

### 4.0 *Fungal structure*

Fungi are predominately multicellular and filamentous in nature and are important ecologically as decomposers. The filamentous structures are known as hyphae and are commonly divided into cells by cross-walls called septa. Cytoplasm flows freely throughout the hyphae passing through pores in the septa. Ultrastructural studies of filamenteous fungi demonstrate a typical eukaryotic cellular organisation with individual hyphal compartments consisting of one or more nuclei (Carlile & Watkinson, 1994). These cellular compartments are enclosed by a plasma membrane and a rigid cell wall structure. Polysaccharides make up to 90% of the main constituents of the cell wall structure and are usually complexed with proteins, lipids, polyphosphates, inorganic ions and pigments such as melanins (Farkas, 1990). The main polysaccharide present in fungal cell walls is chitin, a linear polymer of the acetylated amino sugar *N*-acetylglucosamine. Vegetative growth of filamentous fungi usually takes the from of a multi-branched system of hyphae known as mycelium. Fungal growth is characteristically confined to the tips of the hyphae and as the mycelium extends the cytoplasm tends to disappear from the older central regions leaving behind the cell wall structure, and it is the cell wall components that are considered responsible for the passive adsorption affinities of fungal biomass for metal ions (Remacle, 1990; Gadd, 1993*b*). Filamentous fungi have been found to exhibit low rates of intracellular metal ion uptake, and binding to cell walls appears to be the most significant mechanism (de Rome & Gadd, 1987*b*).

### 4.1 *Biosorption characterisation: discussion*

Although the data reported in *Table 3.1.1* show a slight trend of increasing uptake with pH, the variation between uptake values is typically less than 4%, indicating that at solution pH values of 4 and 6, the initial hydrogen ion concentration has no appreciable effect on the amount of metal adsorbed. This is in keeping with previous studies that report ranges of pH optima from 4-7 (Tsezos & Volesky, 1984; Tobin *et al.*, 1984; Treen-Sears *et al.*, 1984).

#### 4.1.1 *Biosorbent pretreatment effects*

In this work, considerable variation in the effects of biomass pretreatment on the uptake of the test ions is evident, with maximum and minimum adsorption levels observed for freeze-dried and live non-metabolising biomass systems respectively. In the case of non-viable biomass, adsorption is considered to proceed exclusively by metabolically independent passive adsorptive processes (de Rome & Gadd, 1987*b*; Wainwright, 1990), and has been reported to adsorb metal ions in larger quantities than viable biomass (Kuyucak & Volesky, 1988; Wainwright, 1990; Urruita Mera *et al.*, 1992; Brady & Tobin, 1994). Increase in adsorption capacity of non-viable biomass has been attributed to increased surface area and exposure of intracellular binding sites caused by pretreatment (Avery & Tobin, 1992) and the absence of competing $H^+$ ions produced by viable biomass (Urrutia Mera *et al.*, 1992).

In contrast, while freeze drying enhanced uptake for each of the test ions, oven drying diminished uptake values for both $Cd^{2+}$ and $Cu^{2+}$ to the extent that maximum uptake of $Cu^{2+}$ by oven dried biomass was only 60% of the freeze dried value. Uptake levels for $Sr^{2+}$ by both freeze-dried and oven-dried biomass were almost identical.

**4.1.2** *Ionic and covalent binding*

Release of $Ca^{2+}$ and $Mg^{2+}$ ions accounted for between 70-77% of the $Sr^{2+}$ uptake on a molar basis, and a complete absence of $H^+$ ions indicated that ion exchange is the predominant binding mechanism involved. This is consistent with earlier work using the freshwater algae *Vaucheria* (Crist *et al.*, 1990), and overall it was concluded that adsorption of alkaline earth metal ions is an ion-exchange phenomenon based on electrostatic interactions. In contrast, with the yeast *Saccharomyces cerevisiae*, additional covalent binding of $Sr^{2+}$ was reported (Avery & Tobin, 1992; 1993). It was considered that the pH decrease recorded after metal ion addition to live yeast biomass resulted from the covalent bonding of the ion to surface anionic groups which including carboxylate and phosphate (Avery & Tobin, 1992). These sites were presumed to have been occupied previously by $H^+$ ions, and as a result of metal binding, displacement of $H^+$ ions was detected.

During $Cd^{2+}$ binding, appreciable release of $H^+$ ions at *ca.* 2.2 μmol $g^{-1}$, indicated that covalent binding is involved. As for $Sr^{2+}$, ion exchange appears to be the principal mechanism of adsorption, with $Ca^{2+}$ and $Mg^{2+}$ release accounting for between 59-71% of the $Cd^{2+}$ adsorbed. In the $Cu^{2+}$ studies, combined $Ca^{2+}$ and $Mg^{2+}$ release represents only between 34-51% of the total $Cu^{2+}$ adsorbed, whereas $H^+$ displacement was a maximum of *ca.* 120 μmol $g^{-1}$, implying that ion exchange and covalent binding both contribute significantly to uptake. The non-stoichiometry of the exchanges is in keeping with previous work with yeast biomass and suggests that some uptake occurs to sites not previously occupied by $Ca^{2+}$, $Mg^{2+}$ or $H^+$ ions (Avery & Tobin, 1992).

### 4.1.3 *Characterisation of metal binding sites*

#### 4.1.3.1 *Langmuir applications*

The linearity of the reciprocal Langmuir plots for all freeze dried biomass systems suggests the predominance of a single binding mechanism, ion exchange. This agrees well with $Sr^{2+}$ and $Cd^{2+}$ systems, where $Ca^{2+}$ and $Mg^{2+}$ were the main displaceable cations. Similarly, adsorption of $Cd^{2+}$ ions by non-viable brown marine algal biomass and stationary cells of *Saccharomyces cerevisiae* were found to accumulate $Cd^{2+}$ ions exclusively by passive surface adsorption, and a good fit of the Langmuir adsorption model to the adsorption data supported a single layer binding mechanism (Holan, Volesky & Prasetyo, 1993; Volesky *et al.*, 1993).

The linearity of the reciprocal Langmuir plots was unexpected in the case of $Cu^{2+}$, in view of the more complex cation displacement data involving $H^{+}$. In a previous study, adsorption of $Cu^{2+}$ by *Rhizopus arrhizus* followed the BET isotherm for multi-layer adsorption, reflecting more than one type of binding mechanism (de Rome & Gadd, 1987*b*). Furthermore in a study of metal uptake by *Bacillus subtilis* cell walls, it was suggested that carboxyl groups are the major source of metal ion deposition, although $Cu^{2+}$ ions preferentially bind to amines rather than carboxylates (Beveridge & Murray, 1980).

#### 4.1.3.2 *Scatchard transformation and BET applications*

Scatchard transformations of the uptake data demonstrate differences between the test ions. Linear plots, as are evident in all cases for $Sr^{2+}$ and $Cd^{2+}$ freeze-dried biomass systems (see *Table 3.1.3*), represent uptake to a single distinct type of binding site, and

are consistent with the proposed ion exchange binding mechanism. Curved Scatchard plots convex to the origin (see example *Figure 3.1.9*a), have been previously reported for metal binding by microbial biomass and are interpreted as indicating multiple non-equivalent binding sites (Volesky, 1990; Tobin *et al.*, 1990; Avery & Tobin, 1993; Brady & Tobin, 1994; Brady & Duncan; 1994). In the present study, curves concave to the origin (see example *Figure 3.1.9*c) for all the $Cu^{2+}$ adsorption systems (*Table 3.1.3*) may reflect cooperative binding by multiple sites (Chamness & McGuire, 1975). In earlier Scatchard plot studies (Tobin *et al.*, 1990), the primary interactions of metal ions with *Rhizopus arrhizus* biomass were considered to be due a complexation mechanism involving carboxylate and phosphate groups on the surface or within the biomass. A secondary adsorption mechanism involving the electrostatic interactions of positively charged metal ions with negatively charged functional groups was also proposed. However the Brunauer, Emmett, Teller (BET) model, which reflects apparent multilayer adsorption phenomena (Weber, 1972), did not provide good fit to adsorption data from any of the metal-biomass systems in this work. Consequently, it would appear that, although multiple binding sites may be involved, adsorption is a monolayer rather than a multilayer process.

#### **4.1.3.3** *Freundlich applications*

Oven-dried $Sr^{2+}$ biomass systems displayed similar uptake, displacement and adsorption characteristics as freeze-dried systems. However, live non-metabolising systems exhibited lower uptake and conformity to the Freundlich adsorption model only. The Freundlich equation is basically empirical, and represents the case of heterogeneous energies of

adsorption on adsorbent surfaces. This more complex binding may be a result of proton motive forces producing $H^+$ ions that compete or displace surface bound $Sr^{2+}$ ions. A similar result with the same biomass for $Cd^{2+}$ pH 4 systems was also observed.

Overall, with equivalent $Ca^{2+}$ and $Mg^{2+}$ displacement levels (*Table 3.1.2*), it appears that all the biomass types share the same ionic binding characteristics. As with covalent binding (as represented by $H^+$ release), no pretreatment variation effects were observed. For the softer ions $Cd^{2+}$ and $Cu^{2+}$, oven-drying adversely affects binding sites on the biomass not previously occupied by $Ca^{2+}$, $Mg^{2+}$ and $H^+$ ions, reducing overall adsorption capacity. For the hard ion $Sr^{2+}$, these sites do not appear to be involved in uptake, and consequently little variation is observed between biomass types.

In contrast, $Sr^{2+}$ uptake by live *Saccharomyces cerevisiae* cells was previously reported to result in non-linear reciprocal Langmuir plots, reflecting multi-binding site adsorbents, and the displacement of $Ca^{2+}$, $Mg^{2+}$ and $H^+$ ions suggested a combination of both ionic and covalent bonding (Avery & Tobin, 1992). For oven-dried *Saccharomyces cerevisiae* biomass however, $Mg^{2+}$ was the predominant exchangeable cation, indicating primarily electrostatic interaction, and reciprocal Langmuir plots were linear suggesting the existence of a single type of binding site. In another study, chemical modifications of carboxyl groups by esterification, and amino and hydroxyl groups by acetate addition, reduced the quantity of $Cu^{2+}$ ions accumulated by isolated cell walls of *Saccharomyces cerevisiae*. This indicated that both functional groups play a role in $Cu^{2+}$ ion adsorption, and curved Scatchard plots convex to the origin reflected this multiphasic binding (Brady & Duncan, 1994). In general biosorption of metal ions by fungal biomass has been viewed as a relatively non-specific process, with each cation adsorption site being capable of binding a number of different metal species (Tobin *et al.*, 1988; de Rome & Gadd, 1991).

### 4.1.4 *Biosorption characterisation: summary*

In summary, for $Sr^{2+}$ up to 70% of the uptake may be accounted for by ion exchange with negligible covalent binding as evidenced by the absence of $H^+$ release. Covalent bonding contributes to $Cd^{2+}$ uptake but ion exchange is the principal mechanism accounting for up to 60% of the uptake. For $Cu^{2+}$ ion exchange remains important but covalent binding is significant and contributes to the greater uptake levels.

## 4.2 *Application of hard and soft principle: discussion*

$Sr^{2+}$ is a class (a) *hard* metal ion, and $Mn^{2+}$, $Zn^{2+}$, $Cd^{2+}$, $Cu^{2+}$ and $Pb^{2+}$ are classified as borderline *soft* (*Appendix B*). Covalent index and *softness* of the test ions increase in the order: $Sr^{2+} < Mn^{2+} < Zn^{2+} < Cd^{2+} < Cu^{2+} < Pb^{2+}$. In general the greater the covalent index value of a metal ion, the greater its degree of *class (b)* character, and consequently its potential to form covalent bonds with biological ligands (Brady & Tobin, 1994).

### 4.2.1 *Equilibrium cation uptake, displacement and inhibition studies*

The results reported in *Table 3.2.1* demonstrate significant differences in affinity by the same biomass for different metal ions. Equilibrium uptake levels of $t_0$ metals were found to correlate directly with covalent index values as illustrated in *Figure 4.2.1*. This correlation is a further indication that greater binding results from an increased covalent contribution. In a previous study, metal ion adsorption by vacuum dried *Rhizopus arrhizus* was found to be directly related to ionic radii for a range of divalent and trivalent metal ions (Tobin, Cooper & Neufeld, 1984), and it is interesting to note that ionic radius is a factor in the computation of covalent index values. From the Periodic

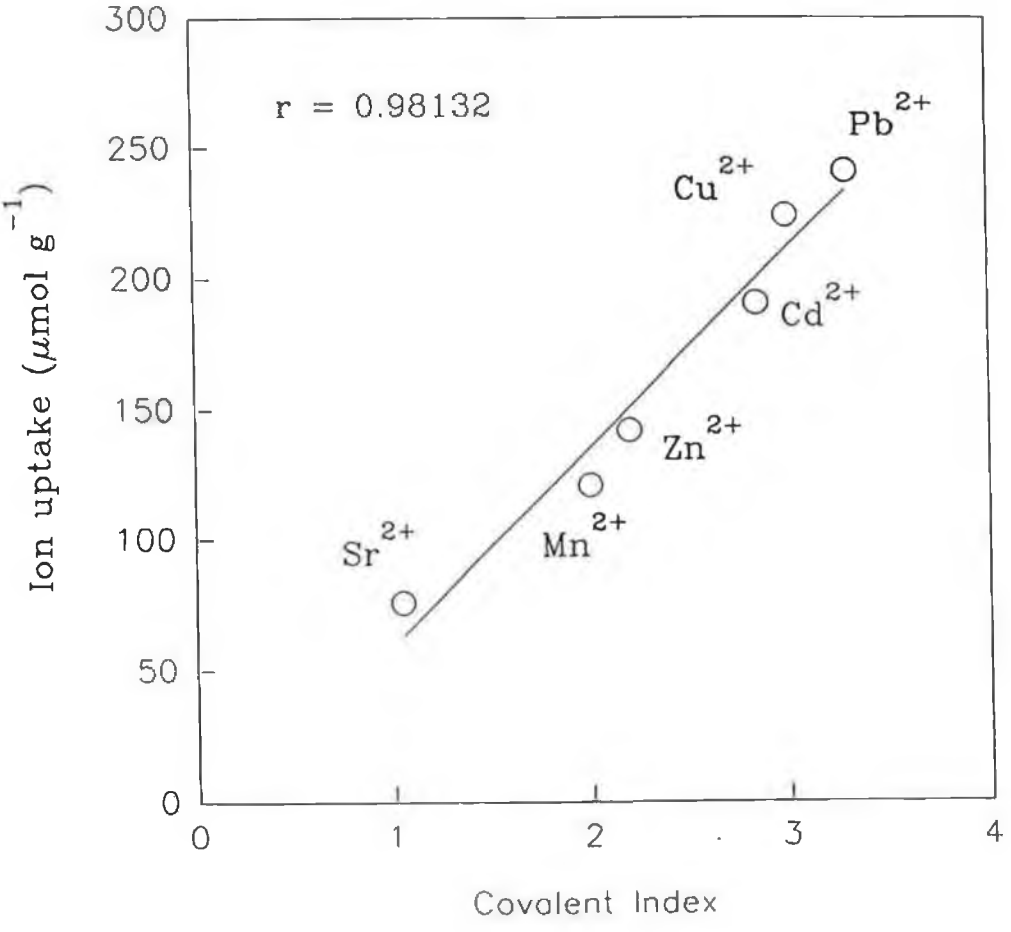


**Figure 4.2.1:** Correlation of equilibrium metal uptake values ($q$) with ion covalent index values.

Table, the ions $Mn^{2+}$, $Zn^{2+}$ and $Cu^{2+}$ are in the first series of transition elements, and according to Hughes & Poole (1989; 1991), $Cu^{2+}$ is the strongest Lewis acid in this group and will bind preferentially to microbial biomass ligands. This is demonstrated in this study with binding increasing with covalent index in the order, $Mn^{2+} < Zn^{2+} < Cu^{2+}$.

In earlier studies, metal ion uptake capacities for native cell walls of *Saccharomyces cerevisiae* and fungal cell walls of *Trichoderma harzianum* increased in the order $Co^{2+} < Cd^{2+} < Cu^{2+}$, and $Zn^{2+} < Cd^{2+} < Hg^{2+}$ respectively (Brady & Duncan, 1994; Rulcker, Frandberg & Schnurer, 1995). Both trends also demonstrate increasing metal adsorption with increasing covalent index.

**4.2.1.1** *Exchange of $Ca^{2+}$, $Mg^{2+}$ and $H^+$ ions*

The displacement of $H^+$ ions has been interpreted to indicate covalent bonding, and release of $Ca^{2+}$ and $Mg^{2+}$ ions denotes ionic interactions (Crist *et al.*, 1990; Avery & Tobin, 1992, 1993; Brady & Tobin, 1994). Release of $H^+$ ions in this study increased in the order: $Mn^{2+} < Zn^{2+} < Cd^{2+} < Cu^{2+} < Pb^{2+}$, as exhibited in *Table 3.2.3*, which supports the view that increased uptake levels result from an increased covalent binding component. Completely stoichiometric exchanges were not observed for the borderline ions, indicating that a significant part of the uptake results from binding processes that do not cause $H^+$, $Ca^{2+}$ or $Mg^{2+}$ release. Since $Sr^{2+}$ is a class (a) metal, it is expected to exhibit ionic binding only. This was confirmed, with 100% of uptake fully accounted for by $Ca^{2+}$ and $Mg^{2+}$ release, and a complete absence of $H^+$ ion displacement. These findings are consistent with work in which $Sr^{2+}$ binding to the freshwater algae *Vaucheria* was attributed solely to ion exchange processes, also detected from equivalent $Ca^{2+}$ and $Mg^{2+}$ release (Crist *et al.*, 1990).

**4.2.1.2** *Test ion displacement and inhibition potentials*

For borderline preloaded systems, and similar to the *time-course* studies, the potential of one ion to displace another increased with increasing covalent index (*Table 3.2.2*) in the following orders:

$Mn^{2+}$ systems: $Sr^{2+} < Zn^{2+} < Cd^{2+} < Cu^{2+} < Pb^{2+}$

$Zn^{2+}$ systems: $Sr^{2+} < Mn^{2+} < Cd^{2+} < Cu^{2+} < Pb^{2+}$

$Cd^{2+}$ systems: $Sr^{2+} < Mn^{2+} < Zn^{2+} < Cu^{2+} < Pb^{2+}$

$Cu^{2+}$ systems: $Sr^{2+} < Mn^{2+} < Zn^{2+} < Cd^{2+} < Pb^{2+}$

$Pb^{2+}$ systems: $Sr^{2+} < Mn^{2+} < Zn^{2+} < Cd^{2+} < Cu^{2+}$

Inhibition potentials increased in an identical manner (*Table 3.2.3*). This suggests that the more covalent the nature of the binding, the stronger the bond.

In the case of preloaded and inhibitory $Sr^{2+}$ systems, almost an opposite trend was apparent.

$Sr^{2+}$ systems: $Cu^{2+} < Cd^{2+} < Zn^{2+} < Mn^{2+} < Pb^{2+}$

Displacement and inhibition capacities decrease with increasing covalent index for all test ions except $Pb^{2+}$. The effects exhibited by $Pb^{2+}$ on $Sr^{2+}$ systems are anomalous, and cannot be accounted for on the basis of covalent index. However, according to Shannon and Prewitt (1969; 1970), ionic radii for both $Pb^{2+}$ and $Sr^{2+}$ are almost identical, and it may be this close similarity in ionic size that introduces additional competition effects. Similarly, inhibition of $Co^{2+}$ and $Cd^{2+}$ uptake by viable *Saccharomyces cerevisiae* cells also was found to be greatest by cations of similar size (Norris & Kelly, 1977). Furthermore, Hughes & Poole (1991) reported that if hard and soft metal ions are present in solution, soft ions tend to bind preferentially to biological ligands and displace essential-hard metal ions from their sites (Hughes & Poole, 1991).

**4.2.2** *Time-course cation adsorption studies*

The results of the *time-course* studies shown in *Figure 3.2.1* demonstrate that the biosorption process is both rapid, and rapidly reversible by the addition of metal co-ions. Equilibrium adsorption is 95% complete within the first 5 min of metal-microbe contact, and the slower adsorptive process may represent diffusion into the biosorbent particles. These findings are similar to other time-course ion adsorption studies, where cation uptake by algal biomass also displayed rapid accumulation, followed by a slower uptake phase (Crist *et al.*, 1988; Sloof & Viragh, 1995). Adsorption equilibrium conditions for $Sr^{2+}$ by non-metabolising *Saccharomyces cerevisiae* systems were reached within 5 minutes of metal-biomass contact (Avery & Tobin, 1992, 1993), and the uptake of uranium by *Saccharomyces cerevisiae* was relatively fast, with 60% of the equilibrium values attained within the first 15 minutes of contact (Kuyucak & Volesky, 1988; Volesky & May-Phillips, 1995).

Overall ion uptake values increase in the order: $Sr^{2+} < Cd^{2+} < Cu^{2+}$, which is consistent with the findings reported in *section 4.1* (Brady & Tobin, 1994). For the dual ion $Cd^{2+}$-$Cu^{2+}$ borderline systems, ion inhibition and displacement potentials increased with covalent index. This trend was reversed for dual ion systems involing $Sr^{2+}$ ions. Biosorption of the borderline ions, $Cd^{2+}$, $Cu^{2+}$ and $Zn^{2+}$, in two-metal systems using formaldehyde-cross-linked *Ascophyllum nodosum* seaweed biomass, also demonstrated that each metal ion can inhibit the adsorption of the others (de Carvalho, Chong & Volesky, 1995). For single metal systems overall uptake increased in the order, $Cd^{2+} < Cu^{2+} < Zn^{2+}$, which is also consistent with increasing covalent index. For $Cu^{2+}$-$Zn^{2+}$ systems, the effect of $Cu^{2+}$ on $Zn^{2+}$ sorption was more pronounced than the effect of $Zn^{2+}$

on $Cu^{2+}$ sorption. Similarly, and identical to observations in this study for $Cd^{2+}$-$Cu^{2+}$ systems, sorption of $Cd^{2+}$ was more sensitive to the presence of $Cu^{2+}$ ions than *vice versa*. For $Zn^{2+}$-$Cd^{2+}$ systems, $Cd^{2+}$ and $Zn^{2+}$ ions interfered with each other's sorption by almost equal proportions. Again it appears that the higher the covalent index value of borderline ions, the greater their inhibitory potential. Similar results were observed too for the uptake of $Zn^{2+}$ and $Cd^{2+}$ by *Saccharomyces cerevisiae*, in equimolar dual-metal systems (Ting & Teo, 1994). Overall $Zn^{2+}$ uptake was impeded by the presence of $Cd^{2+}$ ions, but $Zn^{2+}$ had no effect on the overall long term uptake of $Cd^{2+}$.

### **4.2.3** *Application of hard and soft principle: summary*

In the present study, both the magnitude of adsorption levels and the displacement/inhibition potential of the ions correlated with covalent index, confirming that the classification of metal ions according to the hard and soft principle is of value in the study of metal-microbial interactions.

## **4.3** ***Effects of biomass concentration***

For $Cu^{2+}$ adsorption by yeast and fungi, including *Rhizopus arrhizus*, the amount of metal adsorbed per unit weight was found to be maximal at lower biomass levels, decreasing with increasing amounts of the biosorbent (Gadd & White, 1989*b*; Junghans & Straube, 1991). Similar trends were observed for thorium uptake by a range of fungi (Gadd & White, 1989*b*). These studies proposed that increasing the distance between cells enhanced metal uptake as a result of diminished cell-cell electrostatic interference. An increased biomass density also leads to interference between ion binding sites and

reduced mixing during incubation. Disruption of mycelium biomass for a range of fungal species increased the surface area available for $Cd^{2+}$ adsorption and slightly increased sorption capacities (Azab *et al.*, 1990). In this study it was proposed to examine this relationship between solution biomass levels and metal ion equilibrium adsorption. The ions $Sr^{2+}$, $Cd^{2+}$ and $Cu^{2+}$ were used in conjunction with freeze-dried *Rhizopus arrhizus* biomass to this end.

**4.3.1** *Equilibrium isotherm curves*

The shapes of the $Sr^{2+}$, $Cd^{2+}$ and $Cu^{2+}$ isotherms were independent of solution biomass levels as shown separately for each test ion in *Figure 3.3.1*. Conformity of the adsorption data to single reciprocal Langmuir plots further suggests that biosorption is an equilibrium type reaction independent of solution solute or biosorbent levels (*Figure 3.3.2*). As in the previous two sections, metal uptake levels increased in the order $Sr^{2+} < Cd^{2+} < Cu^{2+}$, yielding maximum values of *ca.* 130, 280 and 400 μmol $g^{-1}$. The equilibrium interphase accumulation of metal ions at the surface of microbial biomass can be described by adsorption isotherms, and as illustrated in this study, such plots are independent of the volume of metal salt solution in contact with the biosorbent, and *vice versa* (Remacle, 1990; Brady and Duncan, 1994).

These results are generally consistent with previous studies, where metal ion adsorption by lignite (Allen & Brown, 1995) and thorium and $Zn^{2+}$ uptake by *Rhizopus arrhizus* (Gadd & White, 1989*b*; Fourest *et al.*, 1991) were found to be independent of both biosorbent solution levels and particle sizes. It was also found that any increase in surface area between sonicated and non-sonicated freeze-dried biomass particles of *Saccharomyces cerevisiae* and a *Candida* species, did not significantly enhance $Cu^{2+}$ and $Ag^{+}$ uptake (Simmons *et al.*, 1995).

**4.3.2** *Cation displacement trends*

Similar to *section 4.1*, $Ca^{2+}$ and $Mg^{2+}$ ion displacement increased with increasing metal uptake until saturation levels were reached (*Figures 3.3.3* and *3.3.4*). As before, maximum displacement values were constant for each test ion, at *ca.* 20 and 95 μmol $g^{-1}$ for $Ca^{2+}$ and $Mg^{2+}$ respectively. Since isotherm plots were constant over a range of solution biomass levels, it was expected that the $Ca^{2+}$ and $Mg^{2+}$ ion displacement data should display similar equilibrium trends. This was indeed the case, with plots of ion levels displaced versus equilibrium $q_{uptake}$ all fitting the same straight lines for each of the test ion systems.

In comparison, $H^+$ ion displacement results displayed more complicated equilibrium trends for $Cd^{2+}$ and $Cu^{2+}$ systems. Levels of $H^+$ ions displaced per unit dry weight of biosorbent increased with decreasing solution biomass concentration for both $Cd^{2+}$ and $Cu^{2+}$ systems. This is an unexpected phenomenon, with $H^+$ release being at a maximum at the lowest biomass concentration, and is in contrast with the trends observed for $q_{uptake}$ and $Ca^{2+}$ and $Mg^{2+}$ ion displacement. It may be possible in this case that cell-cell interactions and electrostatic interferences influence $H^+$ ion adsorption/displacement. The chemistry of $Cd^{2+}$ and $Cu^{2+}$ ions may also change with decreasing pH and perhaps exert an effect on cation equilibrium adsorption.

For $Sr^{2+}$ systems, no pH changes were detected with respect to $q_{uptake}$ over the solution biomass concentration range, confirming the absence of $H^+$ ion displacement as previously observed in *sections 4.1* and *4.2*.

### 4.3.3 *$Ca^{2+}$+$Mg^{2+}$/$H^+$ ratios*

For the $Cd^{2+}$ and $Cu^{2+}$ systems, $Ca^{2+}$+$Mg^{2+}$/$H^+$ ratio values (ionic/covalent) were calculated for the different biomass concentrations, and are presented versus $q_{uptake}$ in *Figure 4.3.1.* In all cases, the ratio appears to decrease linearly with metal uptake, and since the levels of $H^+$ displacement increased with decreasing biosorbent concentrations, the smallest ratio values for both systems were calculated for the lowest solution biomass levels. This indicates ionic binding to be the primary mechanism of cation adsorption followed by covalent interactions, and such trends are more pronounced at the lower solution metal concentrations. As metal levels increased, $H^+$ displacement increased, suggesting covalent binding to be a secondary adsorption mechanism.

### 4.3.4 *Effects of biomass concentration: summary*

In summary, metabolism-independent metal ion adsorption to freeze-dried *Rhizopus arrhizus* biomass is an equilibrium type reaction, and equilibrium positions are independent of the suspended biosorbent levels in the aqueous phase. Primary mechanisms of cation adsorption have been found to involve ionic binding resulting in the displacement of $Ca^{2+}$ and $Mg^{2+}$ ions from the biomass ligands, and a secondary adsorption mechanism includes covalent interactions as evidenced by $H^+$ ion displacement. Future work is merited on the mechanism of $H^+$ ion adsorption/displacement at low biomass concentrations.

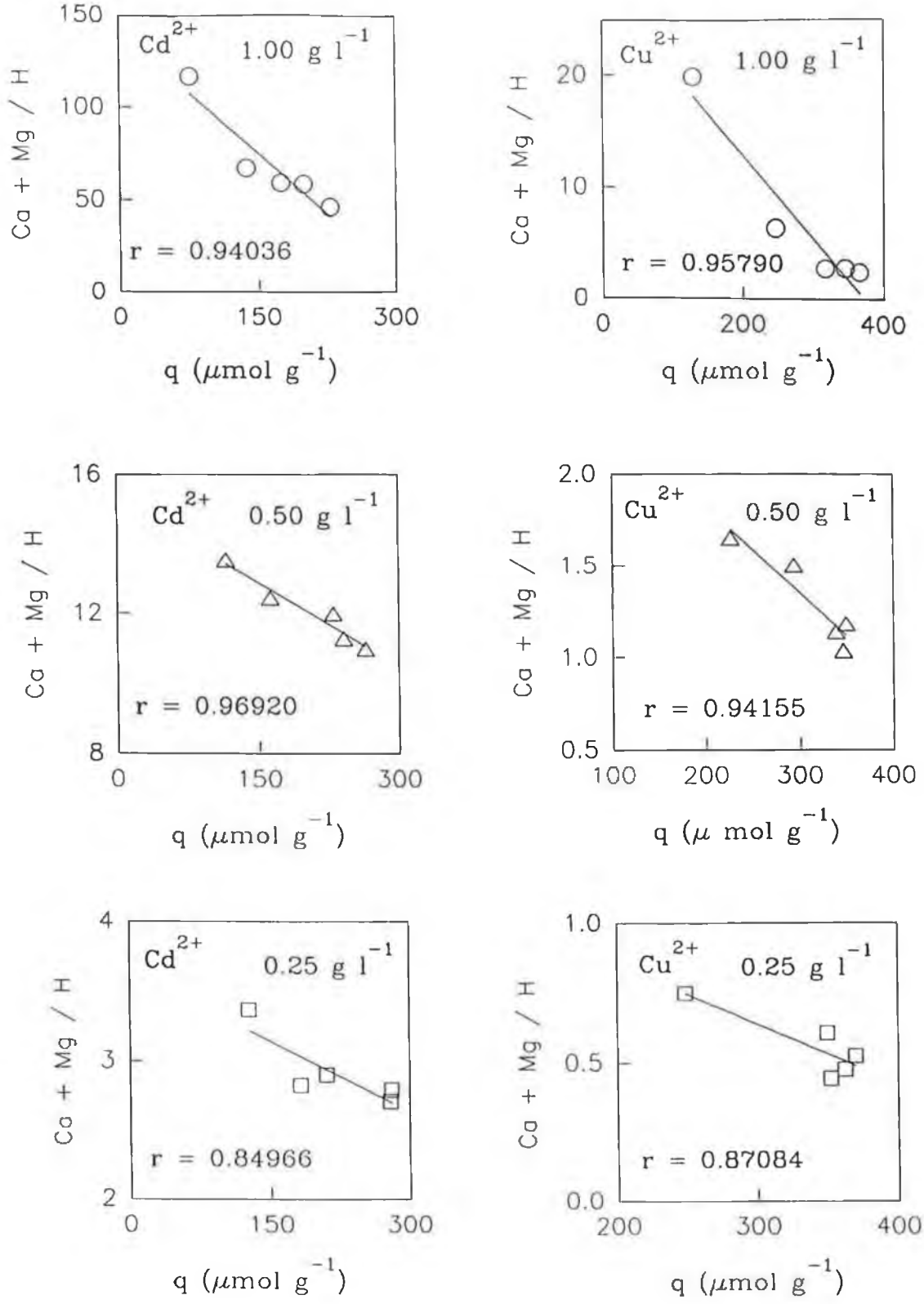


**Figure 4.3.0:** Ionic/covalent ($Ca^{2+}+Mg^{2+}/H^{+}$) ratio plots for $Cd^{2+}$ and $Cu^{2+}$ freeze-dried biomass systems versus metal uptake (*q*).
Biomass concentrations: 1 g $l^{-1}$ ( ○ ), 0.5 g $l^{-1}$ ( △ ) and 0.25 g $l^{-1}$ ( □ ).

## 4.4 *Continuous flow systems*

### 4.4.1 *Batch screening studies*

The organic solvent DCM, was found to have no significant effect on the biosorptive capacity of freeze-dried *Rhizopus arrhizus* biomass for $Cu^{2+}$ ions. Over the initial solution $Cu^{2+}$ concentration range, $Cu^{2+}$ uptake and $Ca^{2+}$, $Mg^{2+}$ and $H^+$ displacement trends were in close agreement for both DCM-treated and -untreated biomass (*tables 3.4.1* and *3.4.2*). As in earlier sections, maximum $Cu^{2+}$ adsorption was *ca.* 425 μmol $g^{-1}$, and overall $Ca^{2+}$, $Mg^{2+}$ and $H^+$ displacement levels, were *ca.* 27, 116 and 139 μmol $g^{-1}$ respectively. Similar to *section 4.1.2* for freeze-dried biomass, $Ca^{2+}$ and $Mg^{2+}$ release accounted for *ca.* 34% of $Cu^{2+}$ adsorption, representing ionic binding.

The absence of effects of DCM on the biosorbent was unexpected. It was originally thought that DCM, as a relatively strong organic solvent might remove cell wall material containing metal binding groups such as carboxylates and phosphates, and therefore reduce the overall surface net negative charge and limit biosorption. Alternatively binding sites might also have been exposed thereby increasing biosorption capacities. In previous studies the treatment of fungal biomass with NaOH (Leuf *et al.*, 1991) and detergent (Gadd & White, 1989*b*) was found to enhance metal ion accumulation by exposing intracellular binding sites for metal deposition.

PVF immobilised biosorbents, with biomass loadings of 40, 50, 60, 70 and 80% (w/w), all adsorbed $Cu^{2+}$ ions to almost identical levels over the initial solution $Cu^{2+}$ concentration range, displaying maximum values of *ca.* 435 μmol $g^{-1}$ (*Table 3.4.3*). Similar ion displacement trends were observed in each case, and maximum levels of *ca.* 20, 125 and 110 μmol $g^{-1}$ were recorded for $Ca^{2+}$, $Mg^{2+}$ and $H^+$ release respectively

(*Tables 3.4.4*, *3.4.5* and *3.4.6*). The biosorbent prepared with a biomass loading of 60% was considered to be more mechanically stable under constant flow conditions and was subsequently used to pack the biosorption columns.

**4.4.2** *Continuous $Cu^{2+}$ elution studies*

The continuous elution of $Cu^{2+}$ ions from aqueous pH 4 solutions was achieved using the biosorbent columns prepared as in *section 2.4.1*. As flowrate increased, the time required for complete column breakthrough (where $C_f = C_i$) decreased as illustrated in *Figure 3.4.1*a. However, experimental breakthrough curves plotted with respect to volume all appear to be similar over the flowrate range 3.40-11.63 ml $min^{-1}$ (*Figure 3.4.1*b). Overall, the $Cu^{2+}$ biosorption capacities of the columns were determined to be relatively constant at *ca.* 208 µmol $g^{-1}$. These maximum values were *ca.* 50% lower then the batch biosorption levels recorded earlier. For the isotherms systems, the biosorbents were not pH equilibrated, and their introduction into pH 4 metal solutions resulted in instantaneous pH increases, decreasing the overall solution $H^+$ ion concentrations. The column immobilised biosorbents, like the influent metal solutions were equilibrated to pH 4 before metal-microbial contact, and the relatively high levels of $H^+$ ions are likely to have interfered competitively with $Cu^{2+}$ ion binding, causing a reduction in adsorption levels relative to non-pH equilibrated biosorbents.

The $Ca^{2+}$ and $Mg^{2+}$ ion displacement potentials were also decreased by pH equilibration of the column biosorbents. Maximum $Ca^{2+}$ and $Mg^{2+}$ displacement values were *ca.* 9 and 39 µmol $g^{-1}$ respectively, collectively representing about 24% of total $Cu^{2+}$ binding by ionic interactions. In contrast to the batch isotherm studies, $Cu^{2+}$ biosorption did not cause any $H^+$ ion displacement from the biosorbents.

**4.4.3** *Mathematical modelling of breakthrough curves*

The two parameter fixed bed adsorption model was successful in modelling the experimental breakthrough curves, and can be used to predict metal ion biosorption breakthrough curves over a range of flowrates. By determining $\sigma$ for two experimental curves, it is possible to calculate $\sigma$ from *equation 3.4.1* for a theoretical flowrate. A value for $t_{50}$ can be determined from *equation 3.4.2*, and by selecting a number of values for $t$ and substituting into *equation 2.4.1*, corresponding $C$ values can be calculated (*Figure 3.4.4*).

By introducing the column length, $L$, into *equation 3.4.1*, the model has scale up potential and the equation becomes

$$\sigma^2 = k_1 Q / L \qquad (4.4.1)$$

By calculating $\sigma$ for two experimental breakthrough curves at various column lengths, curves at theoretical lengths and constant flowrates can be determined using a similar procedure to that described above.

**4.4.4** *Continuous flow systems: summary*

Continuous fixed bed adsorption of $Cu^{2+}$ ions was achieved using the PVF immobilised biomass systems. Overall, 0.8 g of column immobilised biomass was capable of the complete sequestration of $Cu^{2+}$ ions from *ca.* 1.4 l of influent solution (150 µmol $l^{-1}$), at the highest tested flowrate of 11.63 ml $min^{-1}$. The immobilisation procedure was found to have no effect on the biosorption potential of the native freeze-dried *Rhizopus arrhizus* biomass, but equilibration to pH 4 after immobilisation reduced uptake capacities by *ca.* 50%. The two parameter fixed-bed adsorption model was also successful in predicting the $Cu^{2+}$ ion adsorption breakthrough curves over the flowrate range at constant column lengths.

### 4.5 *Selenite adsorption studies: discussion*

In batch equilibrium isotherm type studies, no changes in selenite solution concentration was observed following the addition of either *Rhizopus arrhizus* or the *Penicillium* species as described in *section 3.5*. Clearly no selenite adsorption and/or active accumulation by both live non-metabolising fungi occurred. This absence of affinity of negatively charged fungal cell envelopes for adsorption of the selenium oxyanion $SeO_3^{2-}$ is likely a result of anion-anion repulsion effects. In contrast the uptake of anion complexes was observed by *Rhizopus arrhizus* biomass in a previous study (Tobin *et al.*, 1984) and was found to be strongly pH dependent, and the adsorption of selenium also in the form of the oxyanion selenite was reported for metal oxides and clay minerals (Tan *et al.*, 1994).

#### 4.5.1 *Release of $Ca^{2+}$, $Mg^{2+}$, $H^+$ and $K^+$ ions*

Although no selenite was accumulated by the fungi, $Ca^{2+}$, $Mg^{2+}$, $H^+$ and $K^+$ ions release into the aqueous environment was evident, and levels generally increased with increasing selenite concentrations (*Tables 3.5.1* and *3.5.2*). Maximum ion release levels recorded are presented below in *table 4.5.1* for both fungal species.

**Table 4.5.1**: Maximum equilibrium $Ca^{2+}$, $Mg^{2+}$, $H^+$ and $K^+$ ion release levels for *Rhizopus arrhizus* and the *Penicillium* species following selenite-microbe contact.

| ion | *Rhizopus arrhizus* | *Penicillium species* |
|---|---|---|
| $Ca^{2+}$ | 10 ($\mu mol\ g^{-1}$) | 45 ($\mu mol\ g^{-1}$) |
| $Mg^{2+}$ | 77 ($\mu mol\ g^{-1}$) | 60 ($\mu mol\ g^{-1}$) |
| $H^+$ | 27 ($\mu mol\ g^{-1}$) | 66 ($\mu mol\ g^{-1}$) |
| $K^+$ | 73 ($\mu mol\ g^{-1}$) | 364 ($\mu mol\ g^{-1}$) |

The plasma and vacuolar membranes are the main transport membranes of fungi, and membrane permeability resulting in $K^+$, $H^+$, $Ca^{2+}$ and $Mg^{2+}$ release has been shown to be associated with cation accumulation and toxicity (Gadd, 1993*b*; Karamushka & Gadd, 1994). The most abundant cation in most cells is $K^+$ and is believed to play an essential role in the maintenance of an ionic or osmotic environment in the cytoplasm (Ohsumi, Kitamoto & Anraku, 1988). For the *Penicillium* species, $K^+$ was the most abundantly released cellular cation, and for *Rhizopus arrhizus*, $Mg^{2+}$ and $K^+$ were released to the greatest extent in almost equimolar concentrations.

In similar type studies described in *section 3.1*, $Sr^{2+}$, $Cd^{2+}$ and $Cu^{2+}$ ion adsorption by freeze-dried *Rhizopus arrhizus* biomass resulted in maximum $Ca^{2+}$ and $Mg^{2+}$ displacement levels of *ca.* 20 and 110 μmol $g^{-1}$ respectively. However for the non-viable biomass it is likely that some of the $Ca^{2+}$ and $Mg^{2+}$ ions were directly displaced from surface ligands by the adsorbing cations during the formation of ionic bonds (Crist *et al.*, 1988; 1990; 1992; Avery & Tobin, 1992; 1993; Brady & Tobin, 1994; 1995). In the present study for live non-metabolising biomass, $Ca^{2+}$ and $Mg^{2+}$ release values are *ca.* 50% lower than freeze-dried levels, and since selenite sequestration was not evident, all $Ca^{2+}$, $Mg^{2+}$, $H^+$ and $K^+$ ion release appears to have resulted from passive cellular efflux. However studies on microbial interactions with toxic metals have also reported membrane damage that caused internal cellular cation losses (Gadd & Mowll, 1983; Simmons *et al.*, 1995), although this usually occurred in conjunction with uptake/sorption of the toxic metal in question.

### 4.5.2 *Selenite adsorption studies: summary*

Overall it appears that electrostatic repulsion prevented selenite adsorption by the fungal cell wall surfaces although external selenite in the aqueous environment stimulated cellular $Ca^{2+}$, $Mg^{2+}$, $H^+$ and $K^+$ loss. Whether this cation release was in response to a detoxification mechanism or resulted from membrane damage cannot be established at this point. Overall, $K^+$ and $Mg^{2+}$ were the main cations released, followed in order by $H^+$ and $Ca^{2+}$.

## 4.6 *Selenite transformation studies: discussion*

### 4.6.1 *Effect of selenite on biomass growth*

It appears that the selenite at 1000 μmol $l^{-1}$ concentration exerted no discernable toxic effect on fungal growth. Almost identical growth curves were observed in the presence and absence of sodium selenite, with maximum biomass concentrations of *ca.* 6.0 g $l^{-1}$ (*Figure 3.6.1*a and *Figure 3.6.2*a). Close agreement of the pH profiles of each system further support the similarities in growth patterns (*Figure 3.6.1*b and *Figure 3.6.2*b). Slight pH increases detected during the decline growth phases were consistent for replicate experiments and may be due to the release of $H^+$ complexing moieties by disintegrating biomass. Similar trends were also observed for the growth of *Salmonella heidelberg* in the presence and absence of selenite (McCready *et al.*, 1966).

**4.6.2** *Volatilisation trends*

After 14 d, the sum of selenium in the aqueous phase and selenium associated with the biomass equalled *ca.* 4340 μmol (*Figure 3.6.2*e). A total of 440 μmol of selenium were isolated from the activated charcoal traps representing *ca.* 8.8% volatilisation from the original 5000 μmol concentration. Combining the figures *ca.* 4780 μmol of selenium were accounted for representing *ca.* 95.6% of the total selenium present in the reactor at the start of the experiments. During the lag and rapid growth phases (days 0-7), *ca.* 3.7% volatilisation was determined compared with *ca.* 5.1% during the stationary phase and the decline phase (days 8-14). Clearly volatilisation is both growth-associated and non-growth associated. In earlier studies Thompson-Eagle & Frankenberger (1991) reported that total microbial numbers were directly related to selenium volatilisation rates, and a minimum selenium threshold for alkylselenide production was not found (Karlson & Frankenberger, 1989; Thompson-Eagle & Frankenberger, 1990*a*, 1991).

Overall, *ca.* 220 μmol of selenium remained unaccounted for, representing less than 5% of the initial selenium inventory. It is likely that incomplete trapping may have contributed to this discrepancy since a fourth activated charcoal trap in series also retained volatile selenium compounds as observed in *section 3.7*. Incomplete extraction of the volatile selenium products as well as general experimental error may also have contributed.

**4.6.3** *Nature of volatile selenium compounds*

The extraction of volatile selenium compounds from the activated charcoal traps by methanol indicated that these volatiles were organic in nature. Using the extraction procedure, volatile selenium compounds were isolated only from activated charcoal traps exposed to exhaust gases from bioreactors containing the growing *Penicillium* species in the presence of selenite. As expected, no volatile selenium compounds were detected in the exhaust gases from selenite-free and biomass-free bioreactors. Under laboratory and field conditions, dimethylselenide is reported to be the predominant volatile selenium species evolved by microorganisms under aerobic conditions (Doran & Alexander, 1977; Zieve *et al.*, 1985; Karlson & Frankenberger, 1990; Thompson-Eagle & Frankenberger, 1990*a*, *b*; Thompson-Eagle, Frankenberger & Longley, 1991), and it is likely that the selenium compounds volatilised in this study were dimethylselenide. The water cooled condensers used to minimise media evaporation may have condensed some of this volatile selenium product, since the temperature of the cooling water was *ca.* 16°C, and the boilng point of dimethylselenide is 58°C (TCI, 1996). This may have contributed to the *ca.* 220 µmol of selenium unaccounted for, as observed in *sections 3.6.2* and *4.6.2*.

In other previous studies, effluent gases were flushed directly into concentrated nitric acid in order to trap the volatile selenium species (Zieve *et al.* 1985; Tan *et al.*, 1994). This technique was applied to our earlier studies instead of using activated charcoal but was found not to trap selenium volatiles. It may be that this was due to the inefficiency of room temperature nitric acid at converting organic selenium compounds into inorganic selenium species and the effluent gases being flushed through the acid at relatively high flowrates. Alternatively, traps containing solutions of $Na_2CO_3$ and $Na_2HPO_4$ could also be considered for alkylselenides. This system was used to trap alkylmercury produced by fungal transformations of inorganic mercury (Kimura & Miller, 1960; Yannai, Berdicevsky & Duek, 1991).

**4.6.4** *Temperature, pH and carbon source effects*

The volatilisation of selenium is temperature-dependent, and the bioreactor temperatures were maintained at 25°C in order to favour the biomethylation processes. Biomethylation of selenium in the environment occurs at optimal levels in the daytime during the warm spring and summer months at temperatures ranging between 20°C - 35°C (Thompson-Eagle, Frankenberger & Karlson, 1989; Atkinson *et al.*, 1990, Calderone *et al.*, 1990; Frankenberger & Karlson, 1994). Temperature studies conducted by Calderone *et al.* (1990) postulated that increasing temperature increases the solubility of inorganic selenium and subsequently selenium availabilty for methylation. Frankenberger & Karlson (1989) calculated for every 10°C rise, the rate of selenium biomethylation increased 2.6-fold.

In aqueous environments, neutral to alkaline conditions increase the solubility and availability of selenium for microbial transformations, and chemically the reduction of selenite to dimethylselenide should be favoured at a low pH (see Frankenberger & Karlson, 1989). The media pH values decreased from 3.00 to a low of 2.02 during the growth processes (*Figure 3.6.*2b) thereby enhancing conditions considered favourable for dimethylselenide production. In contrast optimum pH values for selenium biomethylation as reported by Frankenberger & Karlson (1989, 1994) were between 7.7 - 8.0. However in these studies the soil microflora investigated apparently had highest biomethylation activity when exposed to pH conditions similar to their native habitat and bacteria were likely to be responsible for most of the biomethylation activity.

In the present study glucose was used as the carbon source. Previous work using the fungus *Alternaria alternata* in pond water indicated glucose to be a poor promoter of the biomethylation process (Thompson Eagle & Frankenberger, 1990*b*; 1991). However in studies with saline seleniferous soil, among carbon sources tested glucose was most effective in enhancing dimethylselenide production and polysaccharides were least effective (Frankenberger & Karlson, 1989).

**4.6.5** *Accumulation and reduction trends*

Reduction of selenite to amorphous elemental selenium by the *Penicillium* species was observed in the reactors as evidenced by the characteristic red colour of both the aqueous phase and the fungal biomass (Nickerson & Falcone, 1963; McReady *et al.*, 1966; Ramadan *et al.*, 1988; Tomei *et al.*, 1992; Gharieb *et al.*, 1995), and occurred only during the decline phase of growth (days 11-14). The disintegration of the biomass may expose certain intracellular metabolites either bound to the biomass or released into the aqueous environment that in turn may catalyse this reduction. As biomass growth became stationary, selenium associated with the biomass (dry weight) decreased (see *Figure 3.6.2*d). However, during the decline phase of gowth where selenite reduction to amorphous elemntal selenium was obvious, selenium accumulated by the biomass increased to a maximum level of *ca.* 60 μmol $g^{-1}$.

Complete reduction of similar concentrations of selenite has been reported for bacterial cells with maximum reduction also occurring during the stationary growth phase for *Wolinella succinogens* (Tomei *et al.*, 1992) but also concurrently with the rapid growth phase for *Pseudomonas stutzeri* (Lortie *et al.*, 1992). Selenite reduction by *Salmonella heidelberg* was found to be associated primarily with the lag phase of growth presumably as a detoxification procedure preceding growth, and reduction was shown to be directly dependent on the metabolic activity of the microorganism and not on spontaneous chemical reductions occurring as a result of media constituents or pH change during microbial growth (McCready *et al.*, 1966).

### 4.6.6 *Selenite transformation studies: summary*

This work has demonstrated that the *Penicillium* species is capable of selenite transformation in aqueous medium by biomass-associated processes as well as the formation of volatile organic derivatives. Measurement of volatile selenium compounds, selenium in solution and selenium associated with the biomass has enabled the calculation of mass balances and the relative significance of biomethylation and assimilatory/reductive processes. Using a novel methanol/acid extraction method, this work has found that biomethylation accounted for *ca.* 8.8% of the total selenium present in the original culture medium. While it is not possible to separate the processes of selenite reduction, transport and incorporation into selenoproteins within the biomass (which accounted for *ca.* 36.6% of the total selenium originally present), it is clear that these processes are of greater significance than biomethylation in the overall biotransformation of selenite in solution.

## 4.7 *Selenite transformation enhancement studies: discussion*

Acceleration of the biomethylation process has previously been achieved by the addition of complex carbon sources such as pectin and plant residues (Karlson & Frankenberger, 1988*b*; 1989; Calderone *et al.*, 1990; Thompson-Eagle & Frankenberger, 1990*a*). These compounds usually have partially methylated structures which may provide a source for direct transfer of free methyl groups from the carbohydrate to the microbial methylation pathway. Dulbecco's Modified Eagle Medium is a synthetic culture medium composed of a range of amino acids, vitamins, inorganic salts, glucose and phenol red indicator, and is usually used in studies associated with animal cell tissue culture. These

components were made available to the *Penicillium* species at levels outlined in *Table 2.7.1* by additions of 50 ml DMEM *10X* to 5 l of broth media. The amino acid L-methionine, a cofactor in the transfer of methyl groups, is a component of DMEM and in previous studies has been shown to promote methylation reactions, both in native and derivative forms. Dimethylselenide formation from selenite by cell-free extracts of a *Corynebacterium* species was achieved by the addition of *S*-adenosylmethionine (SAM) (Doran & Alexander, 1977). Dimethylselenide production from selenate by the fungus *Alternaria alternata* was stimulated by methyl cobalamine and L-methionine (Thompson-Eagle *et al.*, 1989), and in a saline seleniferous soil, optimum conditions for indigenous microbes dimethylselenide production included the provisions of L-methionine and galacturonic acid (Frankenberger & Karlson, 1989). Other amino acids present in DMEM include L-cysine, L-serine, and L-glycine, and all have been shown to promote dimethylselenide production with the fungus *Alternaria alternata* (Thompson-Eagle & Frankenberger, 1990*a*).

**4.7.1** *Effect of DMEM on fungal growth*

A prolonged period of negligable biomass growth over 6 days occurred following a 50 ml DMEM amendment at $t_0$. This growth inhibition may represent fungal adjustment to the DMEM constituents on a genetic level for the manufacture of selective cellular metabolites. After day 6 biomass levels increased to a maximum of *ca.* 7.5 g $l^{-1}$. For the two other DMEM addition systems, 25 ml at $t_0$ and on day 7, and 50 ml on day 7, and also for no DMEM additions (*section 4.6.1*), maximum biomass levels were of the order of *ca.* 6.0 g $l^{-1}$. It appears therefore that in the 50 ml $t_0$ addition system, the DMEM constituents were utilised for further biomass growth. A 50 ml DMEM addition on day 7 appeared to inhibit fungal growth and induced a decline phase of growth.

### **4.7.2** *DMEM induced volatilisation trends*

#### **4.7.2.1** *Single 50 ml DMEM additions*

For systems unamended with DMEM (*section 4.6.2*), volatilisation levels represented 8.8% of the total selenium inventories, *ca.* 440 µmol overall. Out of a total of *ca.* 5000 µmol, *ca.* 184 and 256 µmol were volatilised from $t_0$ to day 7, and from days 7-14 respectively. During the same time periods, for the 50 ml DMEM addition at $t_0$, selenium volatilised was *ca.* 202 and 219 µmol, 421 µmol overall and representing 8.4% volatilisation from the system. Again, during the same time periods, *ca.* 202 and 240 µmol were volatilised for the 50 ml DMEM day 7 addition. This represented 8.8% volatilisation, a total of 442 µmol. Clearly from these results it is evident that single 50 ml aliquot DMEM additions failed to enhance further the volatilisation process.

#### **4.7.2.2** *Two 25 ml DMEM additions*

Methylation enhancement was detected for two 25 ml DMEM additions. Between days $t_0$-7 and 7-14, 303 and 313 µmol were isolated respectively, reflecting 12.3% volatilisation and 616 µmol of selenium. From the biomass growth curves profiled and described above, it seems likely that 50 ml DMEM aliquots were toxic to the growing fungus, as evidenced by the prolonged lag and instant decline phases observed immediately after addition. Two 25 ml additions may exert reduced toxic effects, and rather than increase active resistance and tolerance mechanism, the fungus can engage in methylation transformations.

### 4.7.3 *DMEM induced accumulation/biosorption trends*

Overall DMEM enhanced selenite accumulation by the *Penicillium* species. It appears that the DMEM components assisted the intracellular accumulation of selenite, probably in the manufacture of essential protective metabolites. The presence of selenite has been reported to increase cellular carbohydrate, protein and lipid levels in a *Fusarium* species, and to induce the biosynthesis of several low molecular weight proteins. This was interpreted as a tolerance mechanism to high levels of selenium as either an equilibrium process, or a compensationary mechanism for the replacement of metabolites damaged by selenium (Ramadan *et al.*, 1988).

In all cases following DMEM addition the nature of the mycelia changed from the finely suspended turbid nature of the fungal inocula to well defined large red pellets, demonstrating selenite reduction to elemental selenium during all phases of growth. In contrast for non-DMEM systems, the bioreactor contents only went red in the decline phases of growth (*section 3.6.2*), and there was an absence of the large well defined mycelium particles. However it is possible that the DMEM components may have adsorbed and precipitated or reduced the selenite within the large mycelium pellets independently of the biomass, accounting for the high accumulation levels described above.

Other observed microbial selenite detoxification procedures include, the formation of needle-like crystal structures of elemental selenium on the surfaces of fungal hyphae, spores and conidia (Ramadan *et al.*, 1988; Gharieb *et al.*, 1995), and intracellular deposition of electron-dense selenium granules in yeast and bacteria (Falcone & Nickerson, 1963; Tomei *et al.*, 1992).

For all DMEM addition systems, pH decreased to final levels of *ca.* 1.95, from initial values of between 3.3-3.8, after inocula additions. This is similar to non-DMEM systems, where pH values decreased from 3.00 to a low of 2.02 (*Section 3.6.2*), and as discussed above, decreasing pH has been reported to enhance selenium volatilisation (Frankenberger & Karlson, 1989).

### **4.7.4** *Selenite transformation enhancement studies: summary*

Overall DMEM enhanced the fungal transformation of selenite to amorphous elemental selenium in all cases, possibly as a result of increases in the manufacture and/or replacement of protective metabolites. Reduction to elemental selenium and subsequent accumulatory/biosorptive processes appear to be the favoured mechanisms of detoxification over volatilisation. Enhancement of the volatilisation processes may be achieved by small incremental additions of DMEM over the 2 wk time periods. Volatilisation enhancement techniques may potentially be applied so that selenium in the form of volatile compounds may be dispersed and diluted by air currents directly away from contaminated areas with possible deposition occurring in selenium-deficient regions.

# CHAPTER 5

# CONCLUSION

*Interactions of metal and metalloid ions with fungal biomass*

*PhD Research Thesis by*

*Joseph M. Brady* B.Sc.

## CHAPTER 5: CONCLUSION

Metal ion accumulation by non-metabolising *Rhizopus arrhizus* biomass occurs exclusively by passive equilibrium adsorption processes as a result of anion-cation interactions, and equilibrium positions are independent of the suspended biomass levels in the aqueous phases. Freeze-drying maintains the integrity of the fungal biomass, thus preserving native metal-binding functional groups. Oven-drying at 55°C reduces the adsorption capacity of the native biological ligands, possibly by damage to the structural integrity of the biomass and protein denaturation.

Both ionic and covalent bonds contribute significantly to the adsorption of $Mn^{2+}$, $Zn^{2+}$, $Cd^{2+}$, $Cu^{2+}$ and $Pb^{2+}$ ions, while only ionic binding was observed for $Sr^{2+}$. The level of ionic binding is constant for each divalent cation, and such interactions are the primary mechanisms of metal ion adsorption. A secondary adsorption mechanism involves covalent type interactions, and levels of covalent binding increase in the order: $Mn^{2+} < Zn^{2+} < Cd^{2+} < Cu^{2+} < Pb^{2+}$. Increasing *softness* and decreasing *hardness* of the ions increase in the order $Sr^{2+} < Mn^{2+} < Zn^{2+} < Cd^{2+} < Cu^{2+} < Pb^{2+}$, where $Sr^{2+}$ is considered a true *hard* ion according to the *hard* and *soft* principle of metal ions, and $Mn^{2+}$, $Zn^{2+}$, $Cd^{2+}$, $Cu^{2+}$ and $Pb^{2+}$ ions are *borderline-soft*. Overall adsorption levels increase in the same order and positively correlate with corresponding ion covalent index values. These index values are a measure of the extent metal ions react covalently with biological ligands, and the higher the value the greater the covalent contributions.

As a result of anion-anion repulsion effects, non-metabolising biomass of both *Rhizopus arrhizus* and the *Penicillium* species exhibit no biosorptive affinity for the oxyanion selenite in solution. The actively metabolising *Penicillium* species however, is capable of transforming selenite in solution to volatile selenium compounds and red amorphous elemental selenium. In minimal media with glucose as the sole carbon source, volatilisation is both growth and non-growth associated, whereas reduction to elemental selenium occurs only during the decline phase of growth. However, collective additions of both amino acids and vitamins can enhance the reduction of the selenium oxyanion to the elemental form throughout the growth cycle.

# REFERENCES


Ahrland, S., Chatt, J. & Davies, N.R. (1958). The relative affinities of ligand atoms for acceptor molecules and ions. *Quarterly Review of the Chemical Society* **12**, 265-276.

Akthar, N., Sastry, S. & Mohan, M. (1995). Biosorption of silver ions by processed *Aspergillus niger* biomass. *Biotechnology Letters* **17**, 551-556.

Allen, S.J. & Brown, P.A. (1995). Isotherm analyses for single component and multi-component metal sorption onto lignite. *Journal of Chemical Technology and Biotechnology* **62**, 17-24.

Allred, A. L. (1961). Electronegativity values from thermochemical data. *Journal of Inorganic and Nuclear Chemistry* **17**, 215-221.

Andreoni, V., Finoli, C., Manfrin, P., Pelosi, M. & Vecchio, A. (1991). Studies on the accumulation of cadium by a strain of *Proteus mirabilis*. *FEMS Microbiology Ecology* **85**, 183-192.

Andreoni, V., Fasoli, R., Sorlini, C. & Finoli, C. (1994). Investigation of lead resistance in a *Brevibacterium* Strain. *Ann. Microbiol. Enzimol.* **44**, 153-161.

Appanna, V.D., Huang, J., Prusak-Sochaczewski, E. & St. Pierre, M. (1995). Microbial adaptation to aluminum. *Biotechnology progress* **11**, 159-163.

Artola, A. & Rigola, M. (1992). Selection of optimum biological sludge for zinc removal from wastewater by a biosorption process. *Biotechnology Letters* **14**, 1199-1204.

Atkinson, R., Aschmann, S.M., Hasegawa, D., Thompson-Eagle, E.T. & Frankenberger, W. T. (1990). Kinetics of atmospherically important reactions of dimethyl selenide. *Environmental Science and Technology* **24**, 1326-1332.

Avery, S.V. (1995). Microbial interactions with caesium-implications for biotechnology. *Journal of Chemical Technology and Biotechnology* **62**, 3-16.

Avery, S.V., Codd, G.A. & Gadd, G.M. (1991). Caesium accumulation and interactions with other monovalent cations in the *Cyanobacterium synechocystis* PCC 6803. *Journal of General Microbiology* **137**, 405-413.

Avery, S.V., Codd, G.A. & Gadd, G.M. (1992). Replacement of cellular potassium by caesium in *Chlorella emersonii*: differential sensitivity of photoautotrophic and chemoheterotrophic growth. *Journal of General Microbiology* **138**, 69-76.

Avery, S.V., Codd, G.A. & Gadd, G.M. (1993). Transport kinetics, cation inhibition and intracellular location of accumulated caesium in the green microalga *Chlorella salina*. *Journal of General Microbiology* **139**, 827-834.

Avery, S.V. & Tobin, J.M. (1992). Mechanisms of strontium uptake by laboratory and brewing strains of *Saccharomyces cerevisiae*. *Applied and Environmental Microbiology* **58**, 3883-3889.

Avery, S.V. & Tobin, J.M. (1993). Mechanism of adsorption of hard and soft ions by *Saccharomyces cerevisiae* and the influence of hard and soft anions. *Applied and Environmental Microbiology* **59**, 2851-2856, 538-542.

Axley, M.J. & Stadtman, T.C. (1989). Selenium metabolism and selenium-dependent enzymes in microorganisms. *Annual Reviews in Nutrition* **9**, 127-137.

Azab, M.S., Peterson, P.J. & Young, T.W.K. (1990). Uptake of cadium by fungal biomass. *Microbios* **62**, 23-28.

Belde, P.J.M., Kessels, B.G.F., Moelans, I.M. & Borst-Pauwels, G.W.F.H. (1988). $Cd^{2+}$ uptake, $Cd^{2+}$ binding and loss of cell $K^{+}$ by a Cd-sensitive and a Cd-resistant strain of *Saccharomyces cerevisiae*. *FEMS Microbiology Letters* **49**, 493-498.

Belter, P.A., Cussler, E.L. & Hu, W.S. (1988). *Bioseparations, Downstream Processing for Biotechnology*. John Wiley & Sons: New York.

Bender, J., Gould, J.P., Vatcharapijarn, Y. & Saha, G. (1991). Uptake, transformation and fixation of Se(VI) by a mixed selenium-tolerant ecosystem. *Water, Air and Soil Pollution* **59**, 359-367.

Berhe, A. Fristedt, U. & Persson, B.L. (1995). Expression and purification of the high-affinity phosphate transporter of *Saccharomyces cerevisiae*. *European Journal of Biochemistry* **227**, 566-572.

Beveridge, T.J. & Murray, R.G.E. (1980). Sites of metal deposition in the cell wall of *Bacillus subtilis*. *Journal of Bacteriology* **141**, 876-887.

Blackwell, K.J., Singleton, I. & Tobin, J.M. (1995). Metal cation uptake by yeast: a review. *Applied Microbiology and Biotechnology* **43**, 579-584.

Blais, J.F., Tyagi, R.D. & Auclair, J.C. (1993). Metals removal from sewadge sludge by indigenous iron-oxidizing bacteria. *Journal of Environmental Science and Health* **A28(2)**, 443-467.

Bode, H.P., Dumschat, M. Garotti, S. & Fuhrmann, G.F. (1995). Iron sequestration by the yeast vacuole. A study with vacuolar mutants of *Saccharomyces cerevisiae*. *European Journal of Biochemistry* **228**, 337-342.

Brady, D. & Duncan, J.R. (1994*a*). Bioaccumulation of metal cations by Saccharomyces cerevisiae. *Applied Microbiology and Biotechnology* **41**, 149-154.

Brady, D. & Duncan, J.R. (1994*b*). Binding of heavy metals by the cell walls of *Saccharomyces cerevisiae*. *Enzyme and Microbial Technology* **16**, 633-638.

Brady, D., Glaum, D. & Duncan, J.R. (1994). Copper tolerance in *Saccharomyces cerevisiae*. *Letters in Applied Microbiology* **18**, 245-250.

Brady, J.M. & Tobin, J.M. (1994). Adsorption of metal ions by *Rhizopus arrhizus* biomass: Characterisation studies. *Enzyme and Microbial Technology* **16**, 671-675.

Brady, J.M. & Tobin, J.M. (1995). Column studies of metal removal by immobilised biomass. *ICHEME Research Event/First European Conference* **1**, 213-215.

Brady, J.M. & Tobin, J.M. (1995). Binding of hard and soft metal ions to *Rhizopus arrhizus* biomass. *Enzyme and Microbial Technology* **17**, 791-796.

Brady, J.M., Tobin, J.M. & Gadd, G.M. (1996). Volatilization of selenite in aqueous medium by a *Penicillium* species. *Mycological Research* **00**, 00-00.

Calderone, S.J., Frankenberger, W.T., Parker, D.R. & Karlson, U. (1990). Influence of temperature and organic amendments on the mobilization of selenium in sediments. *Soil Biology and Biochemistry* **22**, 615-620.

Campbell, R. & Martin, M.H. (1990). Continuous flow fermentation to purify waste water by the removal of cadmium. *Water, Air and Soil Pollution* **50**, 397-408.

Carlile, M.J. & Watkinson, S.C. (1994). *The Fungi*. Academic Press: London.

Chamness, G. C. & McGuire, W. L. (1975). Scatchard plots: common errors in correction and interpretation. *Steroids* **26**, 538-542.

Chen, P. & Ting, Y.P. (1995). Effect of heavy metal uptake on the electrokinetic properties of *Saccharomyces cerevisiae*. *Biotechnology Letters* **17**, 107-112.

Chong, K.H. & Volesky, B. (1995). Description of two-metal biosorption equilibria by Langmuir-type models. *Biotechnology and Bioengineering* **47**, 451-460.

Corzo, J. Leon-Barrios, M. Hernando-Rica, V. & Gutierrez-Navarro, A.M. (1994). Precipitation of metallic cations by the acidic exopolysaccharides from *Bradyrhizobium japonicum* and the *Bradyrhizobium* (*Chamaecytisus*) strain BGA-1. *Applied and Environmental Microbiology* **60**, 4531-4536.

Crist, R. H., Martin, J. R., Guptil, P. W., Eslinger, J. M. & Crist, D. R. (1990). Interaction of metals and protons with algae. 2. Ion exchange in adsorption and metal displacement by protons. *Environmental Science and Technology* **24**, 337-342.

Crist, R. H., Oberholser, K., McGarrity, J., Crist, D. R., Johnson, J. K. & Brittsan, J. M. (1992). Interaction of metals and protons with algae. 3. Marine algae, with emphasis on lead and aluminium. *Environmental Science and Technology* **26**, 496-502.

Crist, R. H., Oberholser, K., Schwartz, D., Marzoff, J. & Ryder, D. (1988). Interaction of metals and protons with algae. *Environmental Science and Technology* **22**, 755-760.

Darnall, D. W., Greene, B., Hosae, M., McPherson, R. A., Henzl, M. & Alexander, M. D. (1986). Recovery of heavy metals by immobilized algae. In: *Trace metal removal from aqueous solution* (ed R. Thompson), pp. 1-24. The Royal Society of Chemistry: London.

Deacon, J.W. (1980). *Introduction to Modern Mycology*. Blackwell Scientific Publications: Oxford, England.

de Carvalho, R.P., Chong, K.K. & Volesky, B. (1995). Evaluation of the Cd, Cu and Zn biosorption in two-metal systems using an algal biosorbent. *Biotechnology Progress* **11**, 39-44.

de Rome, L. & Gadd, G.M. (1987*a*). Measurement of copper uptake in *Saccharomyces cerevisiae* using a $Cu^{2+}$-selective electrode. *FEMS Microbiology Letters* **43**, 283-287.

de Rome, L. & Gadd, G. M. (1987*b*). Copper adsorption by *Rhizopus arrhizus*, *Cladosporium resinae* and *Penicillium italicum*. *Applied Microbiology and Biotechnology* **26**, 84-90.

de Rome, L. & Gadd, G. M. (1991). Use of pelleted and immobilized yeast and fungal biomass for heavy metal and radionuclide recovery. *Journal of Industrial Microbiology* **7**, 97-104.

Donnellan, N., Rollan, A., McHale, L. & McHale, A.P. (1995). The effect of electric field stimulation on the biosorption of uranium by non-living biomass derived from *Kluyeromyces marxianus* IMB3. *Biotechnology Letters* **17**, 439-442.

Doran, J.W. & Alexander, M. (1977). Microbial transformation of selenium. *Applied and Environmental Microbiology* **33**, 31-37.

Engl, A. & Kunz, B. (1995). Biosorption of heavy metals by *Saccharomyces cerevisiae*: Effects of nutrient conditions. *Journal of Chemical Technology and Biotechnlogy* **63**, 257-261.

Enzminger, J. D. (1991) Metal finishing and processing. *Resident Journal Water Pollution Control Federation* **63**, 489-494.

Falcone, G. & Nickerson, W.J. (1963). Reduction of selenite by intact yeast cells and cell-free preparations. *Journal of Bacteriology* **85**, 754-762.

Farcasanu, I.C., Hirata, D., Tsuchiya, E., Nishiyama, F. & Miyakawa, T. (1995). Protein phosphatse 2B of *Saccharomyces cerevisiae* is required for tolerance to manganese, in blocking the entry of ions into the cells. *European Journal of Biochemistry* **232**, 712-717.

Farkas, V. (1990). Fungal cell walls: Their structure, Biosynthesis and Biotechnological aspects. *Acta Biotechnology* **10**, 225-238.

Fourest, E., L'homme, B., Quinkal, I. & Roux, J.C. (1991). Purification of heavy metal loaded waste water by biosorption on fungal by-products. *Med. Fac. Landouww. Rijksuniv. Gent,* **56**, 1579-1584.

Fourest, E. & Roux, J. (1992). Heavy metal biosorption by fungal mycelial by-products: mechanisms and influence of pH. *Applied Microbiology and Biotechnology* **37**, 399-403.

Frankenberger, W.T. & Karlson, U. (1989). Environmental factors affecting microbial production of dimethylselenide in a selenium-contaminated sediment. *Soil Science Society of America Journal* **53**, 1435-1442.

Frankenberger, W.T. & Karlson, U. (1994). Microbial volatilisation of selenium from soils and sediments. In *Selenium in the Environment* (ed W. T. Frankenberger & S. Benson), pp. 369-388. Marcel Dekker Inc.: New York.

Gadd, G.M. (1990). Biosorption. *Chemistry and Industry* **13**, 421-426.

Gadd, G.M. (1992). Metals and microorganisms: A problem of definition. *FEMS Microbiology Letters* **100**, 197-204.

Gadd, G.M. (1993*a*). Microbial formation and transformation of organometallic and organometalloid compounds. *FEMS Microbiology Reviews* **11**, 297-316.

Gadd, G.M. (1993*b*). Interactions of fungi with toxic metals. *New Phytologist* **124**, 25-60.

Gadd, G.M. & de Rome, L. (1988). Biosorption of copper by fungal melanin. *Applied Microbiology and Biotechnology* **29**, 610-617.

Gadd, G.M. & Mowll, J.L. (1983). The relationship between cadmium uptake, potassium release and viability in *Saccharomyces cerevisiae*. *FEMS Microbiology Letters* **16**, 45-48.

Gadd, G.M. & Mowll, J.L. (1985). Copper uptake by yeast-like cells, hyphae, and Chlamydospores of *Aureobasidium pullulans*. *Experimental Mycology* **9**, 230-240.

Gadd, G.M. & White, C. (1985). Copper uptake by *Penicillium ochro-chloron*: Influence of pH on toxicity and demonstration of energy-dependent copper influx using protoplasts. *Journal of General Microbiology* **131**, 1875-1879.

Gadd, G.M. & White, C. (1989*a*). Heavy metal and radionuclide accumulation and toxicity in fungi and yeasts. In *Metal-Microbe Interactions* (ed. R.K. Poole & G.M. Gadd), pp. 19-38. IRL Press: Oxford, UK.

Gadd, G.M. & White, C. (1989*b*). Removal of thorium from simulated acid process streams by fungal biomass. *Biotechnology and Bioengineering* **33**, 592-597.

Gardae-Torresday, J. L., Becker-Hapak, Hosea, J. M. & Darnall, W. (1990). Effect of chemical modifiction of algal carboxyl groups on metal ion binding. *Environmental Science and Technology* **24**, 1372-1378.

Geddie, J.L. & Sutherland, I.W. (1993). Uptake of metals by bacterial polysaccharides. *Journal of Applied Bacteriology* **74**, 467-472.

Gelmi, M., Apostoli, P., Cabibbo, E., Porru, S., Alessio, L. & Turano, A. (1994). Resistance to cadmium salts and metal absorption by different microbial species. *Current Microbiology* **29**, 335-341.

Gharieb, M.M., Wilkinson, S.C. & Gadd, G.M. (1995). Reduction of selenium oxyanions by unicellular, polymorphic and filamentous fungi: cellular location of reduced selenium and implications for tolerance. *Journal of Industrial Microbiology* **14**, 300-311

Golab, Z. & Breitenbach, M. (1995). Sites of copper binding in *Streptomyces Pilosus*. *Water, Air and Soil Pollution* **82**, 713-721.

Guibal, E., Roulph, C. & Le Cloirec, P. (1992). Uranium biosorption by a filamentous fungus *Mucor miehei* pH effect on mechanisms and performances of uptake. *Water Research* **26**, 1139-1145.

Hassett, R. & Kosman, D.J. (1995). Evidence for Cu(II) reduction as a component of copper uptake by *Saccharomyces cerevisiae*. *The Journal of Biological Chemistry* **270**, 128-134.

Haygrath, P.M. (1994). Global importance and global cycling of selenium. In *Selenium in the Environment* (ed. W.T. Frankenberger & S. Benson), pp. 1-28. Marcel Dekker Inc.: New York.

Holan, Z.R., Volesky, B. & Prasety, I. (1993). Biosorption of cadmium by biomass of marine algae. *Biotechnology and Bioengineering* **41**, 819-825.

Hughes, M. N. & Poole, R. K. (1989). *Metals and micro-organisms*. Chapmann and Hall: London.

Hughes, M. N. & Poole, R. K. (1991). Metal speciation and microbial growth - the hard (and soft) facts. *Journal of General Microbiology* **137**, 725-734.

Irving, H & Williams, R.J.P. (1948). Order of stability of metal complexes. *Nature* **162**, 746-747.

Junghans, K. & Straube, G. (1991). Biosorption of copper by yeasts. *Biology of Metals* **4**, 233-237.

Karamushka, V.I. & Gadd, G.M. (1994). Influence of copper on proton efflux from *Saccharomyces cerevisiae* and the protective effect of calcium and magnesium. *FEMS Microbiology Letters* **122**, 33-38.

Karlson, U. & Frankenberger, W.T. (1988*a*). Determination of gaseous selenium-75 evolved from soil. *Soil Science Society of America Journal* **52**, 678-681.

Karlson, U. & Frankenberger, W.T. (1988*b*). Effects of carbon and trace element addition on alkylselenide production by soil. *Soil Science Society of America Journal* **52**, 1640-1644.

Karlson, U. & Frankenberger, W.T. (1989). Accelerated rates of selenium volatilization from California soils. *Soil Science Society of America Journal* **53**, 749-753.

Karlson, U. & Frankenberger, W.T. (1990). Alkylselenide production in salinized soils. *Soil Science* **149**, 56-61.

Karlson, U., Spencer, W.F. & Frankenberger, W.T. (1994). Physicochemical properties of dimethylselenide and dimethyldiselenide. *Journal of Chemical Engineering Data* **39**, 608-610.

Kessels, B.G.F., Belde, P.J.M. & Borst-Pauwels, G.W.F.H. (1985). Protection of *Saccharomyces cerevisiae* against $Cd^{2+}$ toxicity by $Ca^{2+}$. *Journal of General Microbiology* **131**, 2533-2537.

Kimura, Y. & Miller, V.L. (1960). Vapor phase separation of methyl- or ethylmercury compounds and metallic mercury. *Analytical Chemistry* **32**, 420-424.

Klapcinska, B. (1994). Binding of germanium and lead to *Pseudomonas putida* lipopolysaccharides. *Canadian Journal of Microbiology* **40**, 686-690.

Krantz-Rulcker, C., Frandberg. E. & Schnurer, J. (1995). Metal loading and enzymatic degradation of fungal cell walls and chitin. *Biology of Metals* **8**, 12-18.

Kuhn, S.P. & Pfister, R.M. (1989). Adsorption of mixed metals and cadmium by calcium-alginate immobilised *Zoogloea ramigera*. *Applied Microbiology and Biotechnology* **31**, 613-618.

Kuyucak, N. & Volesky, B. (1988). Biosorbents for recovery of metals from industrial solutions. *Biotechnology Letters* **10**, 137-142.

Langmuir, I. (1918). The adsorption of gases on plane surfaces of glass, mica and platinum. *Journal of the American Chemical Society*, **40**, 1361-1403.

Lauchli, A. (1993). Selenium in plants: uptake, functions, and environmental toxicity. *Botanica Acta* **106**, 455-468.

Lin, C.M., Crawford, B.F. & Kosman, D.J. (1993*a*). Distribution of $^{64}Cu$ in *Saccharomyces cerevisiae*: kinetic analyses of partitioning. *Journal of General Microbiology* **139**, 1617-1626.

Lin, C.M., Crawford, B.F. & Kosman, D.J. (1993*b*). Distribution of $^{64}Cu$ in *Saccharomyces cerevisiae*: cellular locale and metabolism. *Journal of General Microbiology* **139**, 1605-1615.

Lortie, L., Gould, W.D., Rajan, S., McReady, R.G.L. & Cheng, K.J. (1992). Reduction of selenate and selenite to elemental selenium by a *Pseudomonas stutzeri* isolate. *Applied and Environmental Microbiology* **58**, 4042-4044.

Lovley, D.R. (1993). Dissimilatory metal reduction. *Annual Review in Microbiology* **47**, 265-290.

Luef, E., Prey, T. & Kubicek, C.P. (1991). Biosorption of zinc by fungal mycelial wastes. *Applied Microbiology and Biotechnology* **34**, 688-692.

Macaskie, L.E. & Dean, A.C.R. (1985). Strontium accumulation by immobilised cells of a *Citrobacter* sp.. *Biotechnology Letters* **7**, 627-630.

Macy, J.M., Lawson, S. & DeMoll-Decker, H. (1993). Bioremediation of selenium oxyanions in San Joaquin drainage water using *Thauera selenatis* in a biological reactor system. *Applied Microbiology and Biotechnology* **40**, 588-594.

Maiers, D.T., Wichlacz, P.L., Thompson, D.L. & Bruhn, D.F. (1988). Selenate reduction by bacteria from a selenium-rich environment. *Applied and Environmental Microbiology* **54**, 2591-2593.

Mayland, H.F. (1994). Selenium in plant and animal nutrition. In *Selenium in the Environment* (ed. W.T. Frankenberger & S. Benson), pp. 29-46. Marcel Dekker Inc.: New York.

McCready, R.G., Campbell, J.N. & Payne, J.I. (1966). Selenite reduction by *Salmonella heidelberg*. *Canadian Journal of Microbiology* **12**, 703-714.

Melcer, H., Monteith, H. & Nutt, S.G. (1992). Activated sludge process response to variable inputs of heavy metals. *Water Science Technology* **25**, 387-394.

Moore, M.D. & Kaplan, S. (1992). Identification of intrinsic high-level resistance to rare-earth oxides and oxyanions in members of the class *Proteobacteria*: characterization of tellurite, selenite, and rhodium sesquioxide reduction in *Rhodobacter sphaeroides*. *Journal of Bacteriology* **174**, 1505-1514.

Morley, G.F., Sayer, J.A., Wilkinson, S.C., Gharieb, M.M. & Gadd, G.M. (1995). Fungal sequestration, mobilisation and transformation of metals and metalloids. In *Fungi and Environmental change* (ed J.C. Frankland, N. Magan & G.M. Gadd), pp. 235-256. Cambridge University Press: Cambridge, Great Britian.

Nakajima, A., Horikoshi, T. & Sakaguchi, T. (1982). Recovery of uranium by immobilised microorganisms. *European Journal of Applied Microbiology and Biotechnology* **16**, 88-91.

Namasivayam, C. & Yamuna, R.T. (1992). Removal of congo red from aqueous solutions by biogas waste slurry. *Journal of Chemical Technology and Biotechnology* **53**, 153-157.

Nickerson, W.J. & Falcone, G. (1963). Enzymatic reduction of selenite. *Journal of Bacteriology* **85**, 763-771.

Nieboer, E. & McBryde, (1973). A. E. Free-energy relationships in coordination chemistry. III. A comprehensive index to complex stability. *Canadian Journal of Chemistry* **51**, 2512-2524.

Nieboer, E. & Richardson, D. H. S. (1980). The replacement of the nondescript term "Heavy metals" by a biologically and chemically significant classification of metal ions. *Environmental Pollution Series B* **1**, 3-26.

Norris, P.R. & Kelly, D.P. (1977). Accumulation of cadium and cobalt by *Saccharomyces cerevisiae*. *Journal of General Microbiology* **99**, 317-324.

Ohsumi, Y. Kitamoto, K. & Anraku, Y. (1988). Changes induced in the permeability barrier of the yeast plasma membrane by the cupric ion. *Journal of Bacteriology* **170**, 2676-2682.

Olivas, R.M. & Donrad, O.F.X. (1994). Analytical techniques applied to the speciation of selenium in environmental matrices. *Analytica Chimica Acta* **286**, 357-370.

Oremland, R.S., Hollibaugh, J.T., Maest, A.S., Presser, T.S., Miller, L.G. & Culbertson, C.W. (1989). Selenate reduction to elemental selenium by anaerobic bacteria in sediments and culture: Biogeochemical significance of a novel selfate-independent respiration. *Applied and Environmental Microbiology* **55**, 2333-2343.

Oremland, R.S., Steinberg, N.A., Maest, A.S., Miller, L.G. & Hollibaugh, J.T. (1990). Measurement of *in situ* rates of selenate removal by dissimilatory bacterial reduction in sediments. *Environmental Science and Technology* **24**, 1157-1164.

Oremland, R.S., Steinberg. N.A., Presser, T.S. & Miller, L.G. (1991). *In situ* bacterial selenate reduction in the agricultural drainage systems of Western Nevada. *Applied and Environmental Microbiology* **57**, 615-617.

Oremland, R.S., Switzer Blum, J., Culbertson, C.W., Visscher, P.T., Miller, L.G., Dowdle, P. & Strohmaier, F.E. (1994). Isolation, growth, and metabolism of an obligately anaerobic, selenate-respiring bacterium, strain SES-3. *Applied and Environmental Microbiology* **60**, 3011-3019.

Pearson, R. G. (1963). Hard and soft acids and bases. *Journal of the American Chemical Society*, **85** 3533-3539.

Perkins, J. & Gadd, G.M. (1993). Accumulation and intracellular compartmentation of lithium ions in *Saccharomyces cerevisiae*. *FEMS Microbiology Letters* **107**, 255-260.

Perkins, J. & Gadd, G.M. (1995). The influence of pH and external $K^+$ concentration on caesium toxicity and accumulation in *Escherichia coli* and *Bacillus subtilis*. *Journal of Industrial Microbiology* **14**, 218-225.

Ramadan, S.E., Razak, A.A., Yousseff, Y.A. & Sedky, N.M. (1988). Selenium metabolism in a strain of *Fusarium*. *Biological Trace Element Research* **18**, 161-170.

Remacle, J. (1990). The cell wall and metal binding. In: *Biosorption of heavy metals* (ed B. Volesky), pp. 83-92. CRC Press: Florida.

Saucedo, I., Guibal, E., Roulph, Ch. & Le Cloirec, P. (1992). Sorption of uranyl ions by a modified chitosan: kinetic and equilibrium studies. *Environmental Technology* **13**, 1101-1115.

Savvaidis, I., Nobar, A., Hughes, M.N. & Poole, R.K. (1990). Displacement of surface-boind cationic dyes: a method for the rapid and semi-quantitative assay of metal binding to microbial surfaces. *Journal of Microbiological Methods* **11**, 95-106.

Scatchard, G. (1949). The attractions of proteins for small molecules and ions. *Ann. NY Acad. Sci.* **51**, 600-672.

Scott, C.D. (1992). Removal of dissolved metals by plant tissue. *Biotechnology and Bioengineering* **39**, 1064-1068.

Shannon, R. D. & Prewitt, C. T. (1969). Effective ionic radii in oxides and flourides. *Acta. Cryst.* **B25**, 925-946.

Shannon, R. D. & Prewitt, C. T. (1970). Revised values of effective ionic radii. *Acta. Cryst.* **B26,** 1046-1048.

Simmons, P., Tobin, J.M. & Singleton, I. (1995). Considerations on the use of commercially available yeast biomass for the treatment of metal-containing effluents. *Journal of Industrial Microbiology* **14**, 240-246.

Singleton, I. & Tobin, J.M. (1996). Fungal interactions with metals and radionuclides for environmental bioremediation. In Fungi and environmental change (ed. J.C. Frankland, N. Magan & G.M. Gadd), pp. 282-298. Cambridge University Press: Great Britian.

Sloof, J.E. & Viragh, A. (1995). Kinetics of cadmium uptake by green algae. *Water Air and Soil Pollution* **83**, 105-122.

Stadtman, T.C. (1990). Selenium biochemistry. *Annual Review of Biochemistry* **59**, 111-127.

Stanier, R.Y., Ingraham, J.L., Wheelis, M.L. & Painter, P.R. (1988). *General Microbiology.* Macmillan Eduction Ltd: London, England.

Steinberg, N.A., Blum, J.S., Hochstein, L. & Oremland, R.S. (1992). Nitrate is a preferred electron acceptor for growth of freshwater selenate-respiring bacteria. *Applied and Environmental Microbiology* **58**, 426-428.

Steinberg, N.A. & Oremland, R.S. (1990). Dissimilatory selenate reduction potentials in a diversity of sediment types. *Applied and Environmental Microbiology* **56**, 3550-3557.

Tan, J.A., Wang, W.Y, Wang, D.C. & Hou, S.F. (1994). Adsorption, volatilization and speciation of selenium in different types of soils in china. In *Selenium in the Environment* (ed. W.T. Frankenberger & S. Benson), pp. 47-67. Marcel Dekker Inc.: New York.

TCI. (1996). *Tokyo Kasei Organic Chemicals-Catalog 33*. Flurochem Ltd: Derbyshire, England.

Tebo, B.M. (1995). Metal precipitation by marine bacteria: Potential for biotechnological applications. *Genetic Engineering* **17**, 231-263.

Terry, N. & Zayed, A.M. (1994). Selenium volatilization by plants. In *Selenium in the Environment* (ed. W.T. Frankenberger & S. Benson), pp. 343-367. Marcel Dekker Inc.: New York.

Thompson-Eagle, E.T. & Frankenberger, W.T. (1991). Selenium biomethylation in a saline environment. *Water Research* **25**, 231-240.

Thompson-Eagle, E.T. & Frankenberger, W.T. (1990*a*). Volatilization of selenium from agricultural evaporation pond water. *Journal of Environmental Quality* **19**, 125-131.

Thompson-Eagle, E.T. & Frankenberger, W.T. (1990*b*). Protein-mediated selenium biomethylation in evaporation pond water. *Environmental Toxicology and Chemistry* **9**, 1435-1462.

Thompson-Eagle, E.T., Frankenberger, W.T. & Karlson, U. (1989). Volatilization of selenium by *Alternaria alternata*. *Applied and Environmental Microbiology* **55**, 1406-1413.

Thompson-Eagle, E.T., Frankenberger, W.T. & Longley, K.E. (1991). Removal of selenium from agricultural drainage water through soil microbial transformations. In: *The Economics and Management of Water and Drainage in Agriculture* (ed. A. Dinar & D. Zilberman, Eds.), pp. 169-186. Kluwer Academic Publishers: Norwell, MA.

Ting, Y.P. & Teo, W.K. (1994). Uptake of cadmium and zinc by yeast: effects of co-metal ion and physical/chemical treatments. *Bioresource Technology* **50**, 113-117.

Tobin, J.M., Cooper, D.G. & Neufeld, R.J. (1984). Uptake of metal ions by *Rhizopus arrhizus* biomass. *Applied and Environmental Microbiology* **47**, 821-824.

Tobin, J.M., Cooper, D.G. & Neufeld, R.J. (1987). Influence of anions on metal adsorption by *Rhizopus arrhizus* biomass. *Biotechnology and Bioengineering* **30**, 882-886.

Tobin, J.M., Cooper, D.G. & Neufeld, R.J. (1988). The effects of cation competition on metal adsorption by *Rhizopus arrhizus* biomass. *Biotechnology and Bioengineering* **31**, 282-286.

Tobin, J.M., Cooper, D.G. & Neufeld, R.J. (1990). Investigation of the mechanism of metal uptake by denatured *Rhizopus arrhizus* biomass. *Enzyme and Microbial Technology* **12**, 591-595.

Tobin, J.M., L'homme, B. & Roux, J.C. (1993). Immobilisation protocols and effects on cadium uptake by *Rhizopus arrhizus* biosorbents. *Biotechnology Techniques* **7**, 739-744.

Tobin, J.M., White, C. & Gadd, G.M. (1994). Metal accumulation by fungi: applications in environmental biotechnology. *Journal of Industrial Microbiology* **13**, 126-130.

Tomei, F.A., Barton, L.L., Lemanski, C.L. & Zocco, T.G. (1992). Reduction of selenate and selenite to elemental selenium by *Wolinella succinogenes*. *Canadian Journal of Microbiology* **38**, 1328-1333.

Treen-Sears, M. E., Volesky, B. & Neufeld, R.J. (1984). Ion exchange/complexation of the uranyl ion by *Rhizopus* biosorbent. *Biotechnology and Bioengineering* **26**, 1323-1329.

Trevors, J.T., Stratton, G.W. & Gadd, G.M. (1986). Cadmium transport, resistance, and toxicity in bacteria, algae and fungi. *Canadian Journal of Microbiology* **32**, 447-464.

Tsezos, M., McCready, R.G.L & Bell, J.P. (1989). The continuous recovery of uranium from biologically leached solutions using immobilized biomass. *Biotechnology and Bioengineering* **34**. 10-17.

Tsezos, M., Noh, S.H. & Baird, M.H.I. (1988). A batch reactor mass transfer kinetic model for immobilized biomass biosorption. *Biotechnology and Bioengineering* **32**, 545-553.

Tsezos, M. & Volesky, B. (1982). The mechanism of uranium biosorption by *Rhizopus arrhizus*. *Biotechnology and Bioengineering* **24**, 385-401.

Urrutia Mera, M., Kemper, M., Doyle, R. & Belveridge, T. J. (1992). The membrane induced proton motive force influences the metal binding ability of *Bacillus subtilus* cell walls. *Applied and Environmental Microbiology* **58**, 3837-3844.

Volesky, B. (1986). Biosorbent materials. *Biotechnology and Bioengineering Symposium* **16**, 121-126.

Volesky, B. (1990). Removal and recovery of heavy metals by biosorption. In: *Biosorption of heavy metals* (ed. B. Volesky), pp. 7-43. CRC Press: Florida.

Volesky, B. & Holan, Z.R. (1995). Biosorption of heavy metals. *Biotechnology Progress* **11**, 235-250.

Volesky, B., May, H. & Holan, Z.R. (1993). Cadmium biosorption by *Saccharomyces cerevisiae*. *Biotechnology and Bioengineering* **41**, 826-829.

Volesky, B. & May-Phillips, H.A. (1995). Biosorption of heavy metals by *Saccharomyces cerevisiae*. *Applied Microbiology and Biotechnology* **42**, 797-806.

Wainwright, M. (1990). Novel uses for fungi in biotechnology. *Chemistry and Industry* **2**, 31-34.

Watson, J.S., Scott, C.D. & Faison, B.D. (1989). Adsorption of Sr by immobilised microorganisms. *Applied Biochemistry and Biotechnology* **20/21**, 699-709.

Weber, W.J. (1972). *Physicochemical Processes for water quality control.* Wiley-Interscience: New York.

White, C. & Gadd, G.M. (1990). Biosorption of radionuclides by fungal biomass. *Journal of Chemical Technology and Biotechnology* **49**, 331-343.

Wnorowski, A.U. (1991). Selection of bacterial and fungal strains for bioaccumulation of heavy metals from aqueous solutions. *Water Science Technology* **23**, 309-318.

Yannai, S., Berdicevsky, I. & Duek, L. (1991). Transformations of inorganic mercury by *Candida albicans* and *Saccharomyces cerevisiae*. *Applied and Environmental Microbiology* **57**, 245-247.

Yazgan, A. & Ozcengiz, G. (1994). Subcellular distribution of accumulated heavy metals in *Saccharomyces cerevisiae* and *Kluyveromyces marxianus*. *Biotechnology Letters* **16**, 871-874.

Yoshida, N. & Murooka, Y. (1994). Adsorption of bacterial cells to crystal particles of heavy metals: Role of electrostatic interaction. *Journal of Fermentation and Bioengineering* **77**, 636-641.

Zabel, T.F. (1993). Diffuse sources of pollution by heavy metals. *Journal of Industrial Waste and Environmental Management* **7**, 513-520.

Zieve, R., Ansell, P.J., Young, T.W.K. & Peterson, P.J. (1985). Selenium volatilization by *Mortierella species*. *Transactions of the British Mycological Society* **84**, 177-179.

Zhou, J. L. & Kiff, R. J. (1991). The uptake of copper from aqueous solution by immobilized fungal biomass. *Journal of Chemical Technology and Biotechnology* **52**, 317-330.

**APPENDIX A**: Pearson's classification of hard and soft acids and bases (1963). The vertical distribution of ions down each group reflect increasing class (b) character.

| Class (a) or "hard" | Class (b) or "soft" | Borderline |
|---|---|---|
| $H^+$ | $Cu^+$ | |
| $Li^+$ | $Ag^+$ | |
| $Na^+$ | $Au^+$ | |
| $K^+$ | $Tl^+$ | |
| | $Hg^+$ | |
| | $Cs^+$ | |
| $Be^{2+}$ | $Pd^{2+}$ | $Fe^{2+}$ |
| $Mg^{2+}$ | $Cd^{2+}$ | $Co^{2+}$ |
| $Ca^{2+}$ | $Pt^{2+}$ | $Ni^{2+}$ |
| $Sr^{2+}$ | $Hg^{2+}$ | $Cu^{2+}$ |
| $Sn^{2+}$ | | $Zn^{2+}$ |
| | | $Pb^{2+}$ |
| $Al^{3+}$ | $Tl^{3+}$ | |
| $Sc^{3+}$ | | |
| $Ga^{3+}$ | | |
| $In^{3+}$ | | |
| $La^{3+}$ | | |
| $Cr^{3+}$ | | |
| $Co^{3+}$ | | |
| $Fe^{3+}$ | | |
| $As^{3+}$ | | |
| $Ir^{3+}$ | | |
| $Si^{4+}$ | | |
| $Ti^{4+}$ | | |
| $Zr^{4+}$ | | |
| $Th^{4+}$ | | |
| $Pu^{4+}$ | | |
| $UO_2^{2+}$ | | |

**APPENDIX B**: Classification of metal ions and computation of covalent index values ($X_m^2 r$). Compiled from Nieboer & Richardson (1980).

| Ion | Electronegativity [a] ($X_m$) | Ionic radius [c] ($r$) | $X_m^2 r$ |
|---|---|---|---|
| **Class (a)** | | | |
| $Li^+$ | 0.98 | 0.740 | 0.711 |
| $Na^+$ | 0.93 | 1.020 | 0.882 |
| $K^+$ | 0.82 | 1.380 | 0.928 |
| $Cs^+$ | 0.79 | 1.700 | 1.061 |
| $Be^{2+}$ | 1.57 | 0.350 | 0.863 |
| $Ca^{2+}$ | 1.00 | 1.000 | 1.000 |
| $Sr^{2+}$ | 0.95 | [d]1.130 | 1.020 |
| $Ba^{2+}$ | 0.89 | 1.360 | 1.077 |
| $Mg^{2+}$ | 1.31 | 0.720 | 1.236 |
| $La^{3+}$ | 1.10 | [d]1.045 | 1.264 |
| $Y^{3+}$ | 1.22 | [d]0.900 | 1.340 |
| $Al^{3+}$ | 1.61 | 0.530 | 1.374 |
| $Sc^{3+}$ | 1.36 | [d]0.745 | 1.378 |
| **Borderline** | | | |
| $Mn^{2+}$ | 1.55 | [d]0.830 | 1.990 |
| $Ti^{2+}$ | 1.54 | 0.860 | 2.040 |
| $V^{2+}$ | 1.63 | 0.790 | 2.100 |
| $Zn^{2+}$ | [b]1.69 | [d]0.750 | 2.128 |
| $Cr^{2+}$ | 1.66 | 0.820 | 2.260 |
| $Ni^{2+}$ | 1.91 | [d]0.690 | 2.517 |
| $Fe^{2+}$ | 1.83 | [d]0.780 | 2.612 |
| $Co^{2+}$ | 1.88 | [d]0.745 | 2.633 |
| $Cd^{2+}$ | 1.69 | 0.950 | 2.713 |
| $Cu^{2+}$ | [b]2.02 | 0.730 | 2.979 |
| $Sn^{2+}$ | 1.80 | 0.930 | 3.013 |
| $Pb^{2+}$ | 1.87 | [b,c]0.940 | 3.287 |
| $Ga^{3+}$ | 1.81 | 0.620 | 2.031 |
| $Fe^{3+}$ | 1.96 | 0.645 | 2.478 |
| $In^{3+}$ | 1.78 | [d]0.800 | 2.535 |
| **Class (b)** | | | |
| $Cu^+$ | 1.90 | 0.960 | 3.466 |
| $Tl^+$ | 1.62 | 1.500 | 3.937 |
| $Ag^+$ | 1.93 | 1.150 | 4.284 |
| $Au^+$ | 2.54 | 1.370 | 7.335 |

| | | | |
|---|---|---|---|
| **Class (b) continued** | | | |
| $Hg^{2+}$ | 2.00 | 1.020 | 4.080 |
| $Pt^{2+}$ | 2.28 | 0.800 | 4.159 |
| $Pd^{2+}$ | 2.20 | 0.860 | 4.162 |
| $Tl^{3+}$ | 2.04 | [d]0.885 | 3.683 |
| $Bi^{3+}$ | 2.02 | 1.020 | 4.160 |

[a](Allred, 1961)
[b](Nieboer & McBryde, 1973)
[c](Shannon & Prewitt, 1969)
[d](Shannon & Prewitt, 1970)

**APPENDIX C**: A survey of metal ion oxidation states. Metal ion classification by Nieboer & Richardson (1980).

---

**Class (a)**

| | |
|---|---|
| Li | $1s^2\ 2s^1$ |
| $Li^+$ | $1s^2$ |
| Na | $1s^2\ 2s^2\ 2p^6\ 3s^1$ |
| $Na^+$ | $1s^2\ 2s^2\ 2p^6$ |
| K | $1s^2\ 2s^2\ 2p^6\ 3s^2\ 3p^6\ 4s^1$ |
| $K^+$ | $1s^2\ 2s^2\ 2p^6\ 3s^2\ 3p^6$ |
| Cs | $1s^2\ 2s^2\ 2p^6\ 3s^2\ 3p^6\ 3d^{10}\ 4s^2\ 4p^6\ 4d^{10}\ 5s^2\ 5p^6\ 6s^1$ |
| $Cs^+$ | $1s^2\ 2s^2\ 2p^6\ 3s^2\ 3p^6\ 3d^{10}\ 4s^2\ 4p^6\ 4d^{10}\ 5s^2\ 5p^6$ |
| | |
| Be | $1s^2\ 2s^2$ |
| $Be^{2+}$ | $1s^2$ |
| Ca | $1s^2\ 2s^2\ 2p^6\ 3s^2\ 3p^6\ 4s^2$ |
| $Ca^{2+}$ | $1s^2\ 2s^2\ 2p^6\ 3s^2\ 3p^6$ |
| Sr | $1s^2\ 2s^2\ 2p^6\ 3s^2\ 3p^6\ 3d^{10}\ 4s^2\ 4p^6\ 5s^2$ |
| $Sr^{2+}$ | $1s^2\ 2s^2\ 2p^6\ 3s^2\ 3p^6\ 3d^{10}\ 4s^2\ 4p^6$ |
| Ba | $1s^2\ 2s^2\ 2p^6\ 3s^2\ 3p^6\ 3d^{10}\ 4s^2\ 4p^6\ 4d^{10}\ 5s^2\ 5p^6\ 6s^2$ |
| $Ba^{2+}$ | $1s^2\ 2s^2\ 2p^6\ 3s^2\ 3p^6\ 3d^{10}\ 4s^2\ 4p^6\ 4d^{10}\ 5s^2\ 5p^6$ |
| Mg | $1s^2\ 2s^2\ 2p^6\ 3s^2$ |
| $Mg^{2+}$ | $1s^2\ 2s^2\ 2p^6$ |
| | |
| La | $1s^2\ 2s^2\ 2p^6\ 3s^2\ 3p^6\ 3d^{10}\ 4s^2\ 4p^6\ 4d^{10}\ 5s^2\ 5p^6\ 5d^1\ 6s^2$ |
| $La^{3+}$ | $1s^2\ 2s^2\ 2p^6\ 3s^2\ 3p^6\ 3d^{10}\ 4s^2\ 4p^6\ 4d^{10}\ 5s^2\ 5p^6$ |
| Y | $1s^2\ 2s^2\ 2p^6\ 3s^2\ 3p^6\ 3d^{10}\ 4s^2\ 4p^6\ 4d^1\ 5s^2$ |
| $Y^{3+}$ | $1s^2\ 2s^2\ 2p^6\ 3s^2\ 3p^6\ 3d^{10}\ 4s^2\ 4p^6$ |
| Gd | $1s^2\ 2s^2\ 2p^6\ 3s^2\ 3p^6\ 3d^{10}\ 4s^2\ 4p^6\ 4d^{10}\ 4f^7\ 5s^2\ 5p^6\ 5d^1\ 6s^2$ |
| $Gd^{3+}$ | $1s^2\ 2s^2\ 2p^6\ 3s^2\ 3p^6\ 3d^{10}\ 4s^2\ 4p^6\ 4d^{10}\ 4f^7\ 5s^2\ 5p^6$ |
| Lu | $1s^2\ 2s^2\ 2p^6\ 3s^2\ 3p^6\ 3d^{10}\ 4s^2\ 4p^6\ 4d^{10}\ 4f^{14}\ 5s^2\ 5p^6\ 5d^1\ 6s^2$ |
| $Lu^{3+}$ | $1s^2\ 2s^2\ 2p^6\ 3s^2\ 3p^6\ 3d^{10}\ 4s^2\ 4p^6\ 4d^{10}\ 4f^{14}\ 5s^2\ 5p^6$ |
| Al | $1s^2\ 2s^2\ 2p^6\ 3s^2\ 3p^1$ |
| $Al^{3+}$ | $1s^2\ 2s^2\ 2p^6$ |
| Sc | $1s^2\ 2s^2\ 2p^6\ 3s^2\ 3p^6\ 3d^1\ 4s^2$ |
| $Sc^{3+}$ | $1s^2\ 2s^2\ 2p^6\ 3s^2\ 3p^6$ |

**Borderline**

| | |
|---|---|
| Mn | $1s^2\ 2s^2\ 2p^6\ 3s^2\ 3p^6\ 3d^5\ 4s^2$ |
| $Mn^{2+}$ | $1s^2\ 2s^2\ 2p^6\ 3s^2\ 3p^6\ 3d^5$ |
| Ti | $1s^2\ 2s^2\ 2p^6\ 3s^2\ 3p^6\ 3d^2\ 4s^2$ |
| $Ti^{2+}$ | $1s^2\ 2s^2\ 2p^6\ 3s^2\ 3p^6\ 3d^2$ |
| V | $1s^2\ 2s^2\ 2p^6\ 3s^2\ 3p^6\ 3d^3\ 4s^2$ |
| $V^{2+}$ | $1s^2\ 2s^2\ 2p^6\ 3s^2\ 3p^6\ 3d^3$ |
| Zn | $1s^2\ 2s^2\ 2p^6\ 3s^2\ 3p^6\ 3d^{10}\ 4s^2$ |
| $Zn^{2+}$ | $1s^2\ 2s^2\ 2p^6\ 3s^2\ 3p^6\ 3d^{10}$ |
| Cr | $1s^2\ 2s^2\ 2p^6\ 3s^2\ 3p^6\ 3d^4\ 4s^2$ |
| $Cr^{2+}$ | $1s^2\ 2s^2\ 2p^6\ 3s^2\ 3p^6\ 3d^4$ |

---

**Borderline** (continued)

| | |
|---|---|
| Ni | $1s^2\ 2s^2\ 2p^6\ 3s^2\ 3p^6\ 3d^8\ 4s^2$ |
| $Ni^{2+}$ | $1s^2\ 2s^2\ 2p^6\ 3s^2\ 3p^6\ 3d^8$ |
| Fe | $1s^2\ 2s^2\ 2p^6\ 3s^2\ 3p^6\ 3d^6\ 4s^2$ |
| $Fe^{2+}$ | $1s^2\ 2s^2\ 2p^6\ 3s^2\ 3p^6\ 3d^6$ |
| Co | $1s^2\ 2s^2\ 2p^6\ 3s^2\ 3p^6\ 3d^7\ 4s^2$ |
| $Co^{2+}$ | $1s^2\ 2s^2\ 2p^6\ 3s^2\ 3p^6\ 3d^7$ |
| Cd | $1s^2\ 2s^2\ 2p^6\ 3s^2\ 3p^6\ 3d^{10}\ 4s^2\ 4p^6\ 4d^{10}\ 5s^2$ |
| $Cd^{2+}$ | $1s^2\ 2s^2\ 2p^6\ 3s^2\ 3p^6\ 3d^{10}\ 4s^2\ 4p^6\ 4d^{10}$ |
| Cu | $1s^2\ 2s^2\ 2p^6\ 3s^2\ 3p^6\ 3d^9\ 4s^2$ |
| $Cu^{2+}$ | $1s^2\ 2s^2\ 2p^6\ 3s^2\ 3p^6\ 3d^9$ |
| Sn | $1s^2\ 2s^2\ 2p^6\ 3s^2\ 3p^6\ 3d^{10}\ 4s^2\ 4p^6\ 4d^{10}\ 5s^2\ 5p^2$ |
| $Sn^{2+}$ | $1s^2\ 2s^2\ 2p^6\ 3s^2\ 3p^6\ 3d^{10}\ 4s^2\ 4p^6\ 4d^{10}\ 5s^2$ |
| Pb | $1s^2\ 2s^2\ 2p^6\ 3s^2\ 3p^6\ 3d^{10}\ 4s^2\ 4p^6\ 4d^{10}\ 4f^{14}\ 5s^2\ 5p^6\ 5d^{10}\ 6s^2\ 6p^2$ |
| $Pb^{2+}$ | $1s^2\ 2s^2\ 2p^6\ 3s^2\ 3p^6\ 3d^{10}\ 4s^2\ 4p^6\ 4d^{10}\ 4f^{14}\ 5s^2\ 5p^6\ 5d^{10}\ 6s^2$ |
| | |
| Ga | $1s^2\ 2s^2\ 2p^6\ 3s^2\ 3p^6\ 3d^{10}\ 4s^2\ 4p^1$ |
| $Ga^{3+}$ | $1s^2\ 2s^2\ 2p^6\ 3s^2\ 3p^6\ 3d^{10}$ |
| Fe | $1s^2\ 2s^2\ 2p^6\ 3s^2\ 3p^6\ 3d^6\ 4s^2$ |
| $Fe^{3+}$ | $1s^2\ 2s^2\ 2p^6\ 3s^2\ 3p^6\ 3d^5$ |
| In | $1s^2\ 2s^2\ 2p^6\ 3s^2\ 3p^6\ 3d^{10}\ 4s^2\ 4p^6\ 4d^{10}\ 5s^2\ 5p^1$ |
| $In^{3+}$ | $1s^2\ 2s^2\ 2p^6\ 3s^2\ 3p^6\ 3d^{10}\ 4s^2\ 4p^6\ 4d^{10}$ |

**Class (b)**

| | |
|---|---|
| Cu | $1s^2\ 2s^2\ 2p^6\ 3s^2\ 3p^6\ 3d^{10}\ 4s^1$ |
| $Cu^+$ | $1s^2\ 2s^2\ 2p^6\ 3s^2\ 3p^6\ 3d^{10}$ |
| Tl | $1s^2\ 2s^2\ 2p^6\ 3s^2\ 3p^6\ 3d^{10}\ 4s^2\ 4p^6\ 4d^{10}\ 4f^{14}\ 5s^2\ 5p^6\ 5d^{10}\ 6s^2\ 6p^1$ |
| $Tl^+$ | $1s^2\ 2s^2\ 2p^6\ 3s^2\ 3p^6\ 3d^{10}\ 4s^2\ 4p^6\ 4d^{10}\ 4f^{14}\ 5s^2\ 5p^6\ 5d^{10}\ 6s^2$ |
| Ag | $1s^2\ 2s^2\ 2p^6\ 3s^2\ 3p^6\ 3d^{10}\ 4s^2\ 4p^6\ 4d^{10}\ 5s^1$ |
| $Ag^+$ | $1s^2\ 2s^2\ 2p^6\ 3s^2\ 3p^6\ 3d^{10}\ 4s^2\ 4p^6\ 4d^{10}$ |
| Au | $1s^2\ 2s^2\ 2p^6\ 3s^2\ 3p^6\ 3d^{10}\ 4s^2\ 4p^6\ 4d^{10}\ 4f^{14}\ 5s^2\ 5p^6\ 5d^{10}\ 6s^1$ |
| $Au^+$ | $1s^2\ 2s^2\ 2p^6\ 3s^2\ 3p^6\ 3d^{10}\ 4s^2\ 4p^6\ 4d^{10}\ 4f^{14}\ 5s^2\ 5p^6\ 5d^{10}$ |
| | |
| Hg | $1s^2\ 2s^2\ 2p^6\ 3s^2\ 3p^6\ 3d^{10}\ 4s^2\ 4p^6\ 4d^{10}\ 4f^{14}\ 5s^2\ 5p^6\ 5d^{10}\ 6s^2$ |
| $Hg^{2+}$ | $1s^2\ 2s^2\ 2p^6\ 3s^2\ 3p^6\ 3d^{10}\ 4s^2\ 4p^6\ 4d^{10}\ 4f^{14}\ 5s^2\ 5p^6\ 5d^{10}$ |
| Pt | $1s^2\ 2s^2\ 2p^6\ 3s^2\ 3p^6\ 3d^{10}\ 4s^2\ 4p^6\ 4d^{10}\ 4f^{14}\ 5s^2\ 5p^6\ 5d^8\ 6s^2$ |
| $Pt^{2+}$ | $1s^2\ 2s^2\ 2p^6\ 3s^2\ 3p^6\ 3d^{10}\ 4s^2\ 4p^6\ 4d^{10}\ 4f^{14}\ 5s^2\ 5p^6\ 5d^8$ |
| Pd | $1s^2\ 2s^2\ 2p^6\ 3s^2\ 3p^6\ 3d^{10}\ 4s^2\ 4p^6\ 4d^8\ 5s^2$ |
| $Pd^{2+}$ | $1s^2\ 2s^2\ 2p^6\ 3s^2\ 3p^6\ 3d^{10}\ 4s^2\ 4p^6\ 4d^8$ |
| | |
| Tl | $1s^2\ 2s^2\ 2p^6\ 3s^2\ 3p^6\ 3d^{10}\ 4s^2\ 4p^6\ 4d^{10}\ 4f^{14}\ 5s^2\ 5p^6\ 5d^{10}\ 6s^2\ 6p^1$ |
| $Tl^{3+}$ | $1s^2\ 2s^2\ 2p^6\ 3s^2\ 3p^6\ 3d^{10}\ 4s^2\ 4p^6\ 4d^{10}\ 4f^{14}\ 5s^2\ 5p^6\ 5d^{10}$ |
| Bi | $1s^2\ 2s^2\ 2p^6\ 3s^2\ 3p^6\ 3d^{10}\ 4s^2\ 4p^6\ 4d^{10}\ 4f^{14}\ 5s^2\ 5p^6\ 5d^{10}\ 6s^2\ 6p^3$ |
| $Bi^{3+}$ | $1s^2\ 2s^2\ 2p^6\ 3s^2\ 3p^6\ 3d^{10}\ 4s^2\ 4p^6\ 4d^{10}\ 4f^{14}\ 5s^2\ 5p^6\ 5d^{10}\ 6s^2$ |

**APPENDIX D**: Hard and soft ligands.

| **Hard** | **Borderline** | **Soft** |
|---|---|---|
| [a]$F^-$ | [a]$Cl^-$ | [a]$H^-$ |
| [a]$O_2^-$ | [a]$Br^-$ | [a]$I^-$ |
| [a]$OH^-$ | [a]$N_3^-$ | [a]$R^-$ |
| [a,b]$H_2O$ | [a]$NO_2^-$ | [a,b]$CN^-$ |
| [a,b]ROH | [a]$SO_3^{2-}$ | [a]$RS^-$ |
| [b]$-CO_2^-$ | [a]$NH_3$ | [b]RSH |
| [a]$CO_3^{2-}$ | [a]$N_2$ | [a,b]$R_2S$ |
| [b]$NH_3$ | [a]$RNH_2$ | [b]$S_2O_3^{2-}$ |
| [b]$RNH_2$ | [a]$R_2NH$ | |
| [b]Porphyrin | [a]$R_3N$ | |
| [b]$Cl^-$ | [a]$-CO-N^--R$ | |
| [b]$PO_4^{3-}$ | [a]$O_2$ | |
| [b]$SO_4^{2-}$ | [a]$O_2^-$ | |
| [a]$ROSO_3^-$ | [a]$O_2^{2-}$ | |
| [a]$NO_3^-$ | [b]Pyridine | |
| [a]$HPO_4^{2-}$ | | |
| [a]$RCOO^-$ | | |
| [a]ROR | | |

The symbol R represents alkyl radicals and may also be an aromatic moiety. Hard metal ions have an absolute preference in aqueous solution for hard ligands outlined in the first column, all of which bind through oxygen. Soft metal ions exhibit a preference for the ligands in column three but are also able to react in aqueous solution with the borderline ligands (second column). Borderline metal ions can react in solution with all the ligands but they may exhibit preferences. The data and explanations have been compiled from [a]Nieboer & Richardson (1980) and [b]Hughes & Poole (1989; 1991).

**APPENDIX E**: Values of erf($x$). Compiled from Belter *et al.* (1988).

| $x$ | 0 | 1 | 2 | 3 | 4 | 5 | 6 | 7 | 8 | 9 |
|---|---|---|---|---|---|---|---|---|---|---|
| **0.0** | .000 | .011 | .023 | .034 | .045 | .056 | .068 | .079 | .090 | .101 |
| **0.1** | .112 | .124 | .135 | .146 | .157 | .168 | .179 | .190 | .201 | .212 |
| **0.2** | .223 | .234 | .244 | .255 | .266 | .276 | .287 | .297 | .308 | .318 |
| **0.3** | .329 | .340 | .349 | .359 | .369 | .379 | .389 | .399 | .409 | .419 |
| **0.4** | .428 | .438 | .447 | .457 | .446 | .475 | .485 | .494 | .503 | .512 |
| **0.5** | .521 | .529 | .538 | .546 | .555 | .563 | .572 | .580 | .588 | .596 |
| **0.6** | .604 | .611 | .619 | .627 | .634 | .642 | .649 | .657 | .664 | .671 |
| **0.7** | .678 | .685 | .691 | .698 | .705 | .711 | .717 | .724 | .730 | .736 |
| **0.8** | .742 | .748 | .754 | .759 | .765 | .771 | .776 | .781 | .787 | .792 |
| **0.9** | .797 | .802 | .807 | .812 | .816 | .821 | .825 | .830 | .834 | .839 |
| **1.0** | .843 | .847 | .851 | .855 | .859 | .862 | .866 | .870 | .873 | .877 |
| **1.1** | .880 | .884 | .887 | .890 | .893 | .896 | .899 | .902 | .905 | .908 |
| **1.2** | .910 | .913 | .916 | .918 | .921 | .923 | .925 | .928 | .930 | .932 |
| **1.3** | .934 | .936 | .938 | .940 | .942 | .944 | .946 | .947 | .949 | .951 |
| **1.4** | .952 | .954 | .955 | .957 | .958 | .960 | .961 | .962 | .964 | .965 |
| **1.5** | .966 | .967 | .968 | .970 | .971 | .972 | .973 | .974 | .975 | .975 |
| **1.6** | .976 | .977 | .978 | .979 | .980 | .980 | .981 | .982 | .982 | .983 |
| **1.7** | .984 | .984 | .985 | .986 | .986 | .987 | .987 | .988 | .988 | .989 |
| **1.8** | .989 | .990 | .990 | .990 | .991 | .991 | .991 | .992 | .992 | .992 |
| **1.9** | .993 | .993 | .993 | .994 | .994 | .994 | .994 | .995 | .995 | .995 |
| **2.0** | .995 | .997 | .998 | .999 | .999 | 1 | 1 | 1 | 1 | 1 |